EUROPEAN COMMISSION

Community Research

SEVENTH FRAMEWORK PROGRAMME

ARCHER

Collaborative Project (CP)

Co-funded by the European Commission under the Euratom Research and Training Programme on Nuclear Energy within the Seventh Framework Programme

Grant Agreement Number : 269892

Start date : 01/02/2011 Duration : 48 Months
www.archer-project.eu

Archer
Advanced Reactor for Cogeneration of Heat & Electricity-R&D

Report on strength measurements of irradiated graphite

Authors : HEIJNA Maurits (NRG)

ARCHER - Contract Number: 269892
Advanced High-Temperature Reactors for Cogeneration of Heat and Electricity R&D
EC Scientific Officer: Dr. Panagiotis Manolatos

Document title	Report on strength measurements of irradiated graphite
Author(s)	HEIJNA Maurits
Number of pages	100
Document type	Deliverable
Work Package	WP 41
Document number	D41.15
Issued by	NRG
Date of completion	24/05/2013
Dissemination level	Confidential, only for members of the consortium (including the Commission Services).

Summary

The irradiation behaviour of modern graphite grades have been investigated at two irradiation temperatures, 750

D41-15: Report on strength measurements on irradiated graphite

Diametric compression
and fractography

Confidential

Under the contract of Euratom grant agreement 269892

rev. no.	date	description
A		Final

author(s):	Heijna, M.C.R.	reviewed:	T.O. van Staveren
name:	Archer D41-15.docx	approved:	R.P.C. Schram
referencenr.:	22906/13.119486		
99 pages	24/04/2013		

Contents

Summary		5
1	Introduction	7
2	Experiments and measurement techniques	9
2.1	Irradiation experiments	9
2.1.1	Graphite grades	9
2.1.2	Specimen types	10
2.1.3	INNOGRAPH irradiation experiments at 750°C	11
2.2	Mechanical strength measurements	13
2.2.1	Test matrix	13
2.2.2	Diametric compression	16
2.2.3	Fractography	19
3	Results	20
3.1	Diametric compression	20
3.2	Fractography	22
3.2.1	NBG-10	22
3.2.2	PCIB	41
4	Conclusions	72
References		73
List of tables		75
List of figures		75
Appendix A	Test Matrix	83
Appendix B	Results of the tensile strength measurements	85
Appendix C	Images of specimens after testing	87
C.1	GrafTech specimens	87
C.2	SGL specimens	92
C.3	Toyo Tanso specimens	97

Summary

In the European graphite irradiation programme, part of the HTR-M1-IP and RAPHAEL-IP, the irradiation behaviour of modern graphite grades is investigated at two irradiation temperatures, 750°C and 950°C. With the full Post-Irradiation Examination (PIE) of the high fluence experiments completed in the ARCHER project, samples are now available for additional destructive PIE such as mechanical strength testing. This report describes the mechanical strength measurements, tensile strength by diametric compression, and fractography on samples from the INNOGRAPH-1A and INNOGRAPH-1B irradiation experiments at 750°C.

The work described was performed with financial support from the European Union and the Dutch Ministry of Economic Affairs, Agriculture, and Innovation. The views expressed in this report are those of the authors and do not necessarily represent those of the European Union, nor those of the Dutch government.

1 Introduction

Graphite is a suitable material to be used as a neutron moderator and reflector in nuclear reactors. Graphite has been used in Advanced Gas-Cooled Reactors, Magnox reactors, RBMK's (a Russian acronym meaning "reactor cooled by water and moderated by graphite"), Research Reactors, Materials Test Reactors and High Temperature Reactors (HTR's). Since the end of the 20th century there has been a renewed interest in HTR's. Two prototypes, one in Japan (HTTR) and one in China (HTR-10) are in operation. A demonstration plant is under construction in China (HTR-PM). The Next Generation Nuclear Plant NGNP in the US is in development. The European Commission is supporting research projects for the development of HTR technology to determine the technological requirements for designing and constructing an HTR in Europe.

Much research has been done on the behaviour of graphite grades in a nuclear reactor environment, because graphite is already being used in reactors for decades. However, many of the historical graphite grades are no longer commercially available since the raw materials no longer exist. In addition, most historical data are from low temperature irradiation experiments (<550°C), whereas for HTR's the graphite temperatures will generally be higher than 550°C. In order to be able to design a European HTR, it is decided by the European commission to create a database that contains data of the materials behaviour of available graphite grades under neutron irradiation at temperatures relevant for the HTR's. This will allow the 'best' graphite(s) to be chosen, and provide the necessary data to allow the core design to be carried out.

Within the RAPHAEL-IP framework, graphite irradiation experiments were performed at 750°C and 950°C in the High Flux Reactor (HFR) in Petten. These were named INNOGRAPH-1B (750°C, high dose), INNOGRAPH-2A (950°C, medium dose) and INNOGRAPH-2B (950°C, high dose). In every experiment a selection of samples were also irradiated at lower temperatures of 650°C (1B) and 850°C (2A and 2B). Figure 1.1 shows schematically the expected volume change of graphite with neutron fluence at the two main irradiation temperatures. The boxes on the curves indicate the four different irradiation experiments. Box 1A indicates the low dose irradiation at 750°C named INNOGRAPH-1A. This has been performed within HTR-M1 in the 5th Framework Programme and had a target dose of 8 dpa [1]. Box 1B indicates INNOGRAPH-1B, the high dose (up to ~25 dpa) experiment at the same temperature. Boxes 2A and 2B indicate the medium and high dose experiments at 950°C, INNOGRAPH-2A and INNOGRAPH-2B respectively. In order to reach the target dose in a short time, the high dose experiments (INNOGRAPH-1B/2B) partly contain specimens that have been irradiated in the low dose experiments. These two high dose experiments had to be built in a hot-cell because of the radioactivity of the samples. The capability to do this delicate work with manipulators is essential to carry out this irradiation programme [2, 3].

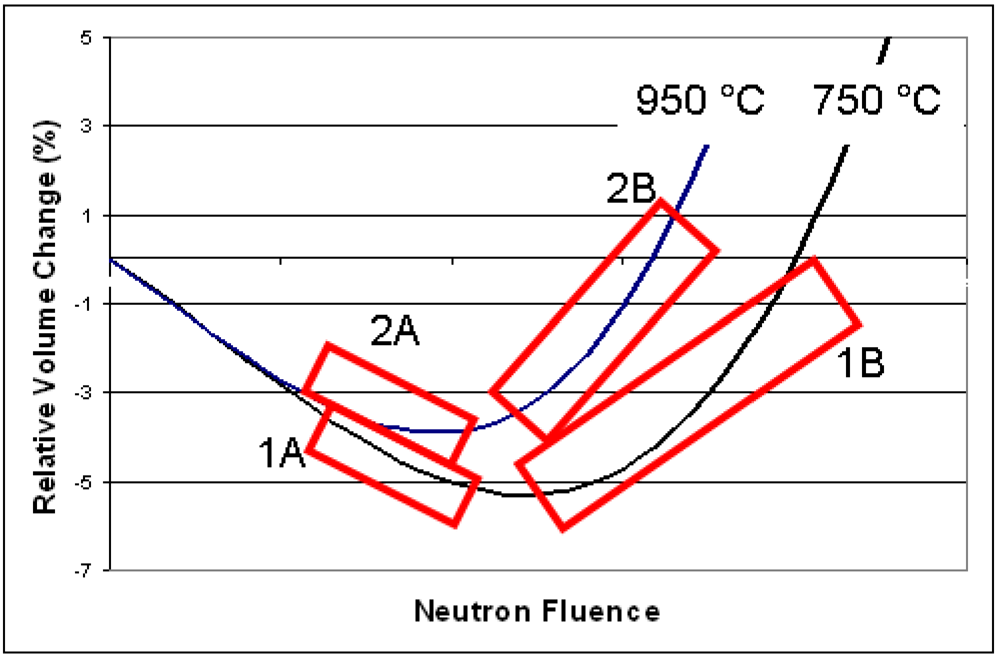

Figure 1-1 Schematic overview of the four INNOGRAPH irradiation experiments

Four graphite grades have been selected as major grades by the project partners in the 5th and 6th Framework projects; two produced by SGL Carbon and two by Graftech. In addition, minor graphite grades are included in the experiments with fewer samples. These also include graphite grades produced by Toyo Tanso.
The following properties were measured and compared before and after irradiation: specimen dimensions, mass, dynamic Young's modulus, coefficient of thermal expansion and thermal diffusivity. Density and thermal conductivity were calculated from the measurements. Full PIE programs have been performed on the INNOGRAPH-1A and -2A in the HTR-M1 and RAPHAEL projects [4, 5]. Full PIE programs on the INNOGRAPH-1B and -2B experiments have been performed in the ARCHER project [6]. Microstructural analysis was performed on a selection of INNOGRAPH-1A and INNOGRAPH-1B samples [7].

This report presents the results of the mechanical strength measurements on irradiated graphite specimens from the INNOGRAPH-1A and INNOGRAPH-1B experiments. With this report, ARCHER deliverable D41.14 is fulfilled.

2 Experiments and measurement techniques

2.1 Irradiation experiments

2.1.1 Graphite grades

The selection of graphite grades for the INNOGRAPH irradiations is based on several HTR design requirements such as thermal and mechanical properties, impurity levels, and availability [2]. The major grades, produced by Graftech and SGL Carbon, are chosen in such a way that the graphites cover a variety of microstructures. This is achieved by selecting grades based on different raw materials, i.e. coal tar pitch coke or petroleum coke, and different manufacturing methods, i.e. extrusion, isostatic moulding, or vibro –moulding.
The minor grades include graphites from three different manufacturers, SGL Carbon, Graftech, and Toyo Tanso. The minor grades include graphites based on needle coke.
The graphite grades used in the INNOGRAPH-1A and -1B experiments are listed in Table 1. Some grades were absent in the INNOGRAPH-1A experiment. For others, due to new insights and availability of new grades, the “major/minor” status for the INNOGRAPH-1B experiment was changed with respect to the INNOGRAPH-1A experiment.

Table 1 Selected grades for the INNOGRAPH-1A and -1B irradiation experiments

Grade	Manufacturer	Coke	Process	Status 1A	Status 1B
IG-110	Toyo Tanso	Petroleum	Iso-moulding	Major	Minor
IG-430	Toyo Tanso	Pitch	Iso-moulding	Minor	Minor
LPEB/BAN	GrafTech	Needle	Extrusion	n/a	Minor
LPIB	GrafTech	Needle	Iso-moulding	n/a	Minor
NBG-10	SGL	Pitch	Extrusion	Major	Major
NBG-17	SGL	Pitch	Vibro-moulding	n/a	Minor
NBG-18	SGL	Pitch	Vibro-moulding	n/a	Major
NBG-20	SGL	Petroleum	Extrusion	Minor	Minor
NBG-25	SGL	Petroleum	Iso-moulding	Major	Minor
PCEA	GrafTech	Petroleum	Extrusion	Major	Major
PCIB	GrafTech	Petroleum	Iso-moulding	Major	Minor
PPEA	GrafTech	Pitch	Extrusion	Minor	Major

2.1.2 Specimen types

All specimens are cylindrical. The diameter of all specimens is 8 mm and the length is either 6 mm or 12 mm; the majority of samples is 6 mm in length. Specimens of these sizes are small enough to allow a sufficient number of specimens in the irradiation rig, and large enough to perform reasonably accurate measurements. Specimens with a length of 6 mm are suitable for all type of standard PIE measurements (dimensional change, dynamic Young's modulus, coefficient of thermal expansion and thermal diffusivity). The 12 mm samples are included to obtain data points with higher measurement accuracy for dimensional change measurements.

Machining of the samples from the graphite blocks is described in a separate report [8]. The cylindrically shaped specimens are flattened by milling a plane with a width of 3 mm along the length. Figure 2-1 schematically shows the flattening. Producing a plane with a width of 3 mm reduces the volume of the cylinders by 1% only. The benefits of this plane are threefold. The first benefit is the possibility to indicate the z-direction from the original graphite blocks in the specimen. The plane is milled perpendicular to the *z*-direction if the axial direction of the cylinder is parallel to the *xy*-direction, and therefore the *z*-direction in the specimen is known after fabrication. The plane is milled on an arbitrary position if the axial direction of the cylinders is parallel to the *z*-direction, because in that case the *z*-direction is already indicated by the axial direction. The grain orientations quoted for samples in this report (e.g. in Table 2, Appendix A) are parallel to cylinder axis. The *z*-direction is the uniquely defined direction with respect to the production method (extrusion or moulding). Depending on the production method either the "with grain" (WG) or "against grain" (AG) direction is the unique direction; for extrusion and vibro-moulding it is the WG direction, for iso-moulding it is the AG direction.

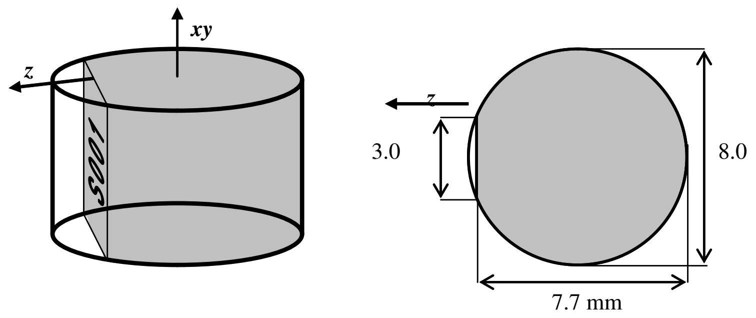

Figure 2-1 Flattening of the specimens. The figure on the left-hand side exaggeratedly shows the flatting of the cylinder. The figure on the right-hand side is a top-view of the specimen

The second benefit of the plane is that it gives an area to engrave the specimen with a unique code. This code is necessary to easily identify a specimen. The code consists of four characters. The first character is a letter that indicates the graphite manufacturer (S= SGL, U= UCAR (Graftech) and T= Toyo Tanso). The last three characters are numbers. A third benefit is that the milled plane can act as a marking that defines the measuring positions during the dimensional measurements before and after irradiation.

2.1.3 INNOGRAPH irradiation experiments at 750°C

The irradiation experiments were performed in the High Flux Reactor (HFR) Petten. The HFR is a tank-in-pool multi-purpose test reactor with a thermal power of 45 MW. Its core arrangement of 9 x 9 positions contains 33 fuel elements, six control rods and 22 beryllium reflector elements, and provides effective 20 in-core positions.

An INNOGRAPH capsule consists of a stack of eight metal drums (Figure 2-2). Each drum has either three or four channels, depending on the experiment, for sample stacks. The capsules are instrumented with 24 thermocouples, placed at different axial and radial positions, to monitor the irradiation temperature. The temperature can be controlled by changing the He/Ne gas mixture in the second containment and by vertical displacement of the capsule in the core.

For purposes of neutron metrology nine activation monitor sets were prepared. Five monitor sets were placed in the central channel of the specimen holder at various vertical levels. The remaining monitor sets were placed in the northern (2), eastern (1) and southern (1) channels, useful for an indication of the radial gradients and the orientation of the experiment. The neutron fluence is measured at the end of the experiment, after the monitoring sets have been removed.

It is important to keep the level of radioactivity of the graphite samples as low as reasonably possible, to make handling of the samples more practical after the irradiation experiment (for post irradiation examinations and reloading in next irradiation experiment) of the samples. Aside from extra purification steps that were made by the manufacturers, some measures are taken in the design. Contact between the metal drum and graphite samples is avoided by placing a graphite foil between them. Contamination of the graphite samples by the drum material is therefore not possible. For the same reason the inner containment is purged with high purity Helium. The design of the INNOGRAPH capsules is kept as simple as possible to allow loading and assembling in a lead shielded hot cell.

INNOGRAPH-1A consists of eight molybdenum drums (Ti-Zr-Mb:TZM alloy) all having a height of 60 mm. There are four stacks of samples in each drum. The irradiation temperature in the lower six drums was 750ºC, the irradiation temperature in the upper two drums was 650ºC.

The second irradiation capsule at 750ºC (INNOGRAPH-1B) contained samples that are irradiated to fluences above cross-over, i.e. the diameter of the samples might be larger than the original 8 mm. To make space for this potential swelling, the diameter of the sample stacks in the drums is larger in this capsule. Therefore, there is only space for three columns of samples in INNOGRAPH-1B. This capsule consists of seven drums (six drums of 60 mm and one drum with a height of 30 mm) that were irradiated at 750ºC. An extra drum at the top, having a height of 60 mm was irradiated at a temperature of 650ºC. The high vertical position of this upper drum makes it not feasible to reach 750ºC, because of the low gamma heating at this position. The extra drum is separated from the other drums by a thermal barrier.

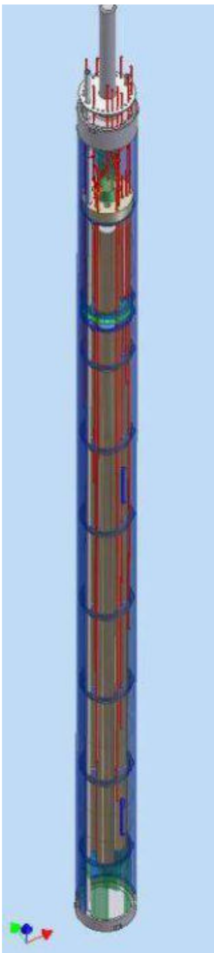

Figure 2-2 Schematic drawing of the INNOGRAPH-1B experiment, showing the eight drums that contain the graphite samples

2.2 Mechanical strength measurements

2.2.1 Test matrix

The mechanical strength measurements consist of diametric compression tests on the specimens used for diametric compression. 47 irradiated samples and 30 unirradiated (reference) samples were selected for diametric compression. The irradiated samples are all samples that were irradiated at 750°C in the INNOGRAPH-1A or INNOGRAPH-1B experiment or both. From these samples, 10 samples were selected for fractography. The fractography samples comprise fine-grain graphite, PCIB, and coarse-grain graphite, NBG-10. All samples are samples with “against grain” orientation for fair comparison.

The decision to select samples only from experiments at 750°C was made for two reasons. First of all, the project allows for only a limited number of specimens to be tested on mechanical strength. Rather than having only a few specimens per dpa per grade per irradiation temperature, we decided to investigate per grade specimens over the whole dpa range but only at one irradiation temperature. Secondly and more important, the availability of specimens of the 950°C INNOGRAPH-2B experiment is limited. Due to activity levels and the amount of swelling only a limited amount of INNOGRAPH-2B samples have their physical property measurements completed [6]. Only samples that have their standard PIE completed can be selected for diametric compression, because diametric compression is a destructive test method due to the required sample preparation.

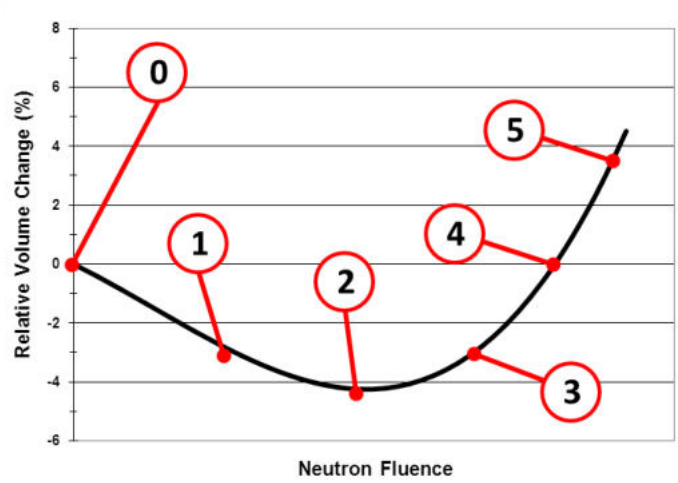

Figure 2-3 Schematic volume change versus neutron fluence curve, with indicated characteristic regions in these type of curves: 0) Virgin. 1) Shrinking. 2) Turn-around. 3) Swelling. 4) Cross-over. 5) Swollen.

Figure 2-3 shows a schematic representation of the volume change versus neutron fluence (dpa) curve typical for nuclear graphites. Indicated are the typical states graphite undergoes during irradiation. Starting from virgin state (0) after an initial shrinkage (1), at turn-around fluence (2) graphite starts to swell again (3). At a certain fluence the sample reaches its original size again (cross-over, 4), after which the sample continues to swell beyond the original sample volume (5). Samples for mechanical strength measurements are selected to have a good spread over the different states of irradiated graphite. Both “with grain” and “against grain” series are selected to investigate anisotropy in mechanical strength.

Table 2 in Appendix A shows the specimens selected for diametric compression and fractography ordered by graphite grade and increasing neutron fluence. Figure 2-4 to Figure 2-6 show the position in the volume change curve of the selected samples, specifying “with grain” and “against grain” samples.

Next to irradiated samples, also a number of reference, unirradiated, samples is selected. For some grades only one or two reference samples are tested. These have been more extensively tested on diametric compression in internal NRG project. The current tests verify that the current set-up produces comparable results to those in the other project. For the other grades, more reference samples are tested to determine the typical spread in tensile strength for the test method and graphite grade.

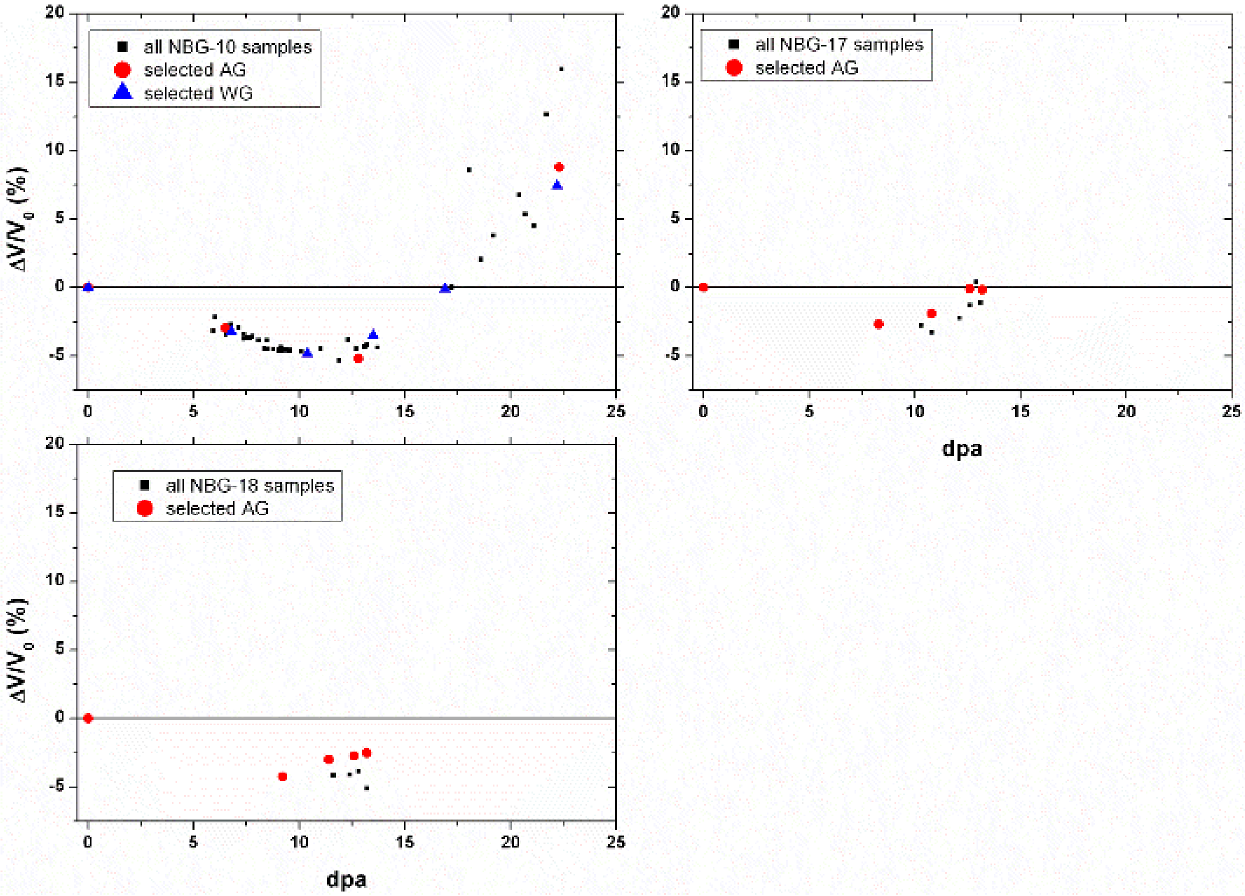

Figure 2-4 Plots of the relative volume change versus dpa for SGL graphite grades irradiated at 750°C in which the samples selected for diametric compression are indicated.

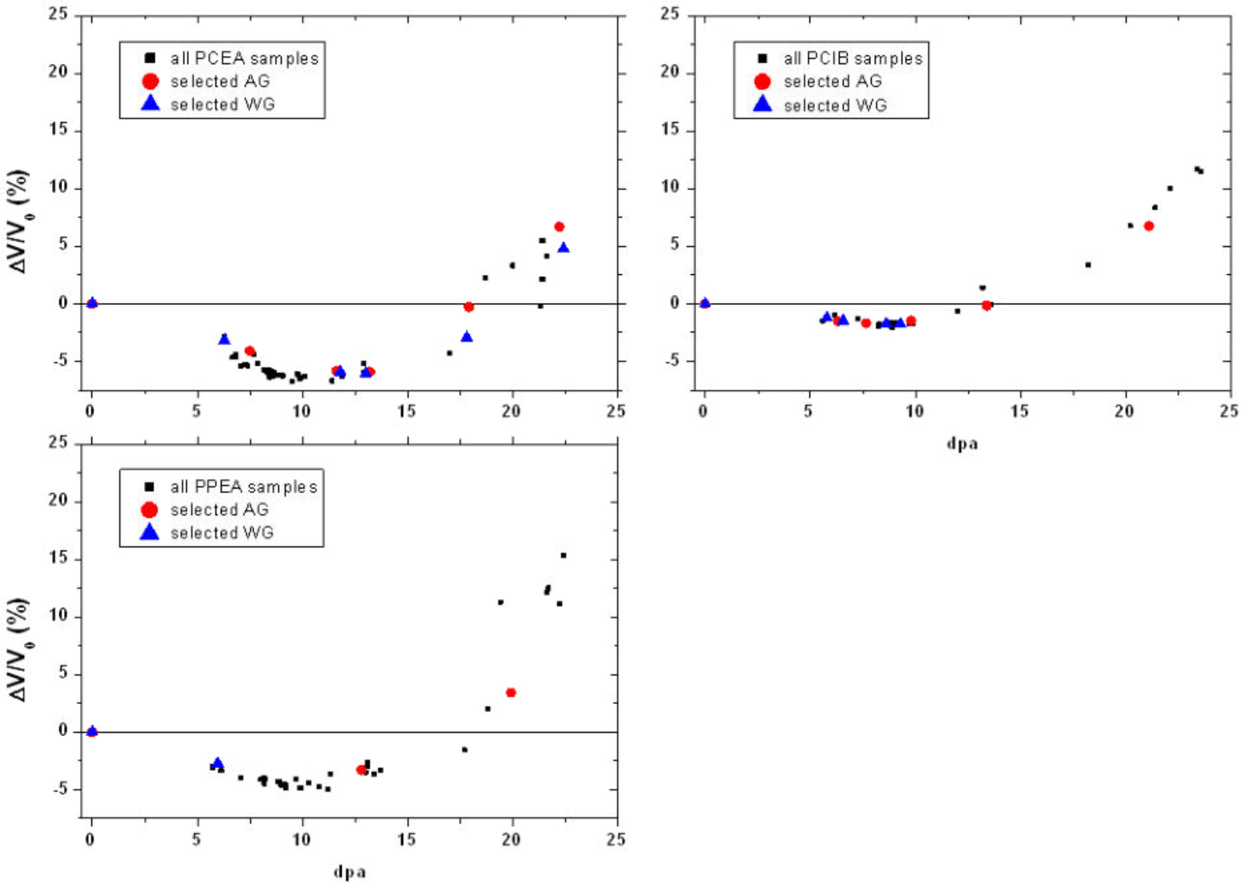

Figure 2-5 Plots of the relative volume change versus dpa for GrafTech graphite grades irradiated at 750°C in which the samples selected for diametric compression are indicated.

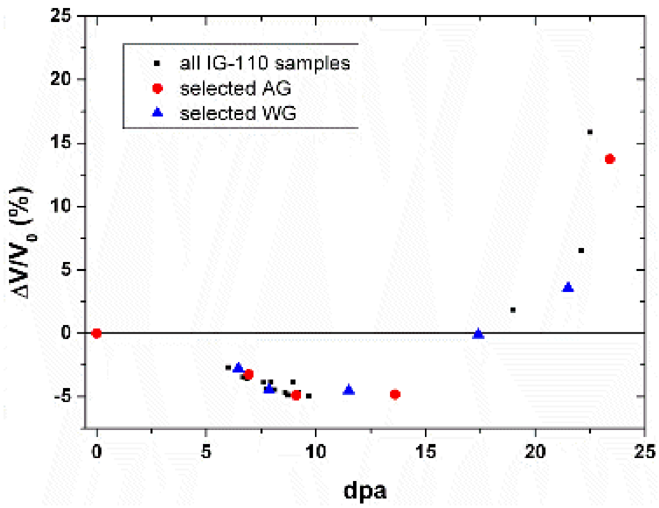

Figure 2-6 Plot of the relative volume change versus dpa for Toyo Tanso IG-110 graphite irradiated at 750°C in which the samples selected for diametric compression are indicated.

2.2.2 Diametric compression

The graphite samples irradiated in the INNOGRAPH irradiation experiments are relatively small with respect to sizes required by tensile strength tests for graphite (ASTM C749). Also, they do not have the required tensile test sample geometry. A strength test that can be performed is the diametric compression test. The diametric compression test, also known as the Brazilian disc test [9, 10], consists of applying a compressive force across the diameter of a specimen until failure. From the applied load at cracking and the contact surface area made by the anvil on the sample, one can calculate the tensile strength of the specimen. A successful diametric compression test comprises crack initiation in the centre of the disc and crack propagation along the loading diameter [11]. For failure to initiate in the centre of the disc, the compressive load must be symmetric.

For the case that the load F is applied on one point of a disc (Figure 2-7), the tensile stress at the centre of the disc is given by [12]:

$$\sigma_P = \frac{2F}{\pi D t} \quad , \tag{1}$$

in which D is the diameter of the sample, and t the thickness of the sample.

However, in general load is not applied to a single point but distributed over a small contact area between the flat anvil and the sample. The contact area is not a constant during the compression test but changes due to elastic deformation of the sample. The contact area at failure determines the load distribution that is to be used for calculating the tensile strength. Following an analysis by Awaji [13], the maximum tensile strength at the centre of the disc can be approximated by:

$$\sigma_H = \sigma_P \left(1 - \left(\frac{b}{R}\right)^2\right) \quad , \tag{2}$$

with R the radius of the disc, and b half the width of the contact area between the anvil and the specimen at failure (see Figure 2-7).

To improve the reliability of the Brazilian disc method, the use of specimens with parallel flat sides on the load bearing areas was introduced by Wang and Xin [14] (see Figure 2-7). The advantages over the use of circular discs are:

i.) the applied loading is evenly distributed over the flat surface,
ii.) the contact surface areas do not vary as loading increases, and
iii.) for flat angles 2a>20°, the crack forms in the centre of the disc.

Following an analysis by Kaklis et al. [15], the maximum tensile stress in the centre of the disc is given by:

$$\sigma_\alpha = \sigma_P(\sin 2\alpha - \alpha) \quad , \tag{3}$$

in which α is half the angle of the flat side in radians.

The INNOGRAPH specimens are a mixture of the traditional disc shape and the disc with flattened sides; they possess one flat side. To minimise contact stresses, a curved anvil is used for the round side instead of a flat anvil (see Figure 2-7). Finite element modelling shows that the stresses become more evenly distributed and maximum stress to occur in the centre of the disc [16]. Equation 2, expressing σ_H, can also be used for obtaining the tensile strength from the Brazilian disc test on specimens with one flat side [16]. Therefore, in this report, σ_H is used in the Results section and graphs. For completeness, σ_H, σ_P, and σ_α are presented together for comparison in tabular form in Appendix B.

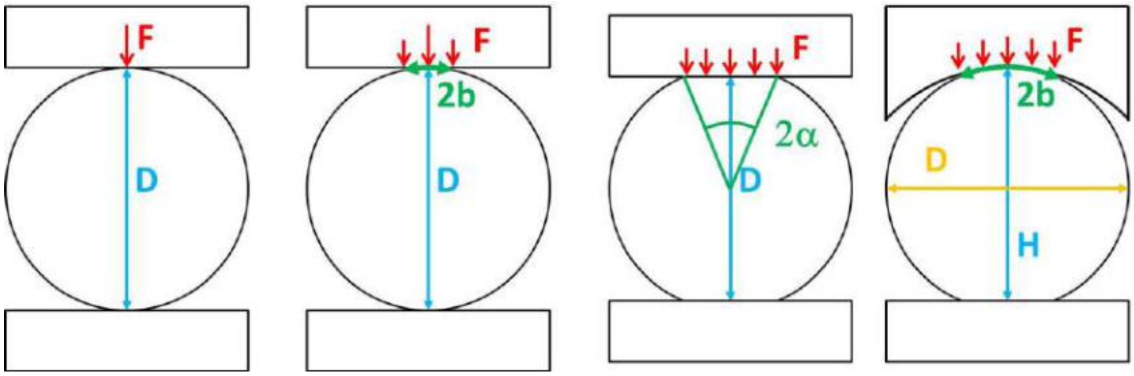

Figure 2-7 Schematic representation of the diametric compression load distribution for, from left to right, a point contact, distributed contact, a sample with flattened sides, and a sample with one flat side and using a curved anvil.

The INNOGRAPH specimens are indicated to be “with grain” (WG) or “against grain” (AG) oriented samples (see section 2.1.2). This direction indicates how the samples are cut out of the block of graphite and corresponds to the direction parallel to the cylinder axis of the samples (see Figure 2-1). In a diametric compression test, the applied force is always perpendicular to the cutting direction (see Figure 2-8). If the cutting direction is perpendicular to the unique direction, the tensile strength following from diametric compression is tested in the *xy*-plane and thus in the non-unique direction. If the cutting direction is parallel to the unique direction, the tensile strength is tested in the plane defined by the unique direction and a non-unique direction.

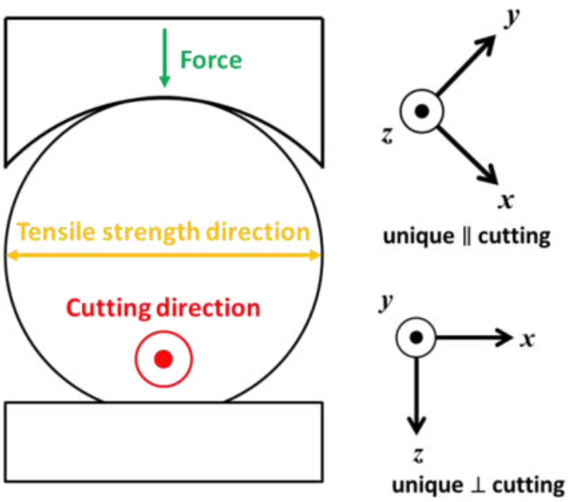

Figure 2-8 Schematic representation of the cutting and tensile strength directions in diametric compression tests. The axes on the right show how the unique axis and non-unique plane are defined for two situations: unique direction parallel to the cutting direction, and unique direction orthogonal to the cutting directions.

For the Brazilian disc test, an Instron 5566A tensile stage was used with a 10 kN load cell. A curved anvil with a radius of 5.014 mm was used for distribution of the load over a larger-than-point contact area. The tensile stage is placed inside a glovebox to be able to handle contaminated, radioactive samples. The sample is placed with its flat side onto the bottom anvil. Samples are tested with a displacement speed of 0.1 mm/min. Loading was stopped when the force dropped by 10% with respect to the start of the drop. A webcam is used to record the experiments and take photographs of the sample before and after testing.

The contact area of the top anvil is determined using a small piece of rolling paper in between sample and anvil (see Figure 2-9). The graphite leaves a marking onto the paper of which a webcam image is taken inside the glove box. From the image that includes a ruler to determine the scale the contact area is determined.

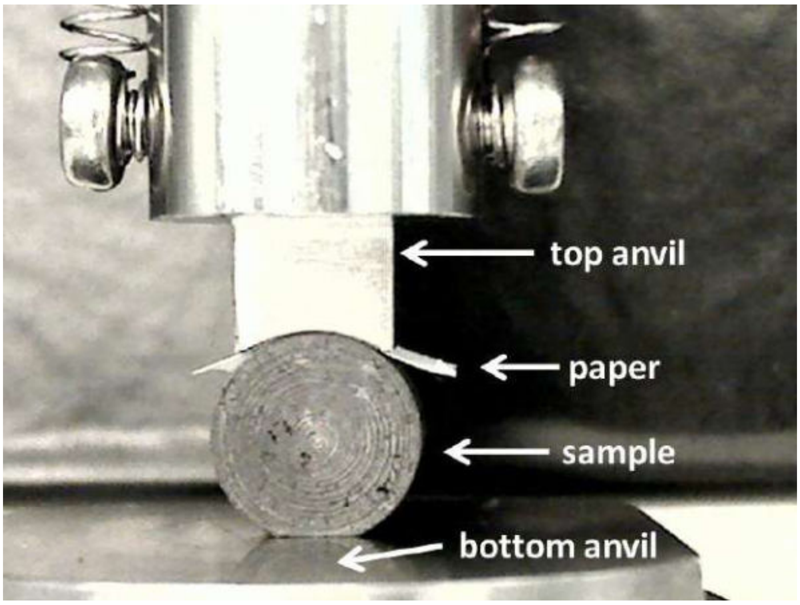

Figure 2-9 Graphite sample mounted in the tensile stage for diametric compression testing.

To calculate the tensile strength by any of equation 1 to 3, the length and diameter of the sample are required. These were measured in the standard post irradiation examinations of INNOGRAPH-1A and -1B. The dimensions were determined using inductive probes (Mahr, Type P 2104 MB) with a measurement range of 4 mm and accuracy of 0.1 um. The measurement is a comparison of the dimension of the sample and the dimension of a well-known calibre. The dimensions are measured on multiple positions on the respective sides and values averaged over these positions are used as input for the calculations.

The graphite specimens that are irradiated in the INNOGRAPH experiments have been machined to have flat sides with a nominal width of 3 mm prior to irradiation. Due to the neutron irradiation, however, dimensions change and the nominal 3 mm width typically is not a valid value for the flat side width anymore. For the irradiated samples, the width of the flat side is measured using an optical microscope in a glovebox. The microscope used is a system dedicated to measuring dimensions, including software tools to process microscope images.

2.2.3 Fractography

Fractography is performed using a scanning electron microscope (SEM). At NRG, a JEOL JSM 6490 SEM, equipped with several detectors (EDS, WDS and EBSD), is available. The SEM is placed in an alpha tight hot-cell to allow analysing radioactive samples emitting α, γ and β radiation, therefore both nuclear structural materials and nuclear fuels can be analysed.

In fractography one investigates fracture surfaces; no special sample surface preparation is performed. Samples are attached to an aluminium sample holder by carbon tape, with the fracture surface visibly facing upward. The graphite samples were found sufficiently conductive to perform SEM measurements without an extra conducting layer deposited onto the surfaces. Most of the SEM images are taken under a 30° angle to get a 3D impression of the surface morphology.

Some samples showed a fracture but did not have separated halves. For these specimens, parts were carefully separated by hand to expose the fracture surfaces.

3 Results

3.1 Diametric compression

The diametric compression tests have been conducted successfully on all unirradiated and irradiated samples. Figure 3-1 shows two typical load displacement curves of the diametric compression tests. Ideally, only a single drop in load occurs during the compression test (red dashed line). However, sometimes a small drop, less than the 10% drop set-point, occurs after which load build-up continues (black solid line). In such cases the video and images of the experiment are assessed to see which drop in load is taken as the maximum load for the specimen. Images of the samples after the compression test are included in Appendix C.

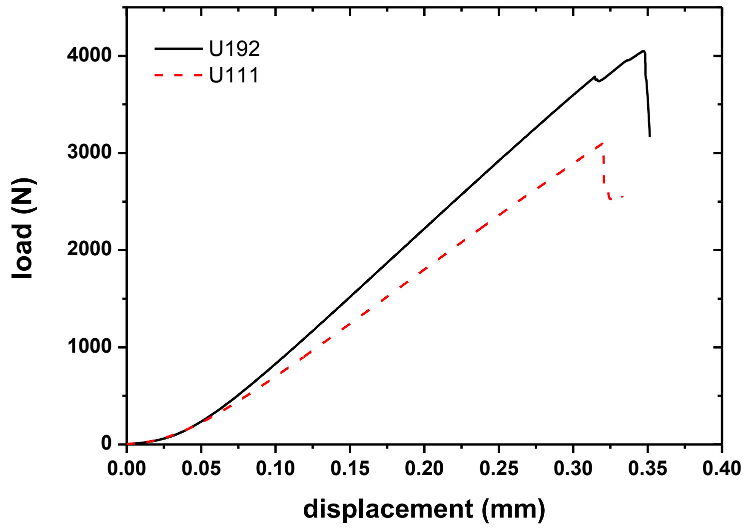

Figure 3-1 Two typical load-displacement curves for the diametric compression tests on irradiated graphite samples. The black solid line shows failure in two steps, the red dashed line failure in a single step.

The widths of the flat side of the specimens (w) are measured using an optical microscope. The contact area of the top anvil ($2b$) is determined from the imprint of the specimen on a piece of paper in between anvil and specimen. Both results are included in the results table in Appendix B.

Figure 3-2, Figure 3-3, and Figure 3-4 show the tensile strengths, σ_H, of graphite specimens irradiated at 750° versus neutron fluence (dpa) arranged by graphite manufacturer as obtained using equation 2. In general, all graphite grades show an increase in strength with increasing neutron fluence. For those grades that have high neutron dose samples available, the results show a decrease in strength at high neutron fluence. For some grades, the strength reduces to approximately its unirradiated value. For others, the strength levels out after the maximum in tensile strength is reached.

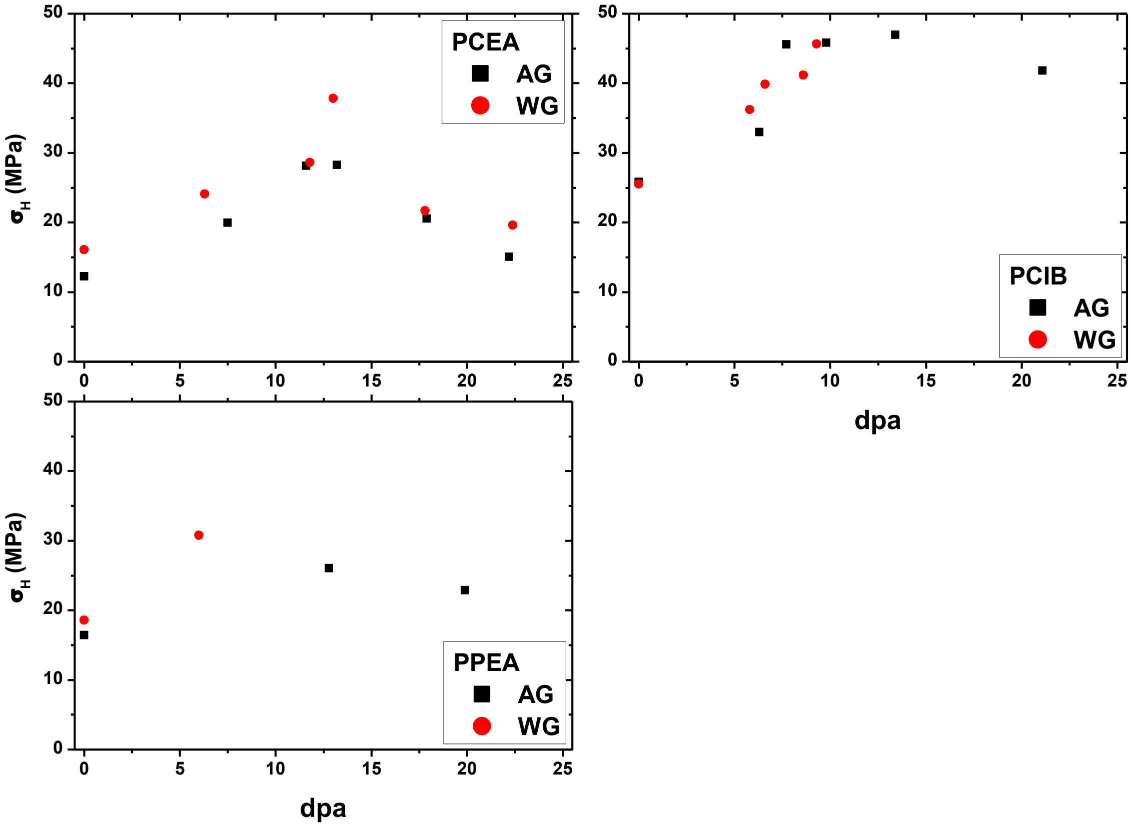

Figure 3-2 Tensile strength as determined from diametric compression for GrafTech graphite grades PCEA, PCIB, and PPEA irradiated at 750°C. Note that the AG and WG directions are sample cutting directions and not tensile strength directions.

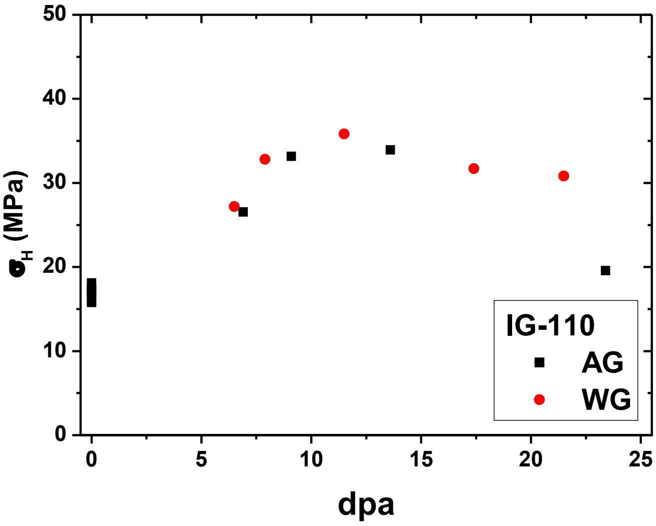

Figure 3-3 Tensile strength as determined from diametric compression for Toyo Tanso IG-110 graphite irradiated at 750°C. Note that the AG and WG directions are sample cutting directions and not tensile strength directions.

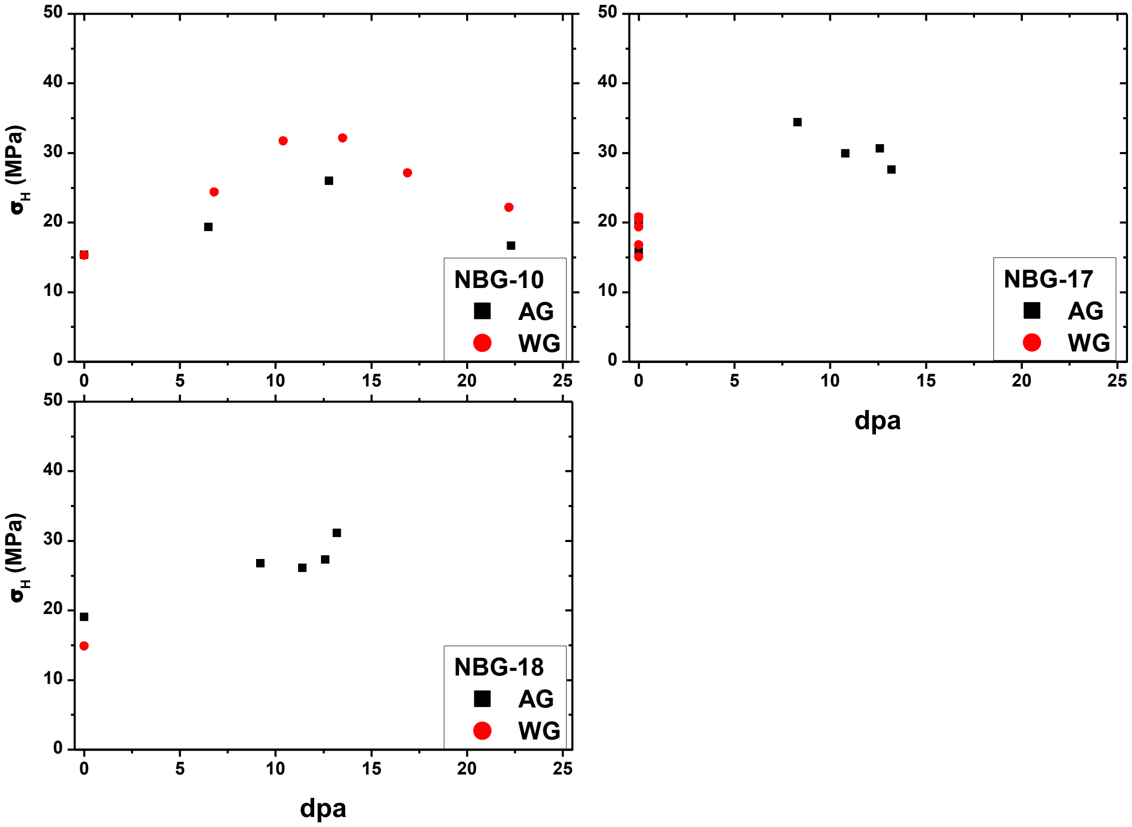

Figure 3-4 Tensile strength as determined from diametric compression for SGL graphite grades NBG-10, NBG-17, and NBG-18 irradiated at 750°C. Note that the AG and WG directions are sample cutting directions and not tensile strength directions.

3.2 Fractography

3.2.1 NBG-10

0S31, NBG-10, 0 dpa

Figure 3-5 to Figure 3-12 show the fracture surface of unirradiated NBG-10 sample 0S31.

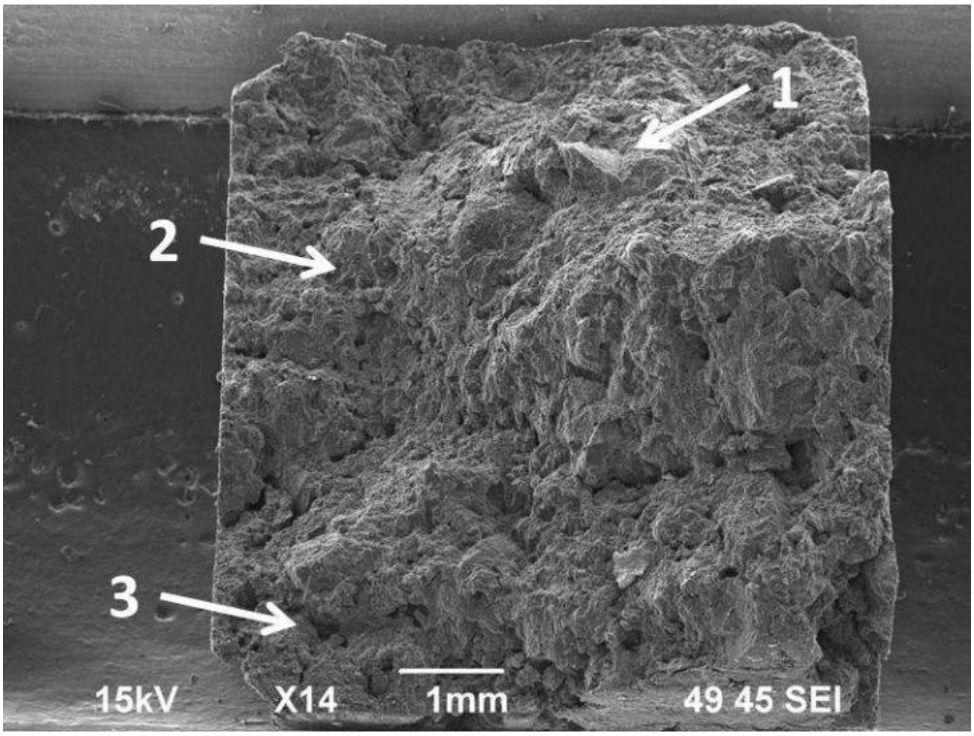

Figure 3-5 Overview SEM image under 30° angle of NBG-10 sample 0S31, 0 dpa. The numbers indicate the locations of the detail SEM images.

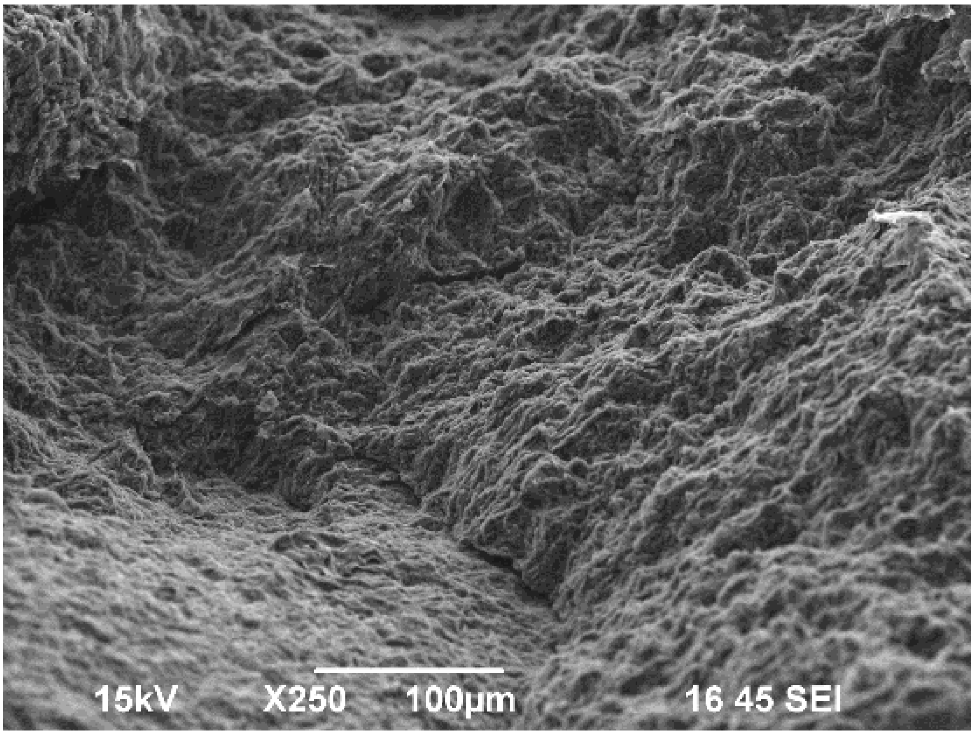

Figure 3-6 Detail SEM image under 30° angle of NBG-10 sample 0S31 at detail location 1.

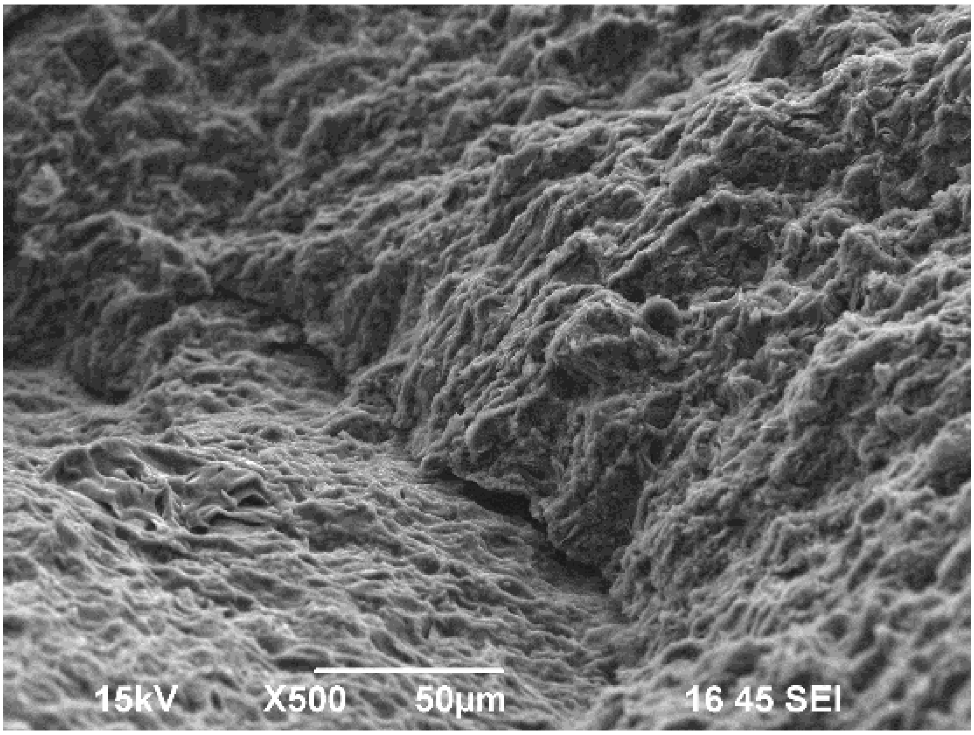

Figure 3-7 Detail SEM image under 30° angle of NBG-10 sample 0S31 at detail location 1.

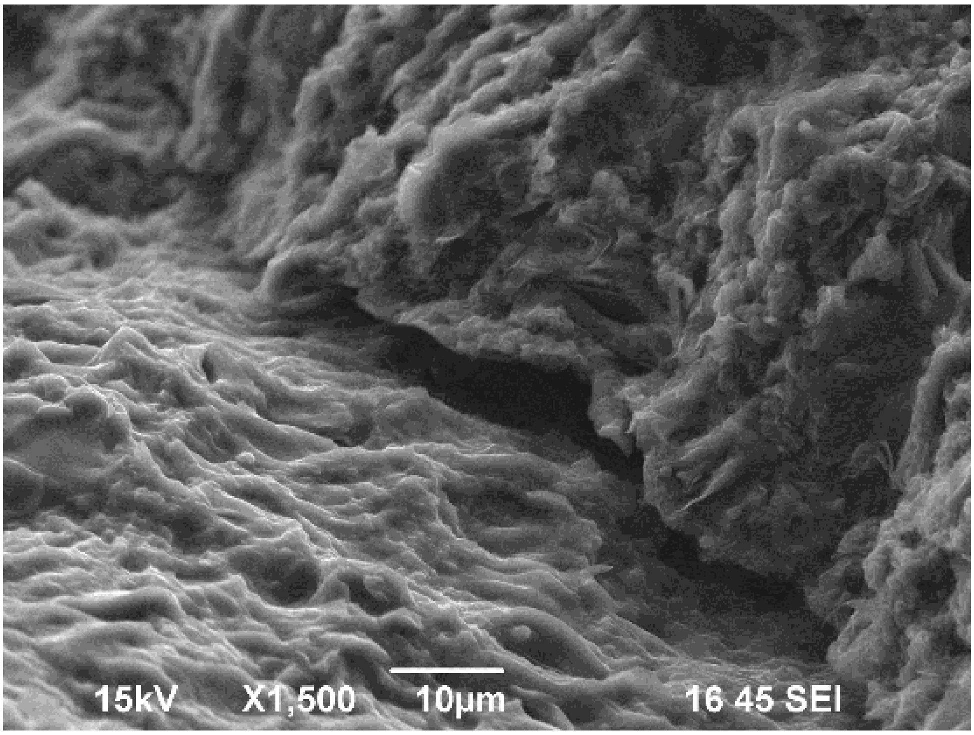

Figure 3-8 Detail SEM image under 30° angle of NBG-10 sample 0S31 at detail location 1.

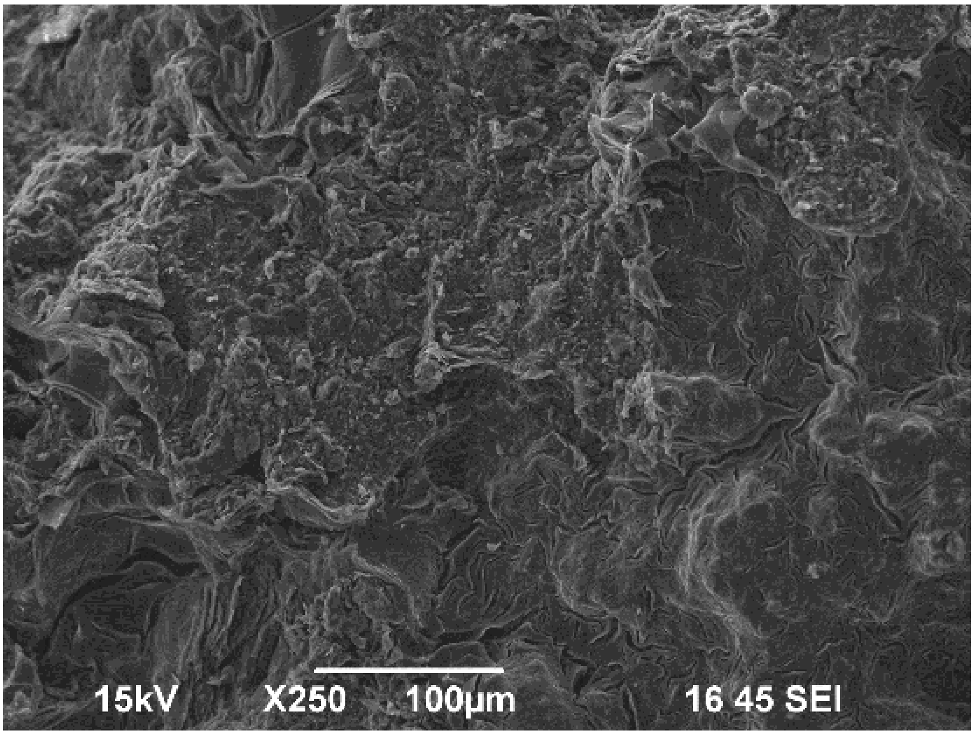

Figure 3-9 Detail SEM image under 30° angle of NBG-10 sample 0S31 at detail location 2.

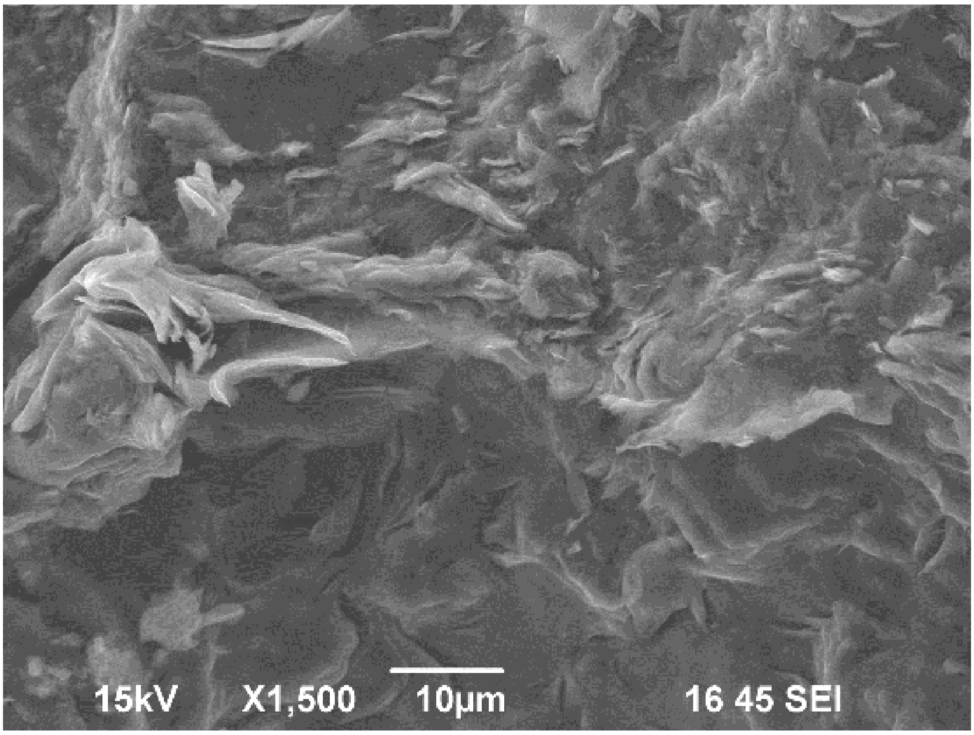

Figure 3-10 Detail SEM image under 30° angle of NBG-10 sample 0S31 at detail location 2.

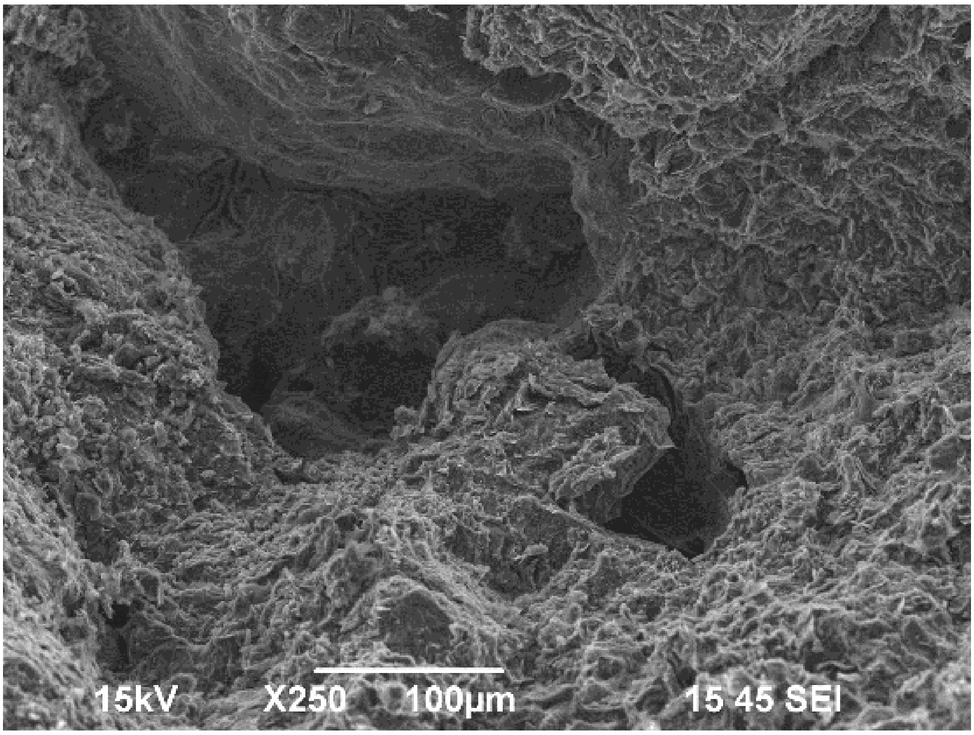

Figure 3-11 Detail SEM image under 30° angle of NBG-10 sample 0S31 at detail location 3.

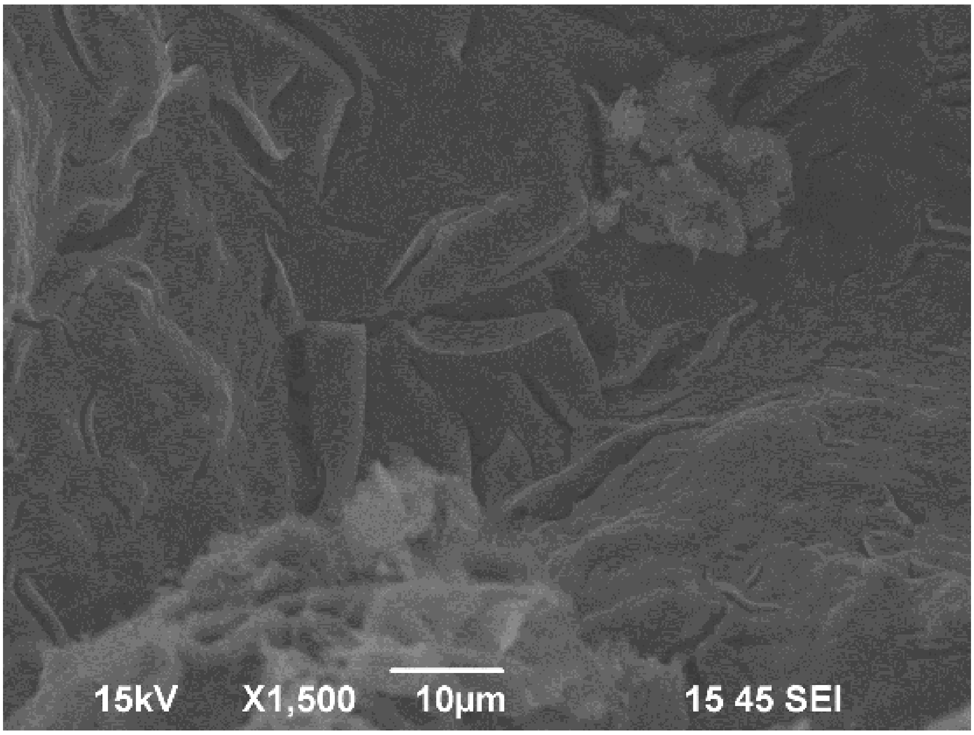

Figure 3-12 Detail SEM image under 30° angle of NBG-10 sample 0S31 at detail location 3.

S050, NBG-10, 6.5 dpa

Figure 3-13 to Figure 3-21 show the fracture surfaces of both halves of NBG-10 sample S050, irradiated at 750°C to 6.5 dpa.

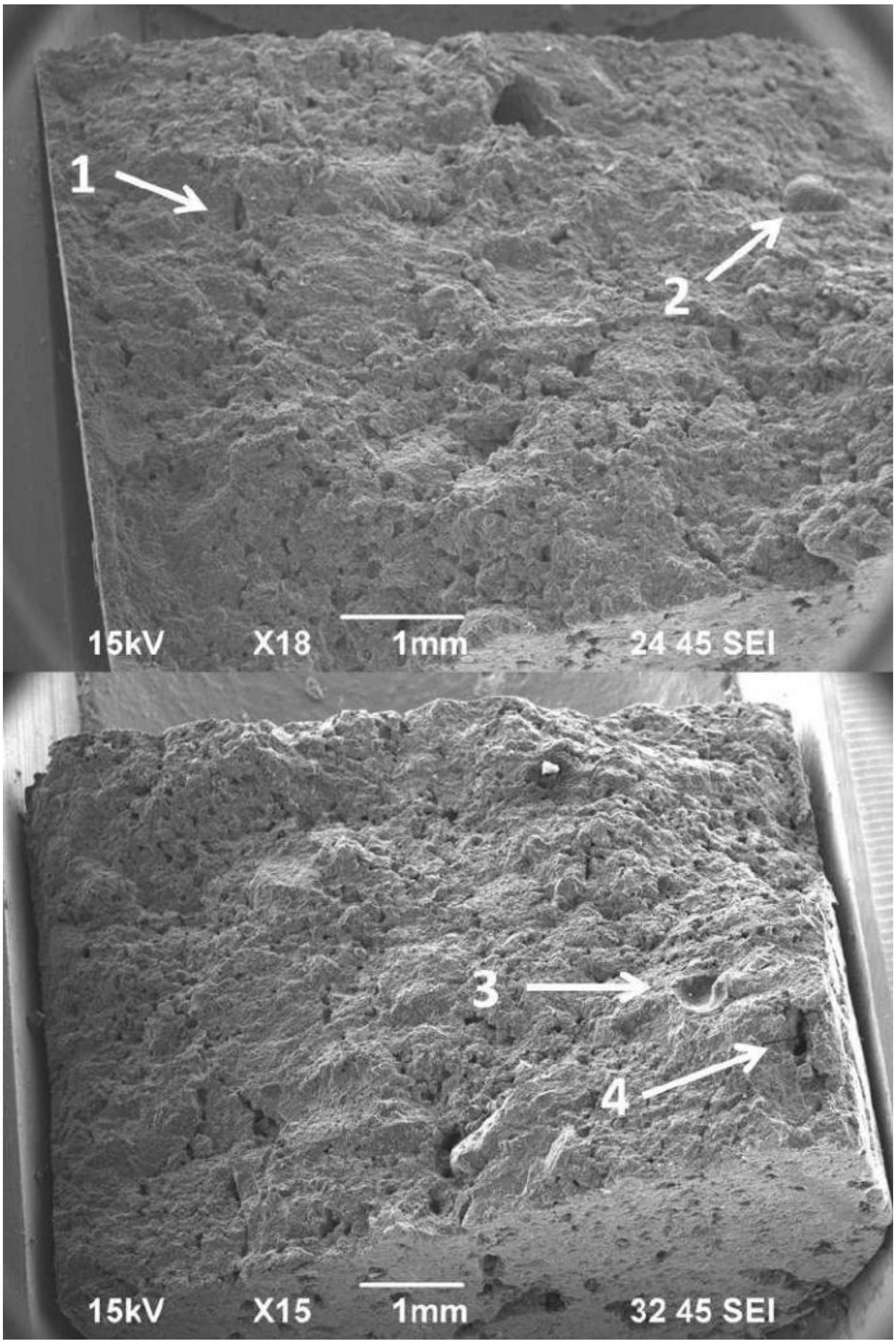

Figure 3-13 Overview SEM images under 30° angle of both halves of NBG-10 sample S050, 6.5 dpa. The numbers indicate the locations of the detail SEM images.

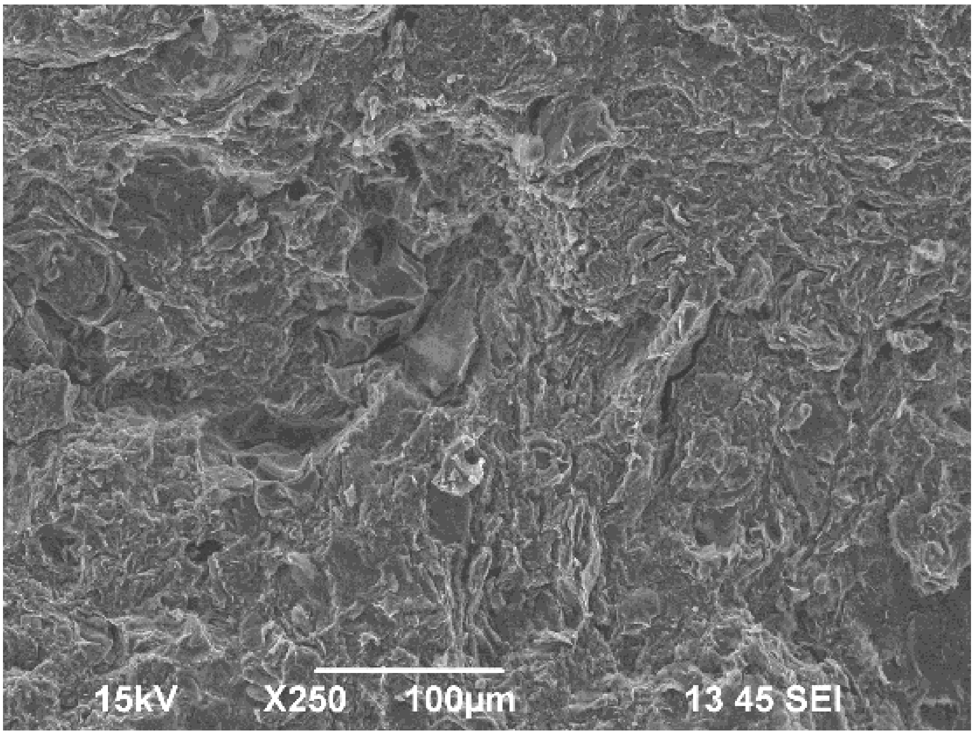

Figure 3-14 Detail SEM image under 0° angle of NBG-10 sample S050 at detail location 1.

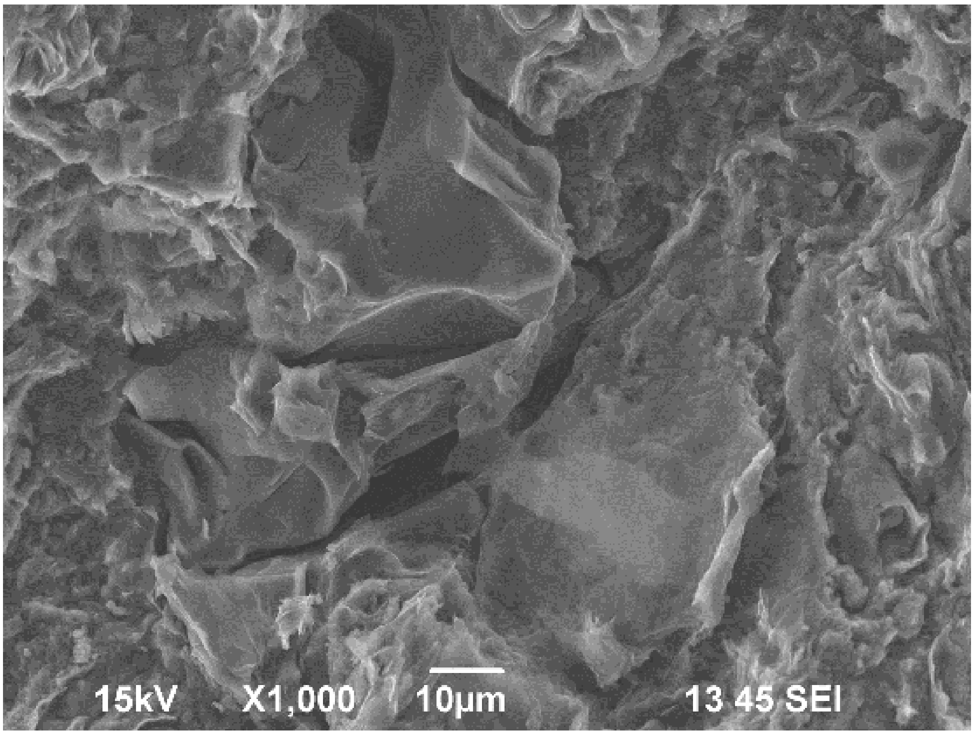

Figure 3-15 Detail SEM image under 0° angle of NBG-10 sample S050 at detail location 1.

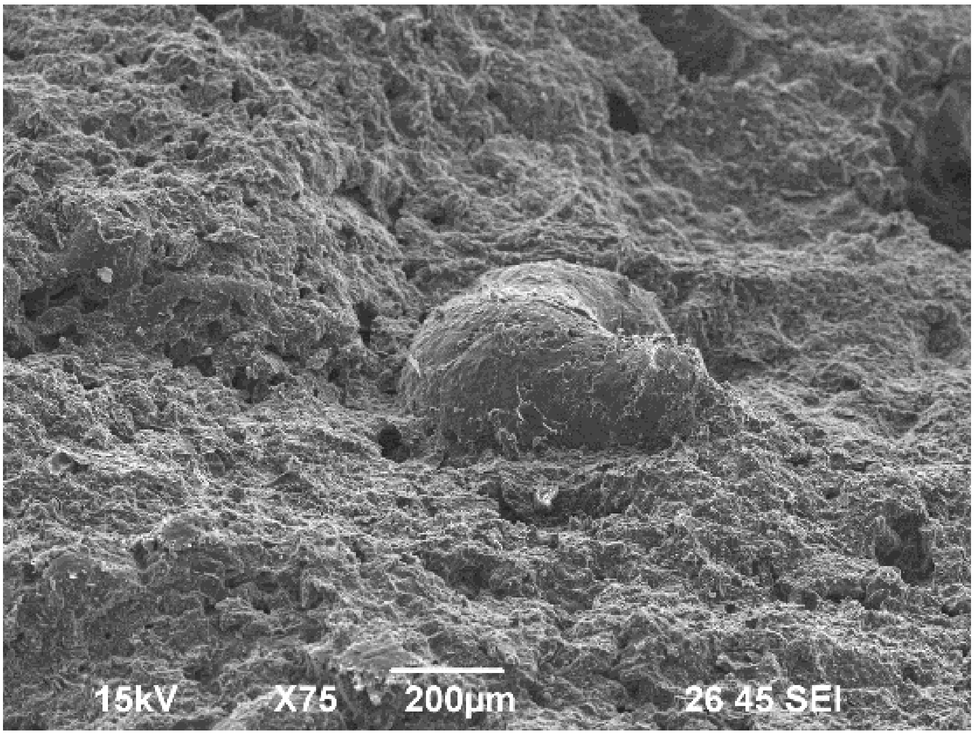

Figure 3-16 Detail SEM image under 30° angle of NBG-10 sample S050 at detail location 2.

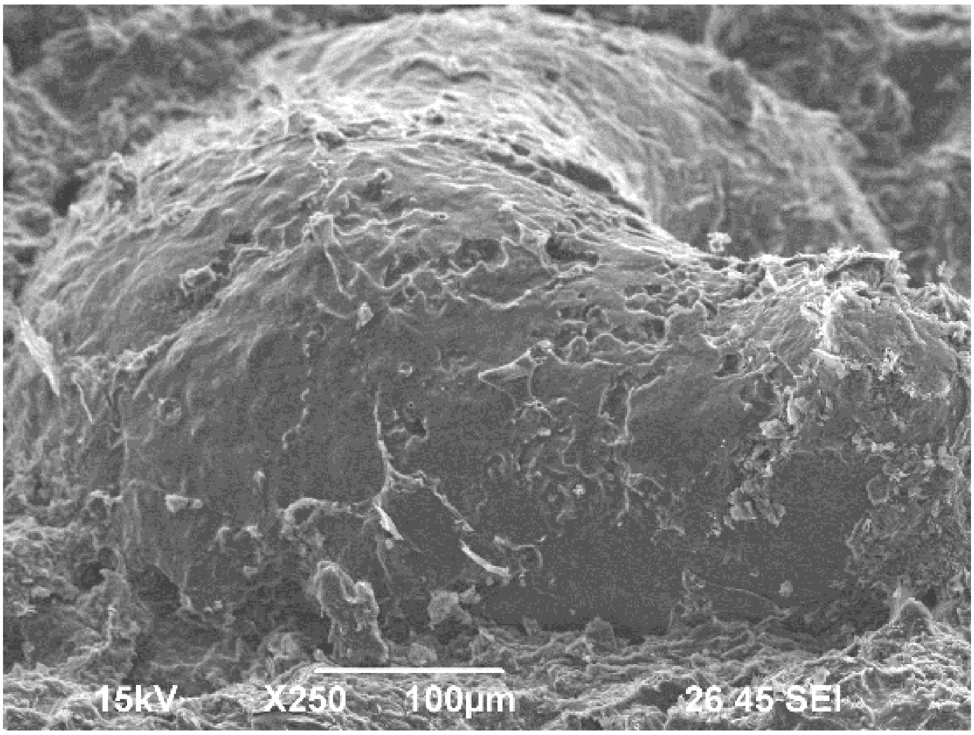

Figure 3-17 Detail SEM image under 30° angle of NBG-10 sample S050 at detail location 2.

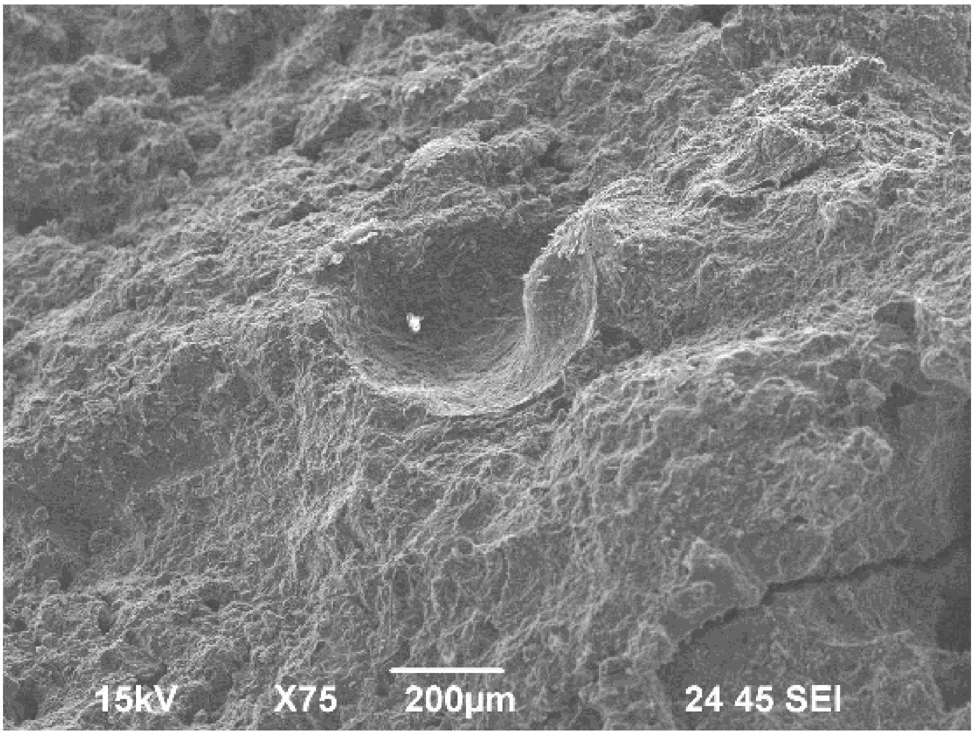

Figure 3-18 Detail SEM image under 30° angle of NBG-10 sample S050 at detail location 3. This feature is the inverse of the feature shown in Figure 3-17.

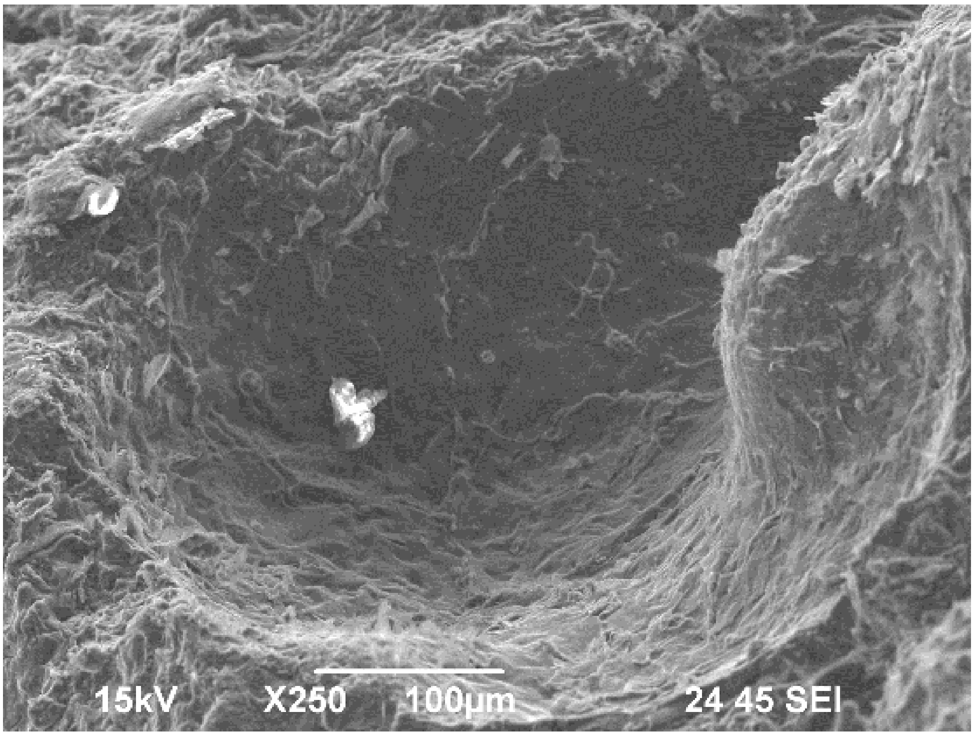

Figure 3-19 Detail SEM image under 30° angle of NBG-10 sample S050 at detail location 3. This feature is the inverse of the feature shown in Figure 3-18.

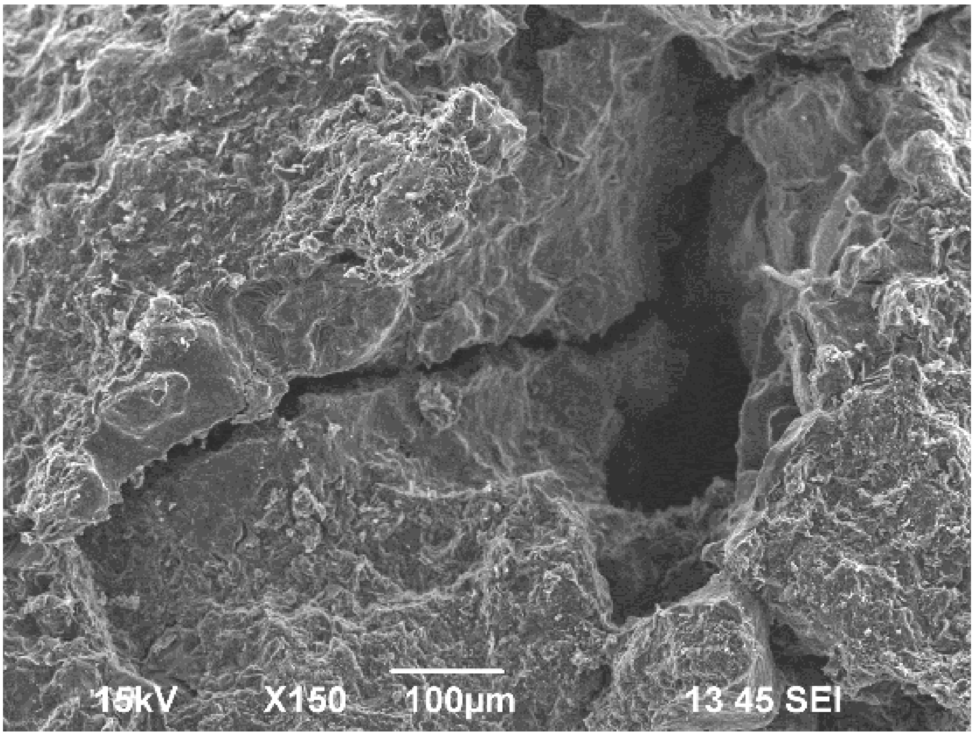

Figure 3-20 Detail SEM image under 30° angle of NBG-10 sample S050 at detail location 4.

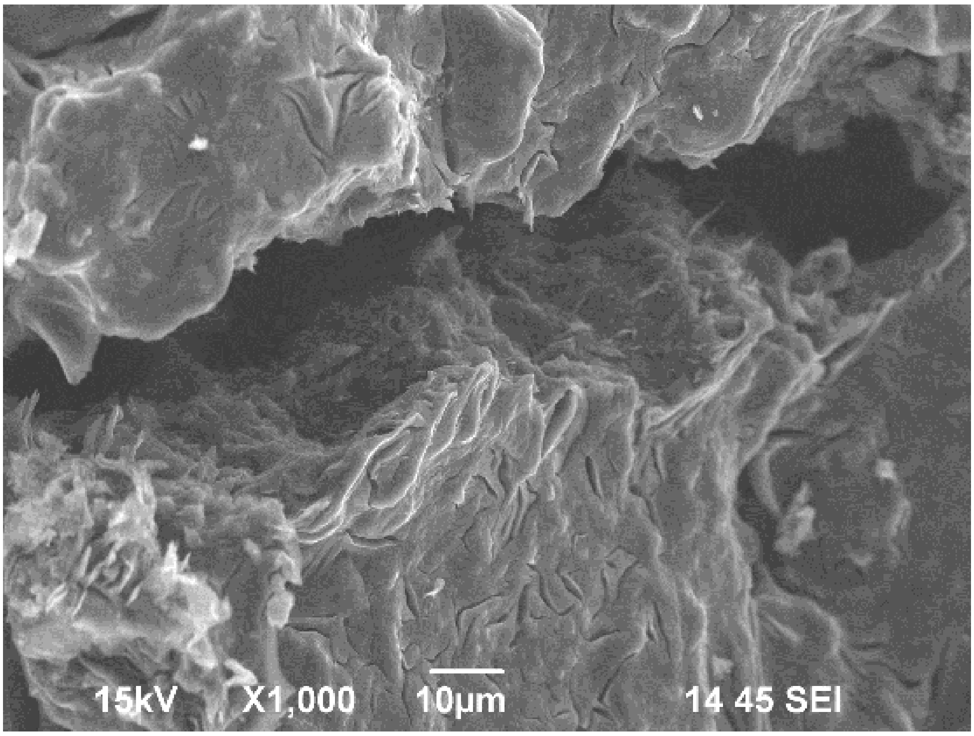

Figure 3-21 Detail SEM image under 30° angle of NBG-10 sample S050 at detail location 4.

S051, NBG-10, 12.8 dpa

Figure 3-22 to Figure 3-30 show the fracture surface of NBG-10 sample S051, irradiated at 750°C to 12.8 dpa.

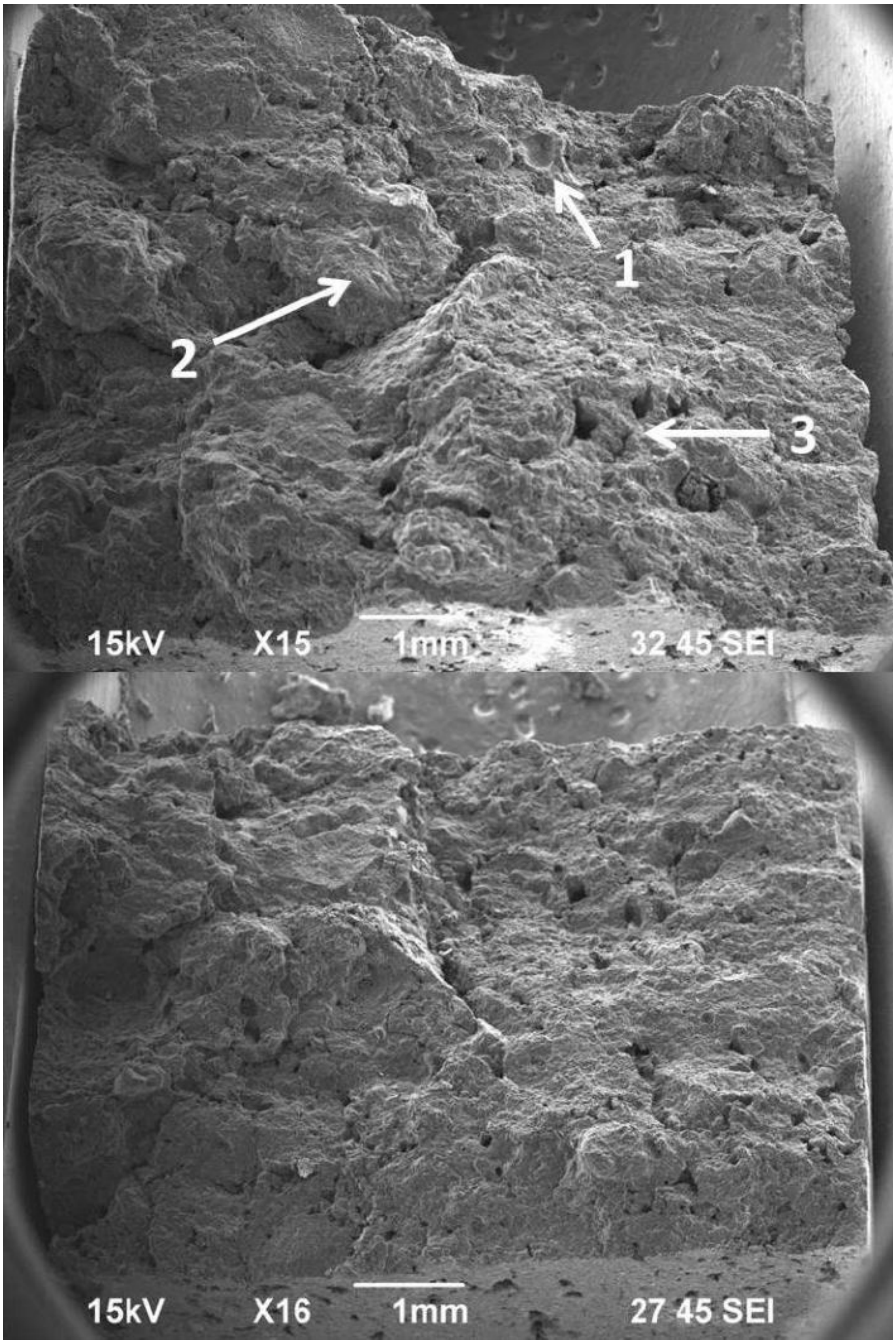

Figure 3-22 Overview SEM images under 30° angle of both halves of NBG-10 sample S051, 12.8 dpa. The numbers indicate the locations of the detail SEM images.

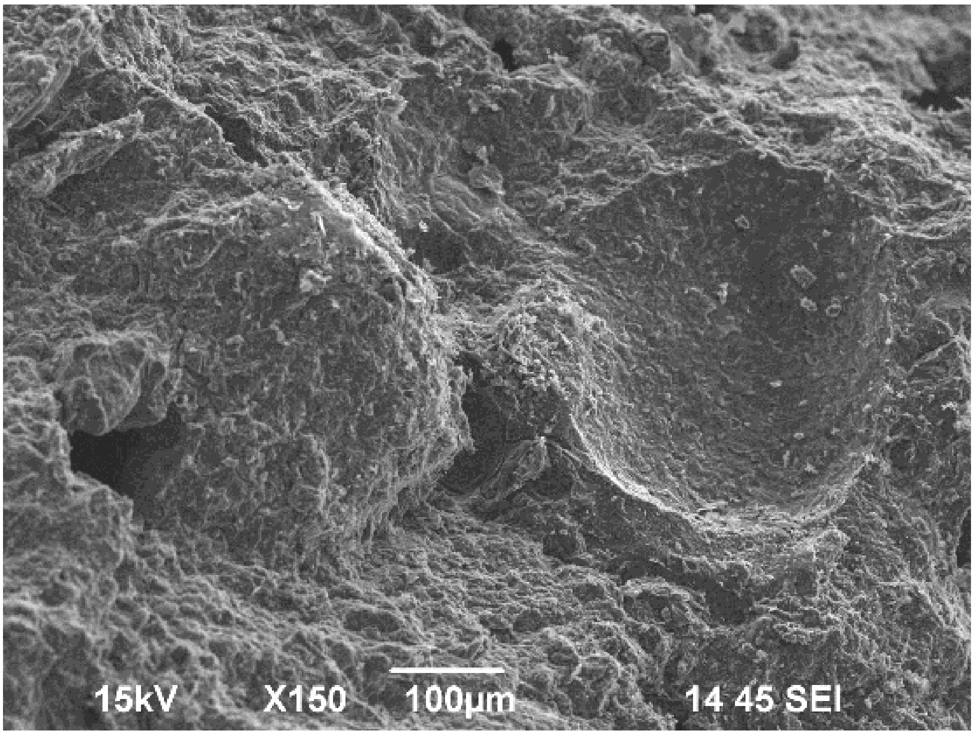

Figure 3-23 Detail SEM image under 30° angle of NBG-10 sample S051 at detail location 1.

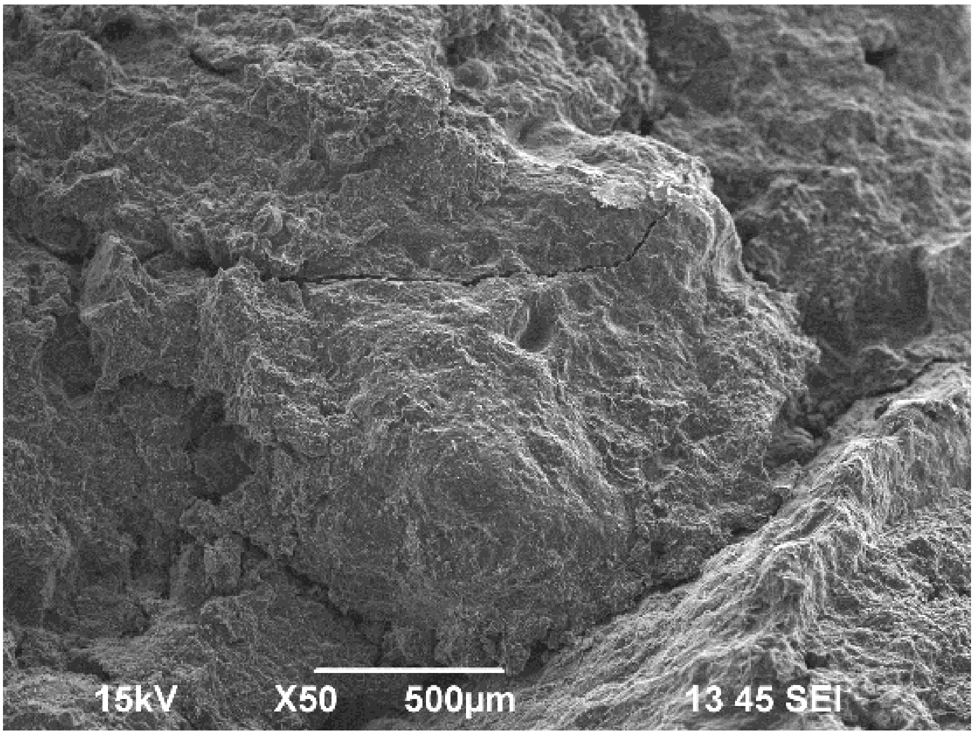

Figure 3-24 Detail SEM image under 30° angle of NBG-10 sample S051 at detail location 2.

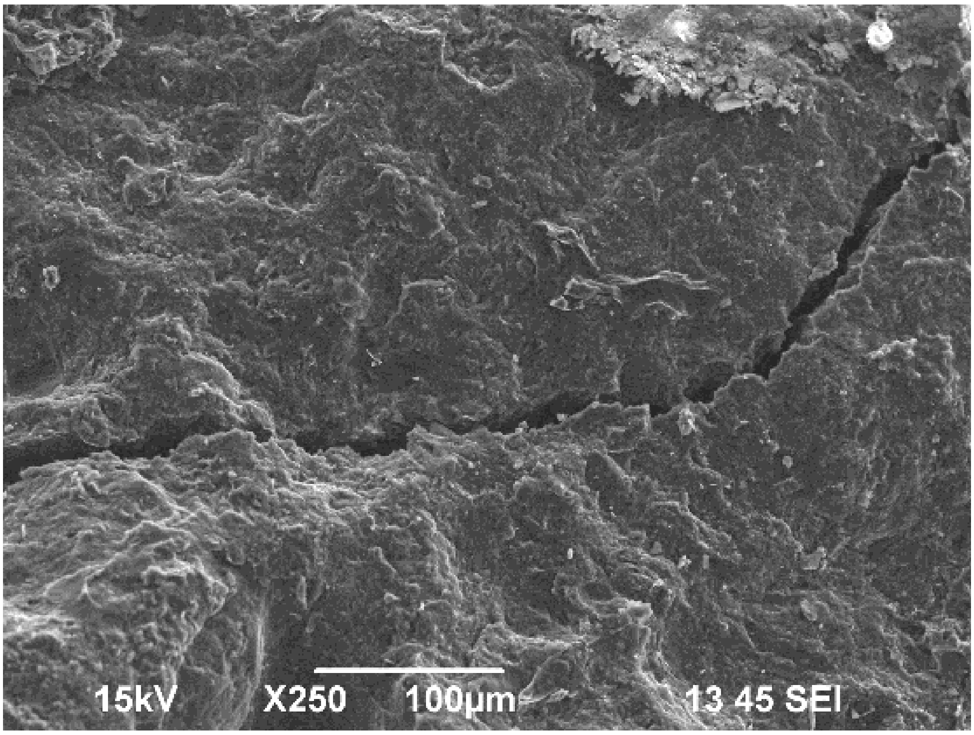

Figure 3-25 Detail SEM image under 30° angle of NBG-10 sample S051 at detail location 2.

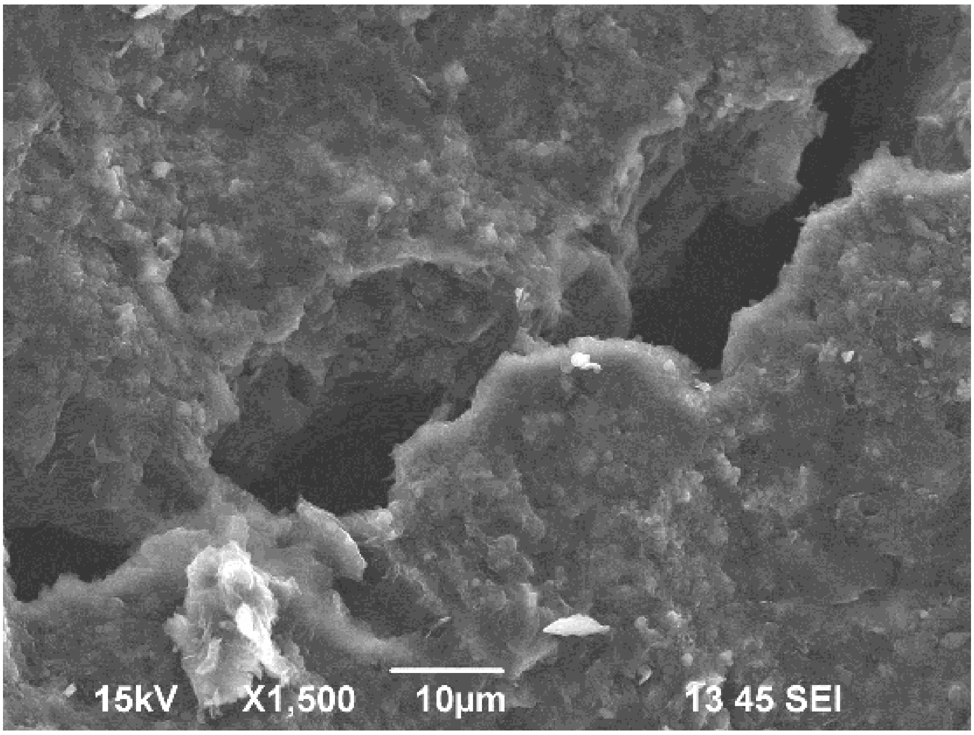

Figure 3-26 Detail SEM image under 30° angle of NBG-10 sample S051 at detail location 2.

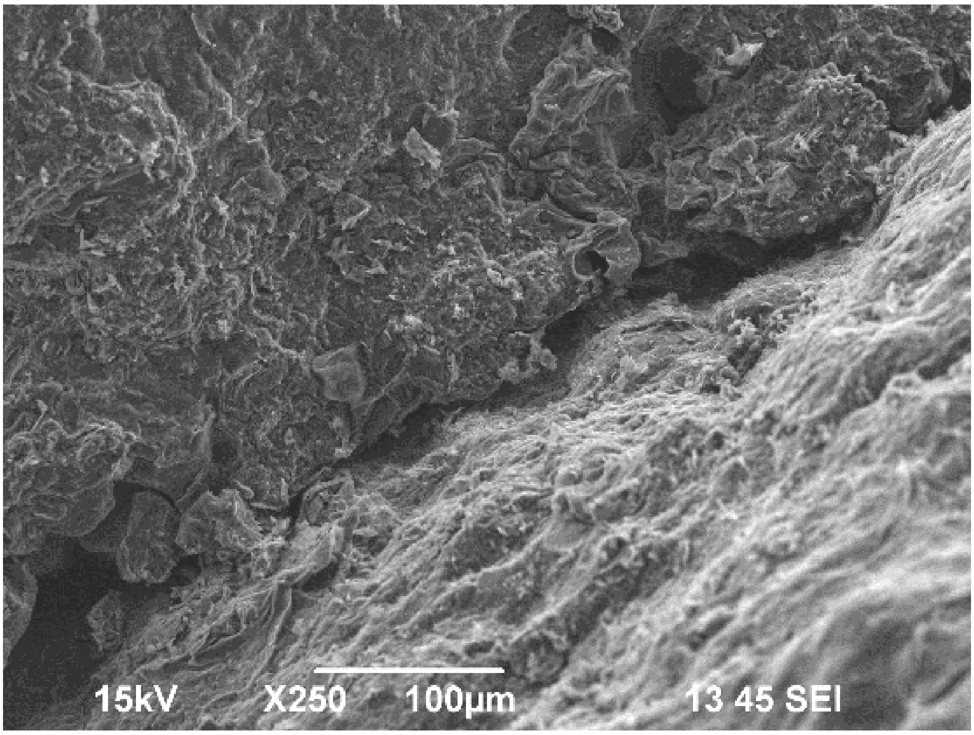

Figure 3-27 Detail SEM image under 30° angle of NBG-10 sample S051 at detail location 2.

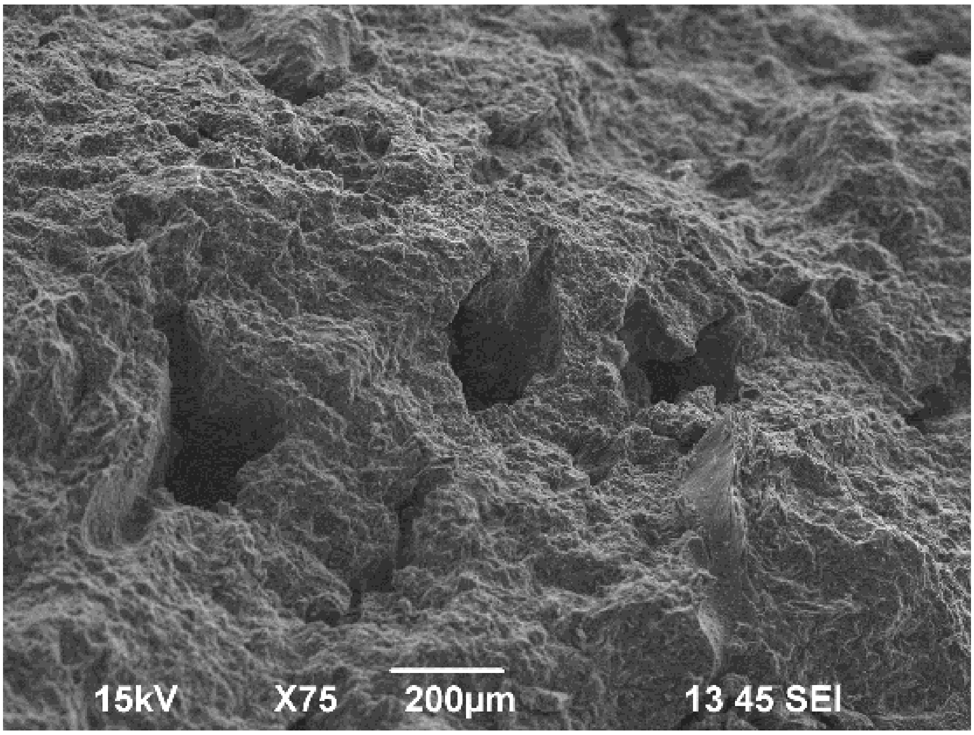

Figure 3-28 Detail SEM image under 30° angle of NBG-10 sample S051 at detail location 3.

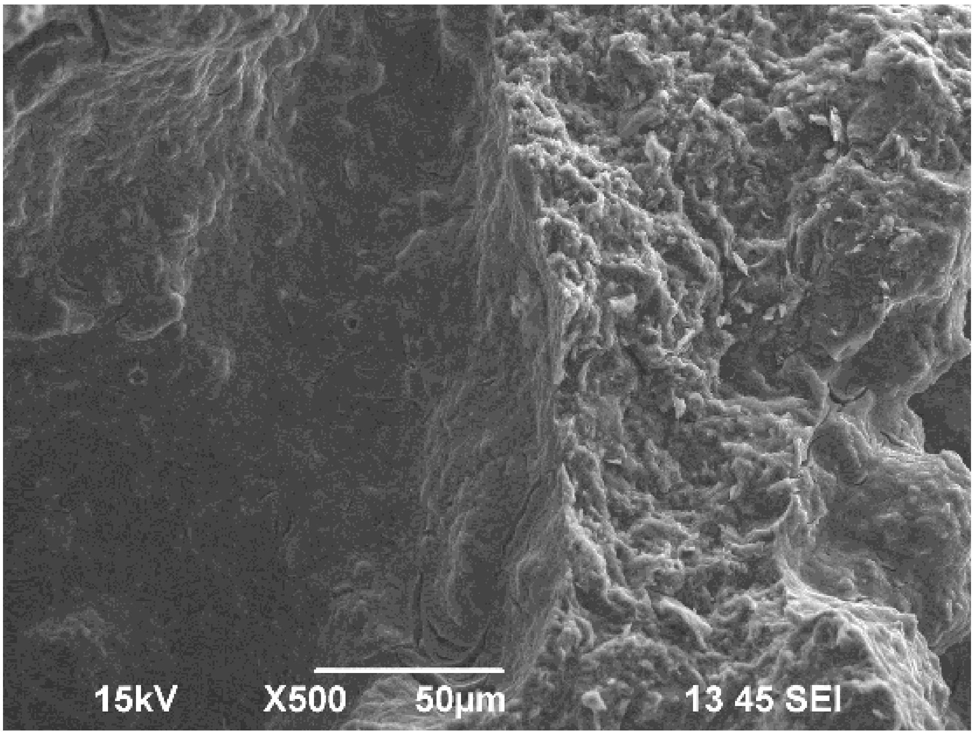

Figure 3-29 Detail SEM image under 30° angle of NBG-10 sample S051 at detail location 3.

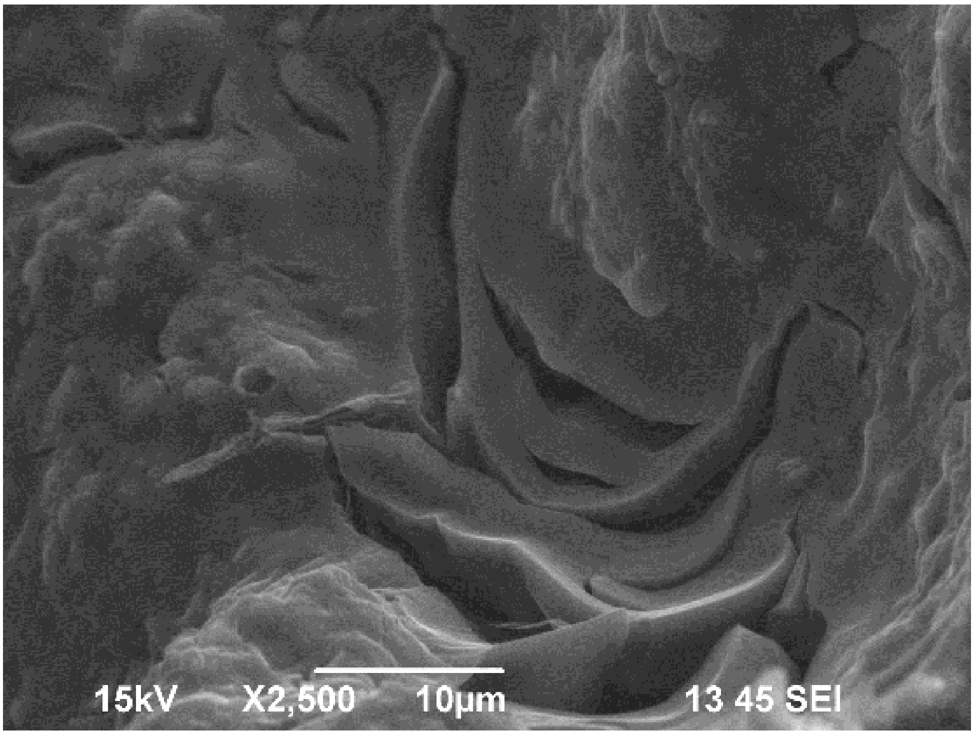

Figure 3-30 Detail SEM image under 30° angle of NBG-10 sample S051 at detail location 3.

S043, NBG-10, 22.3 dpa

Figure 3-31 to Figure 3-37 show the fracture surface of NBG-10 sample S042, irradiated at 750°C to 22.3 dpa.

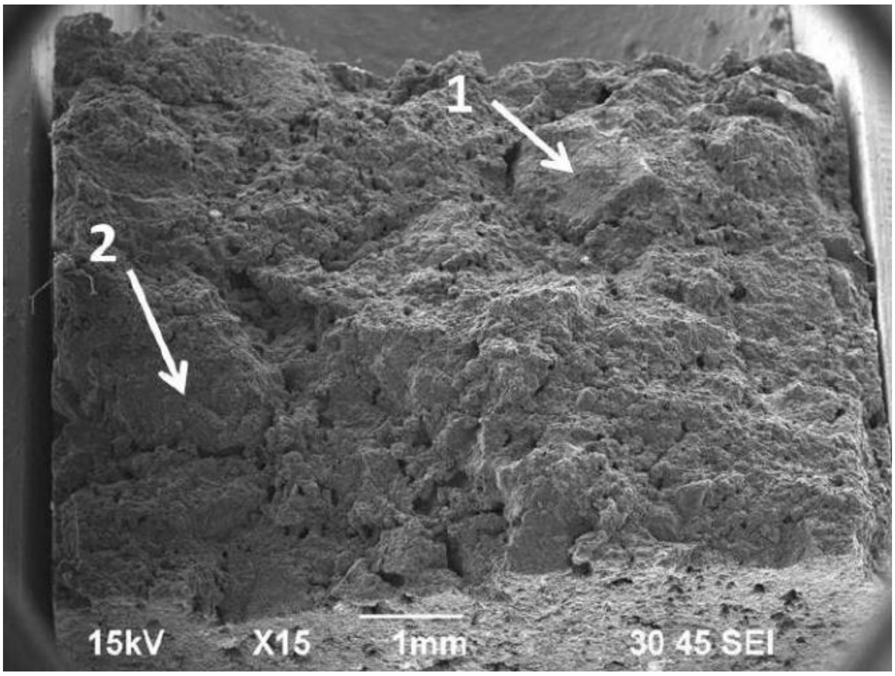

Figure 3-31 Overview SEM images under 30° angle of NBG-10 sample S042, 22.3 dpa. The numbers indicate the locations of the detail SEM images.

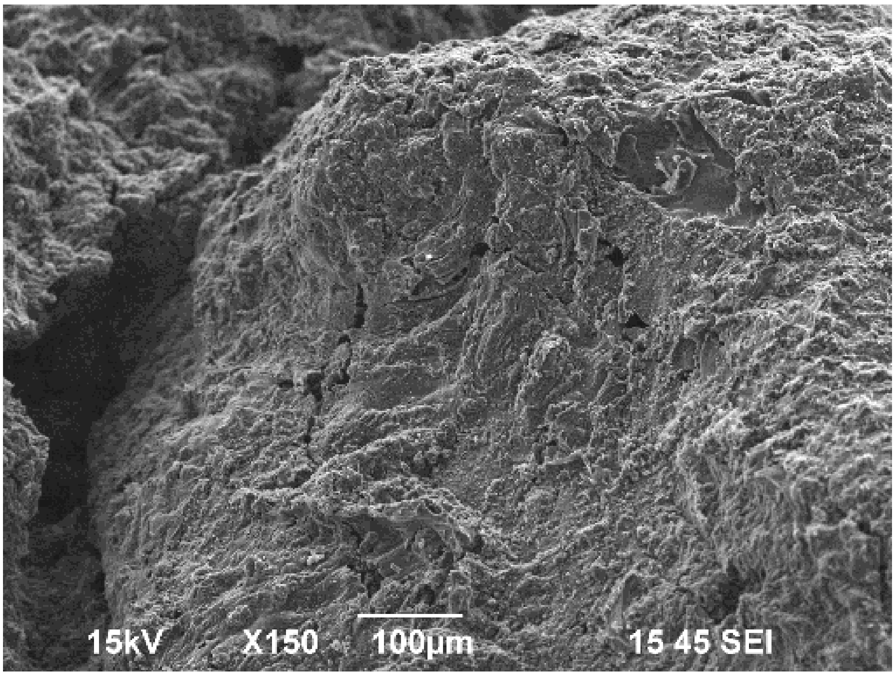

Figure 3-32 Detail SEM image under 30° angle of NBG-10 sample S042 at detail location 1.

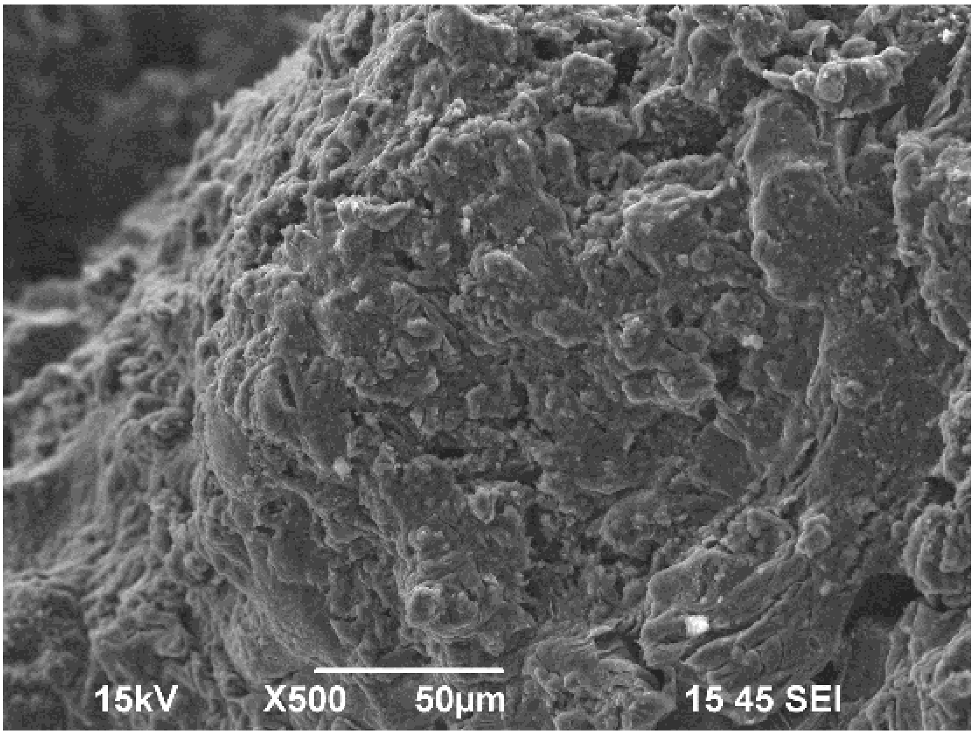

Figure 3-33 Detail SEM image under 30° angle of NBG-10 sample S042 at detail location 1.

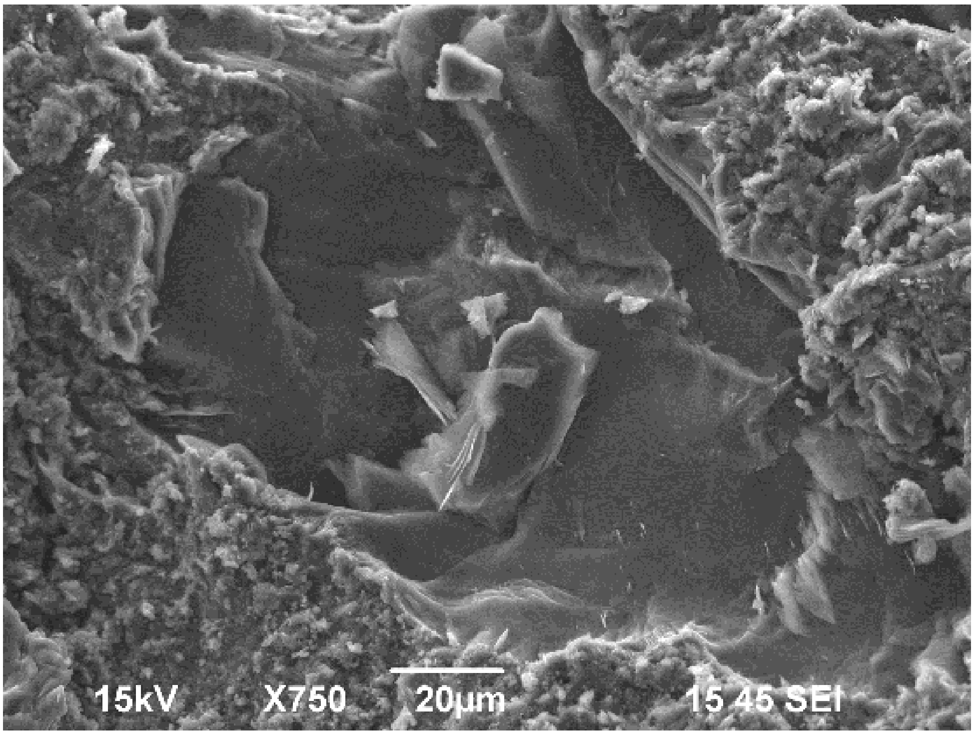

Figure 3-34 Detail SEM image under 30° angle of NBG-10 sample S042 at detail location 1.

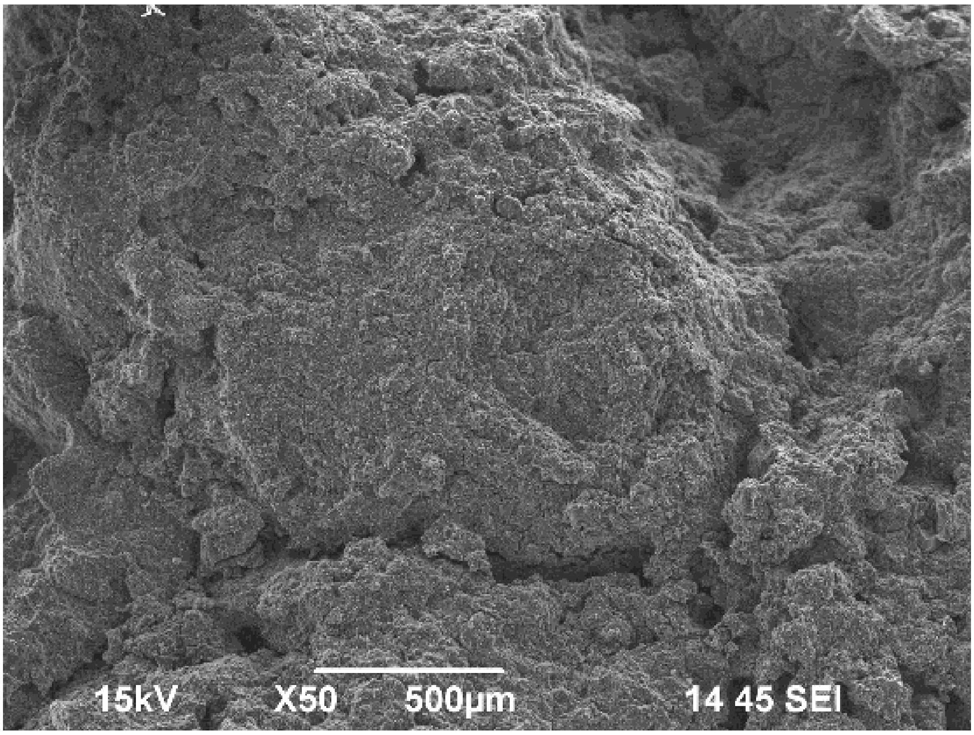

Figure 3-35 Detail SEM image under 30° angle of NBG-10 sample S042 at detail location 2.

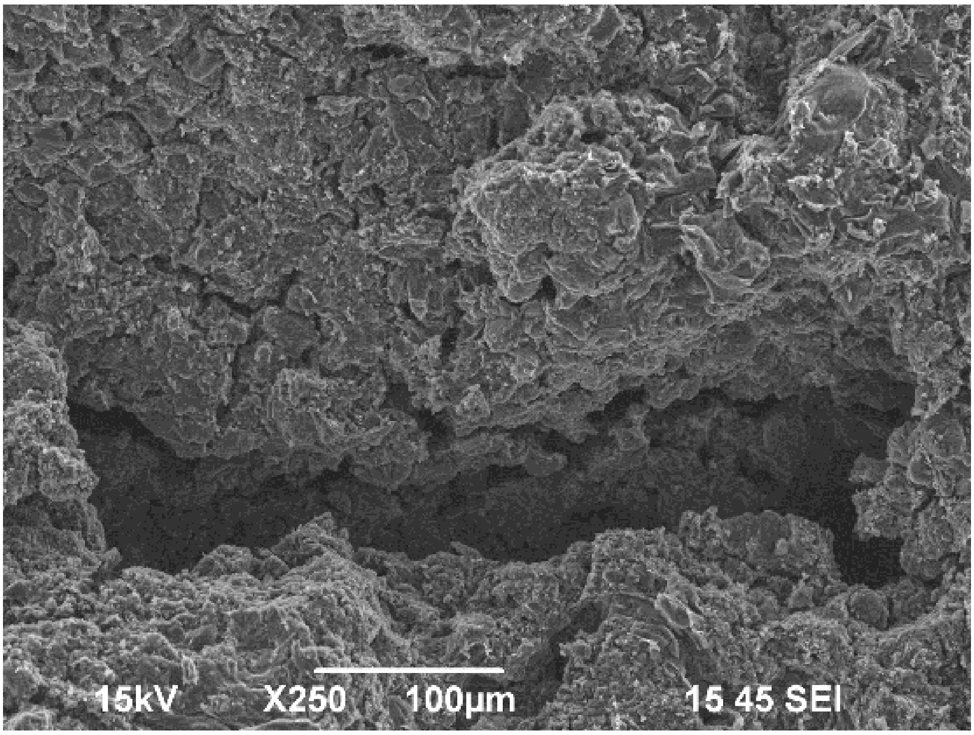

Figure 3-36 Detail SEM image under 30° angle of NBG-10 sample S042 at detail location 2.

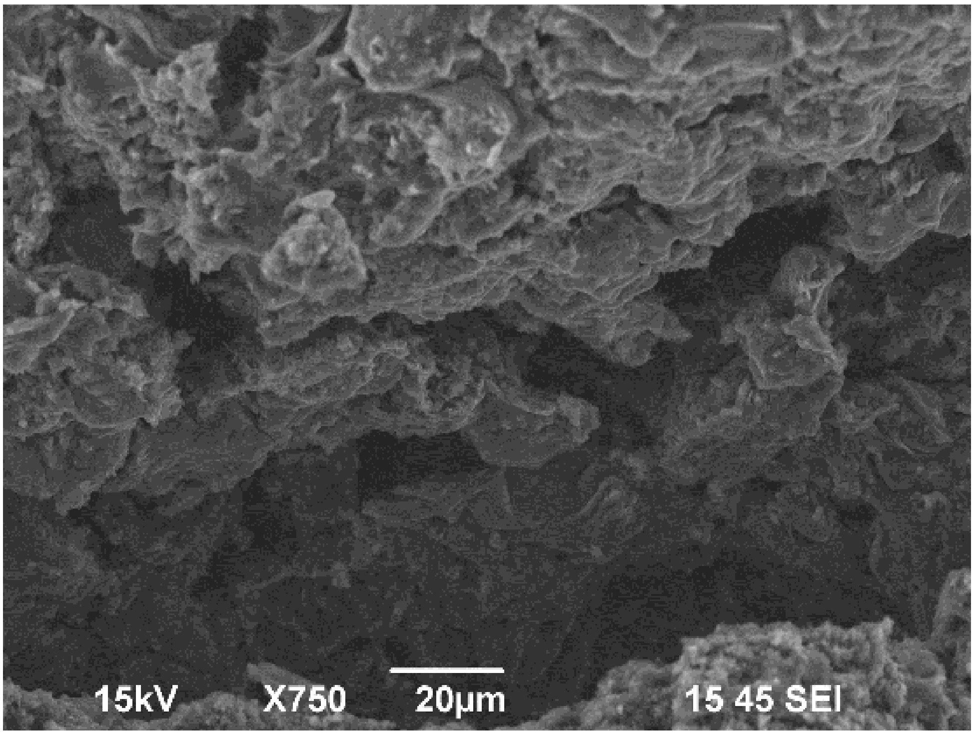

Figure 3-37 Detail SEM image under 30° angle of NBG-10 sample S042 at detail location 2.

3.2.2 PCIB

1U00, PCIB, 0 dpa

Figure 3-38 to Figure 3-48 show the fracture surface of unirradiated PCIB sample 1U00.

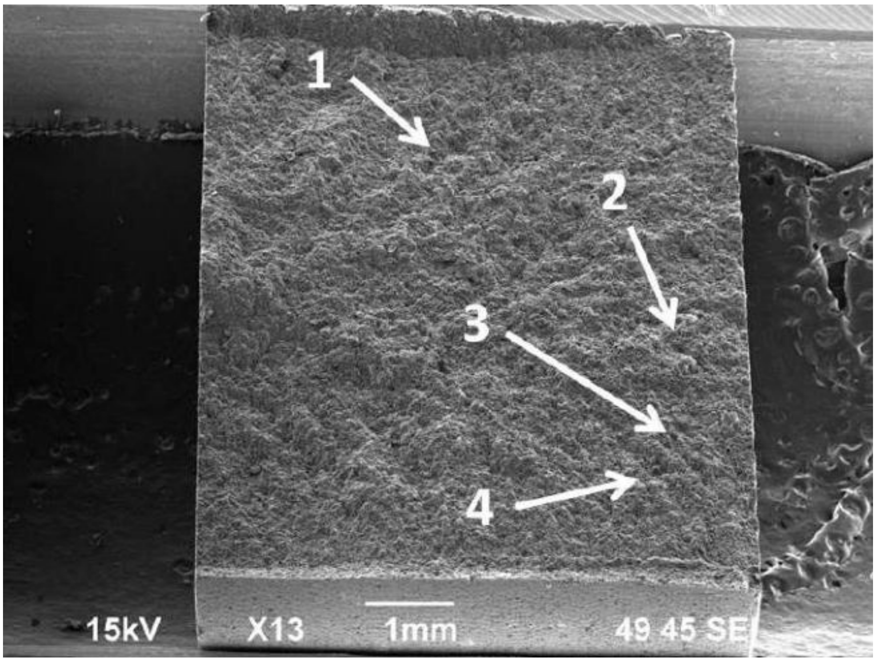

Figure 3-38 Overview SEM images under 30° angle of PCIB sample 1U00, 0 dpa. The numbers indicate the locations of the detail SEM images.

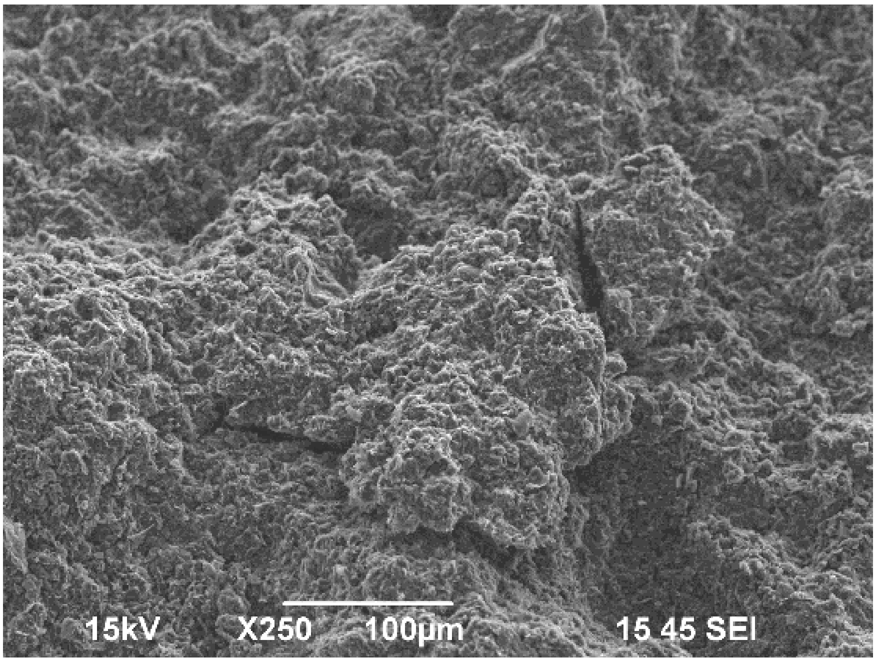

Figure 3-39 Detail SEM image under 30° angle of PCIB sample 1U00 at detail location 1.

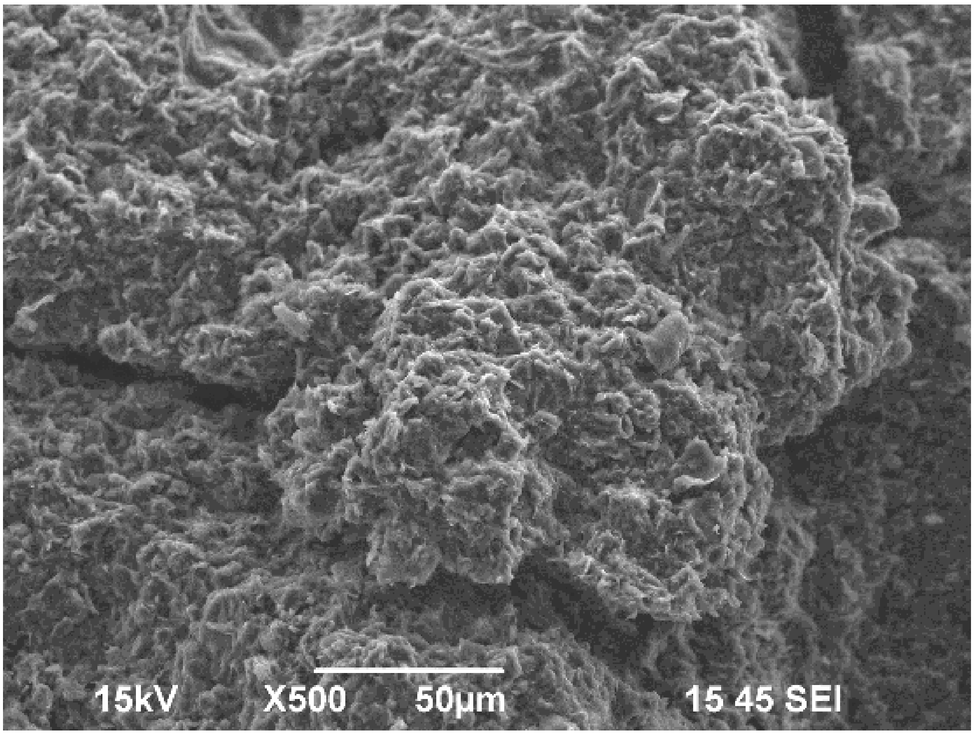

Figure 3-40 Detail SEM image under 30° angle of PCIB sample 1U00 at detail location 1.

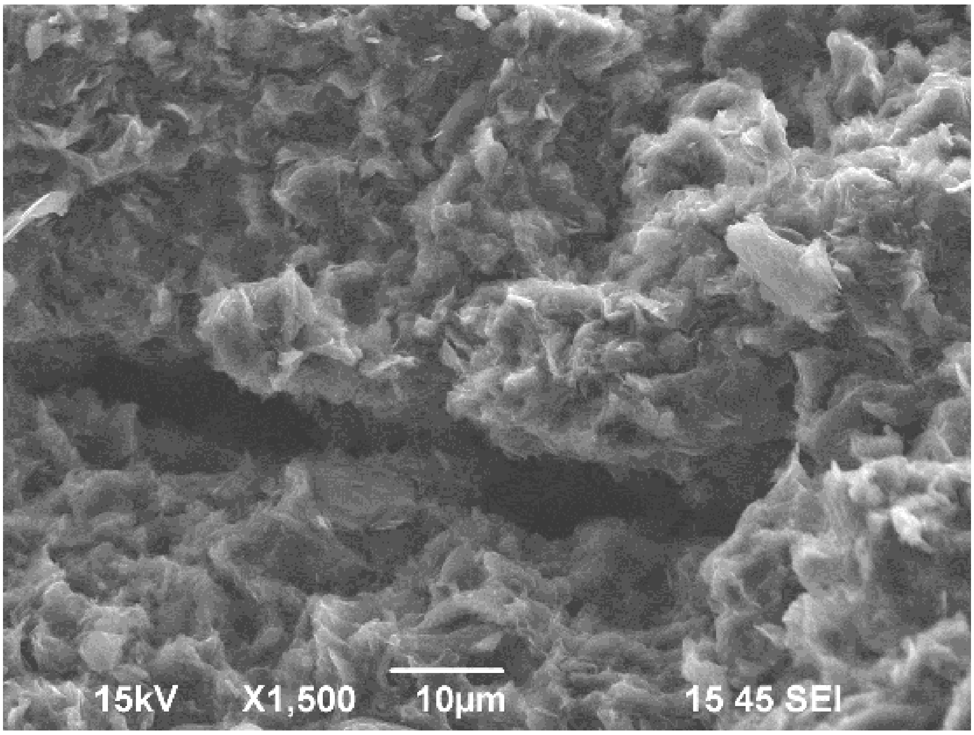

Figure 3-41 Detail SEM image under 30° angle of PCIB sample 1U00 at detail location 1.

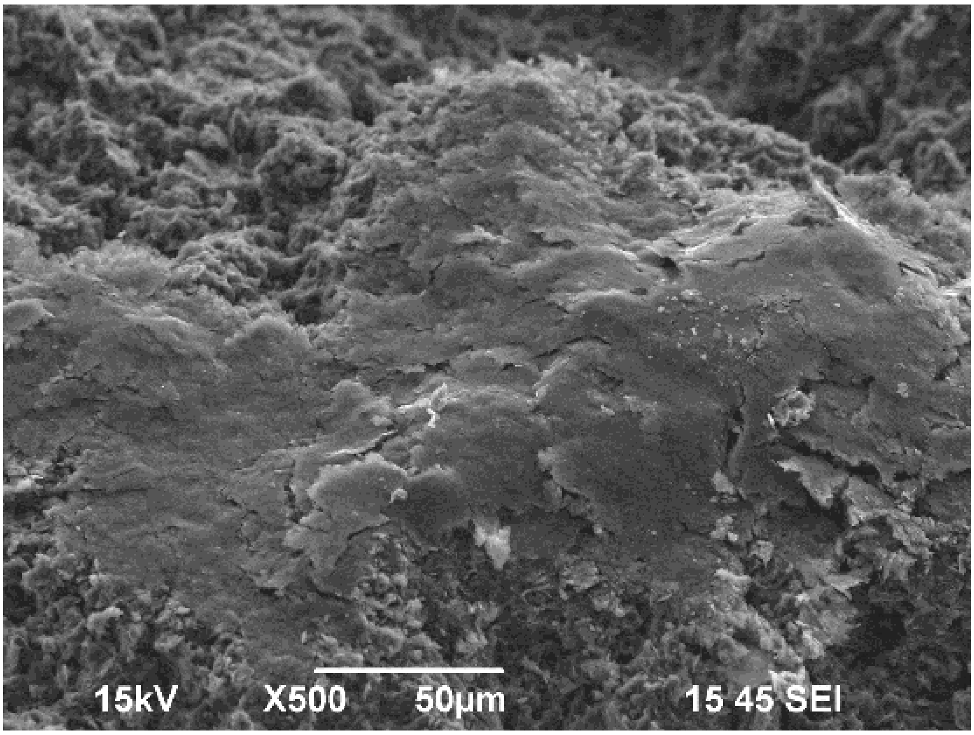

Figure 3-42 Detail SEM image under 30° angle of PCIB sample 1U00 at detail location 2.

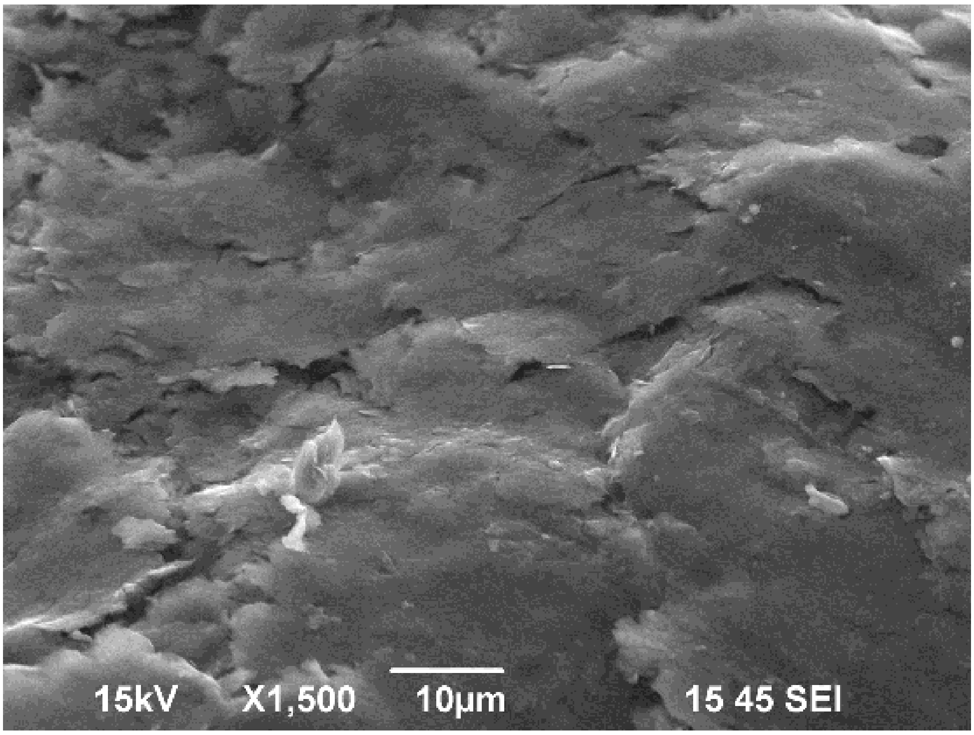

Figure 3-43 Detail SEM image under 30° angle of PCIB sample 1U00 at detail location 2.

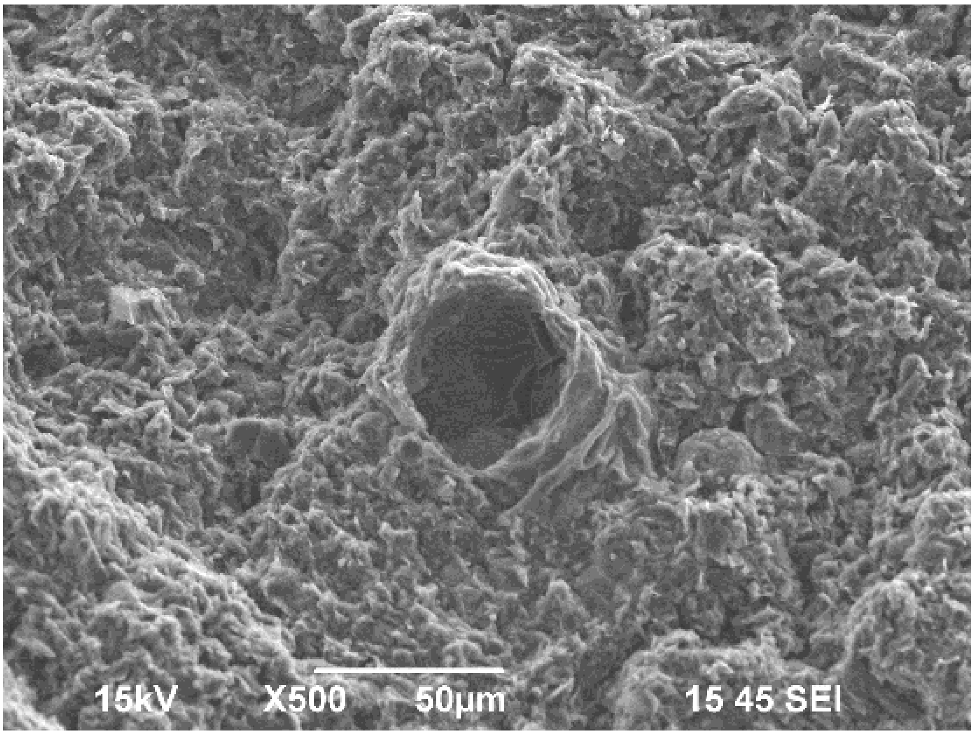

Figure 3-44 Detail SEM image under 30° angle of PCIB sample 1U00 at detail location 3.

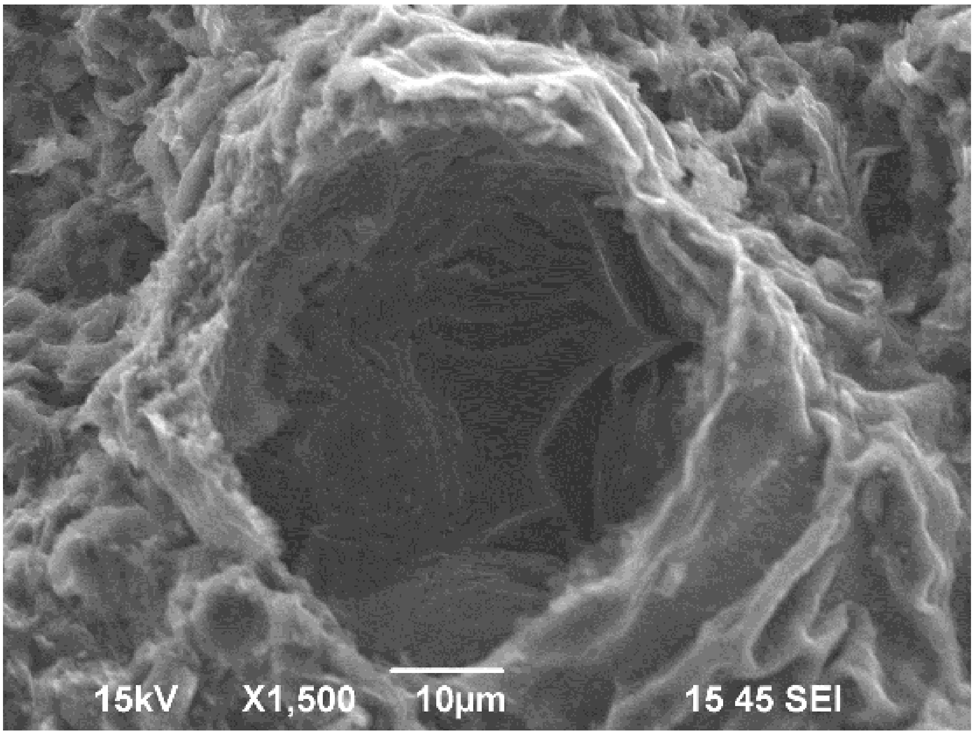

Figure 3-45 Detail SEM image under 30° angle of PCIB sample 1U00 at detail location 3.

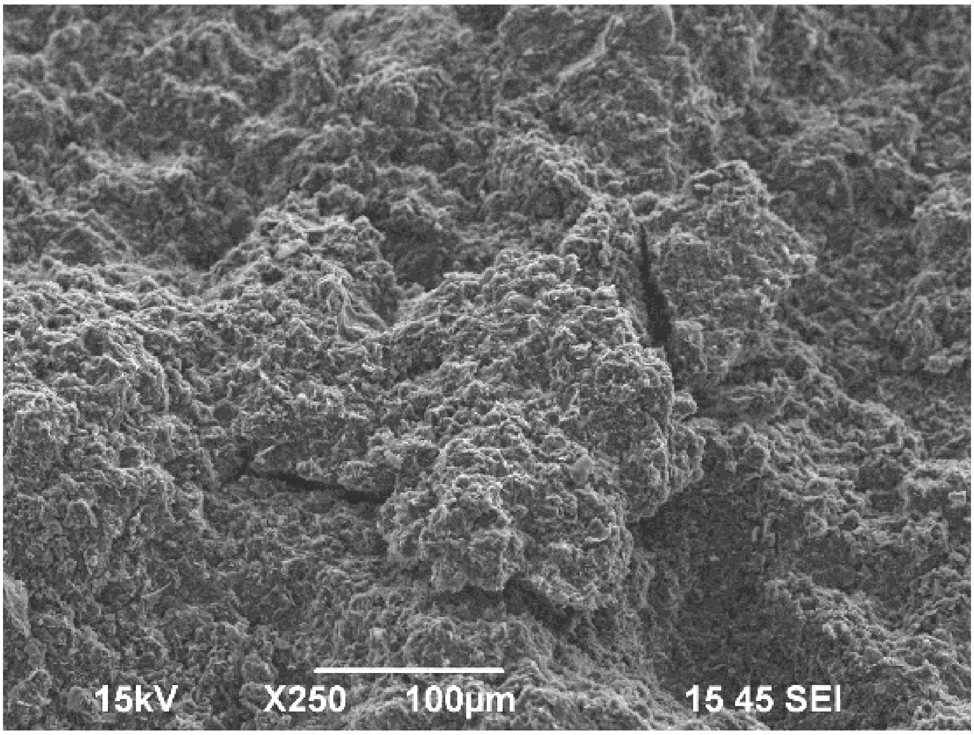

Figure 3-46 Detail SEM image under 30° angle of PCIB sample 1U00 at detail location 4.

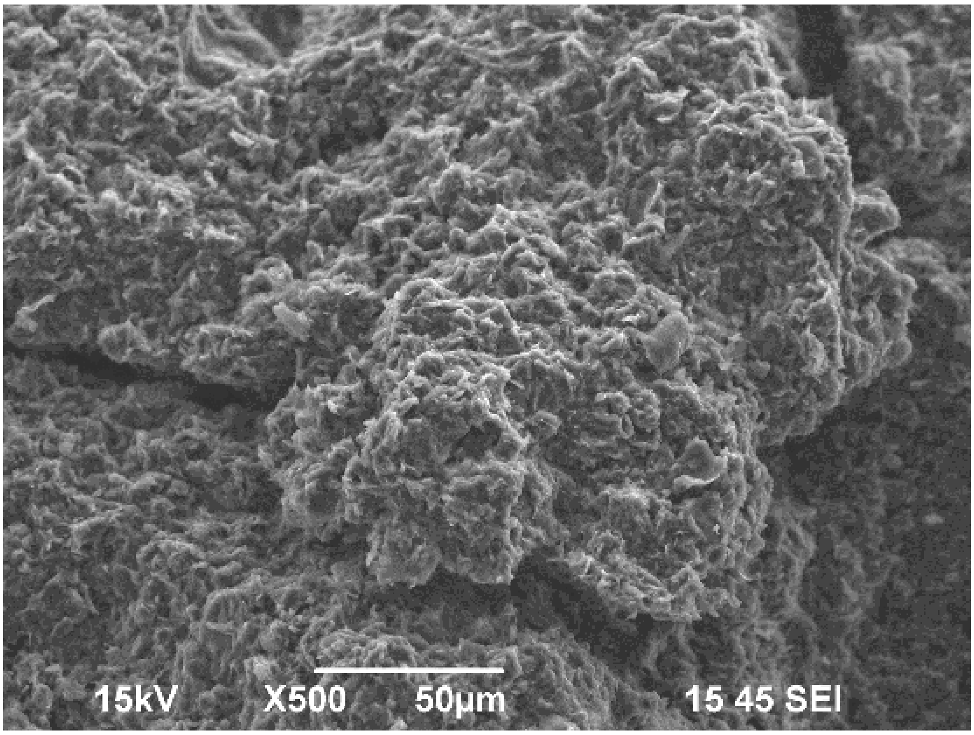

Figure 3-47 Detail SEM image under 30° angle of PCIB sample 1U00 at detail location 4.

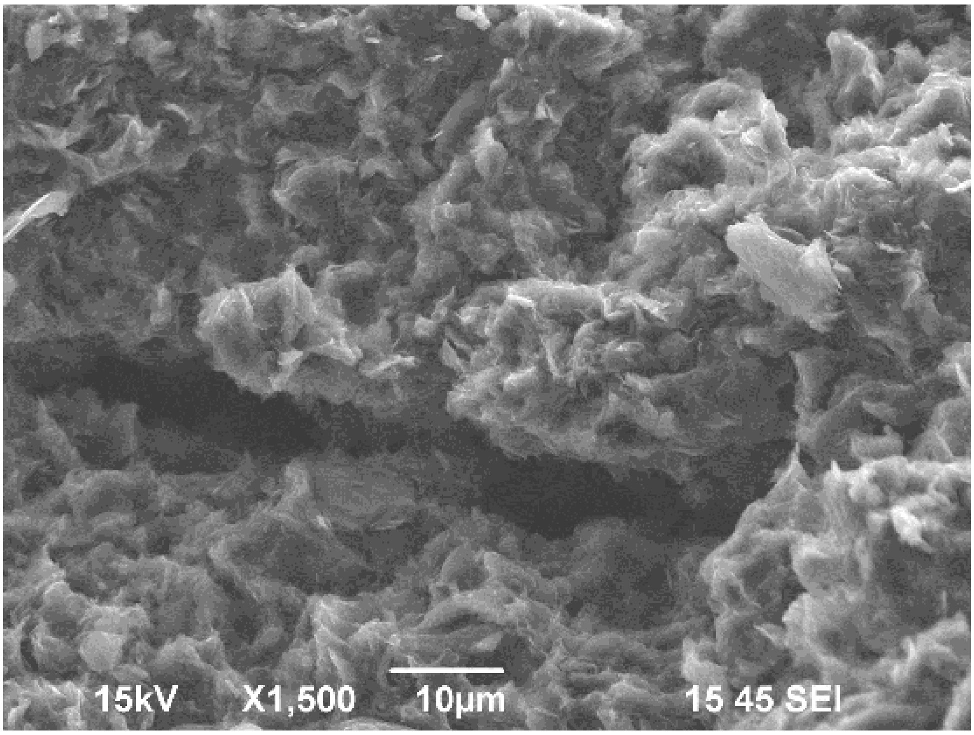

Figure 3-48 Detail SEM image under 30° angle of PCIB sample 1U00 at detail location 4.

U111, PCIB, 6.3 dpa

Figure 3-50 to Figure 3-58 show the fracture surface of PCIB sample U111, irradiated at 750°C to 6.3 dpa.

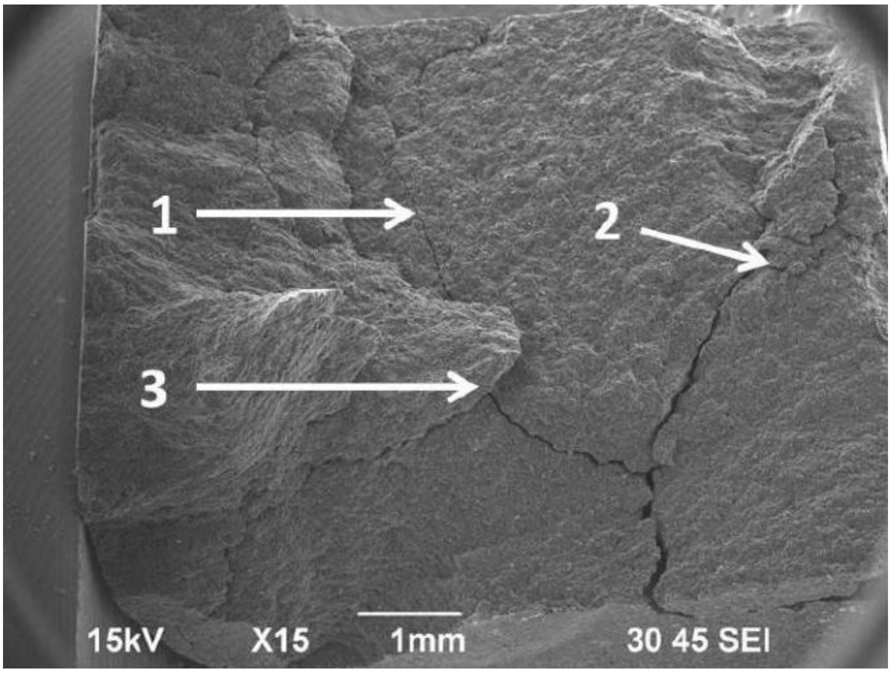

Figure 3-49 Overview SEM images under 30° angle of PCIB sample U111, 6.3 dpa. The numbers indicate the locations of the detail SEM images.

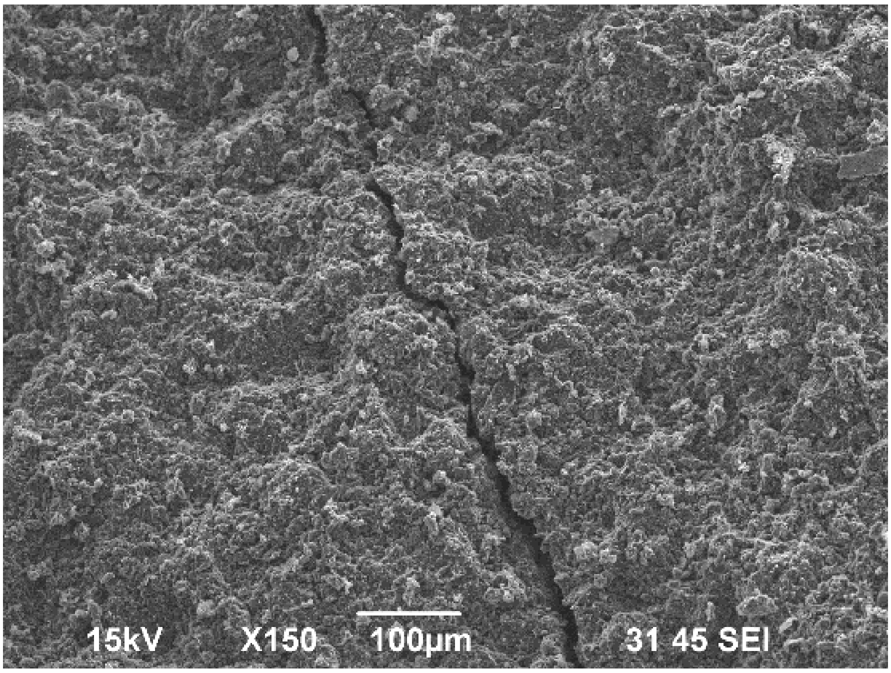

Figure 3-50 Detail SEM image under 30° angle of PCIB sample U111 at detail location 1.

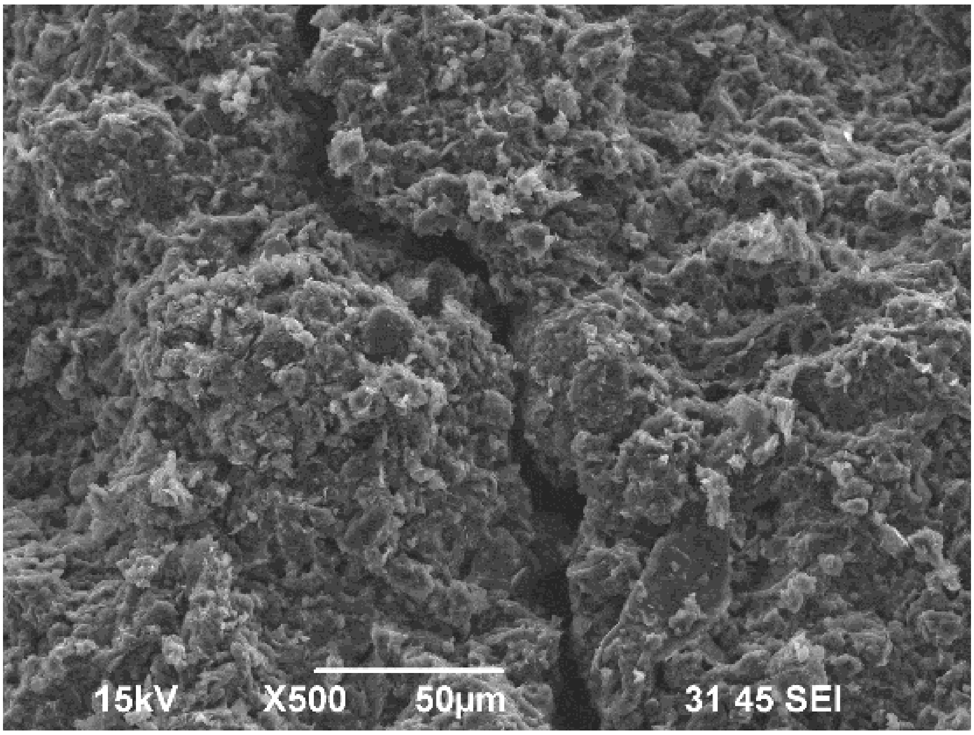

Figure 3-51 Detail SEM image under 30° angle of PCIB sample U111 at detail location 1.

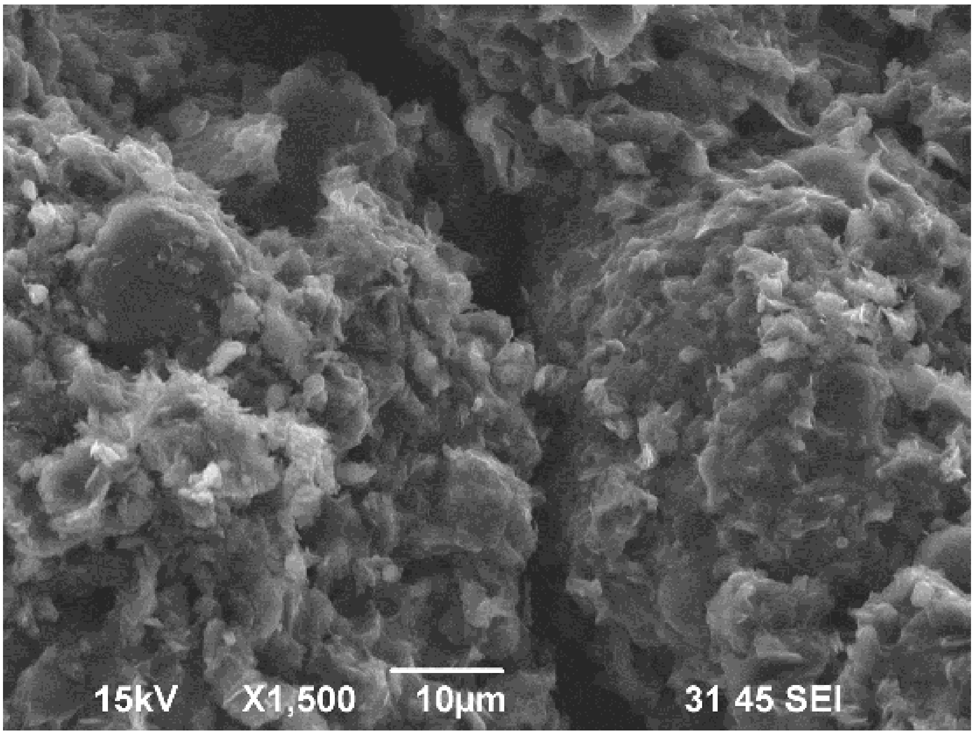

Figure 3-52 Detail SEM image under 30° angle of PCIB sample U111 at detail location 1.

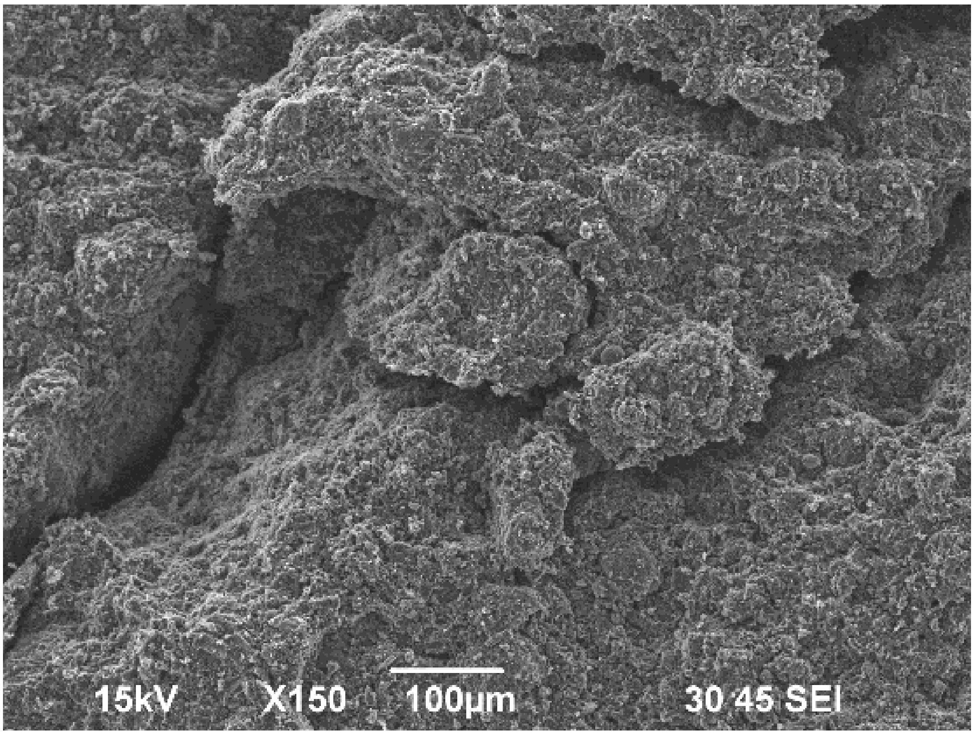

Figure 3-53 Detail SEM image under 30° angle of PCIB sample U111 at detail location 2.

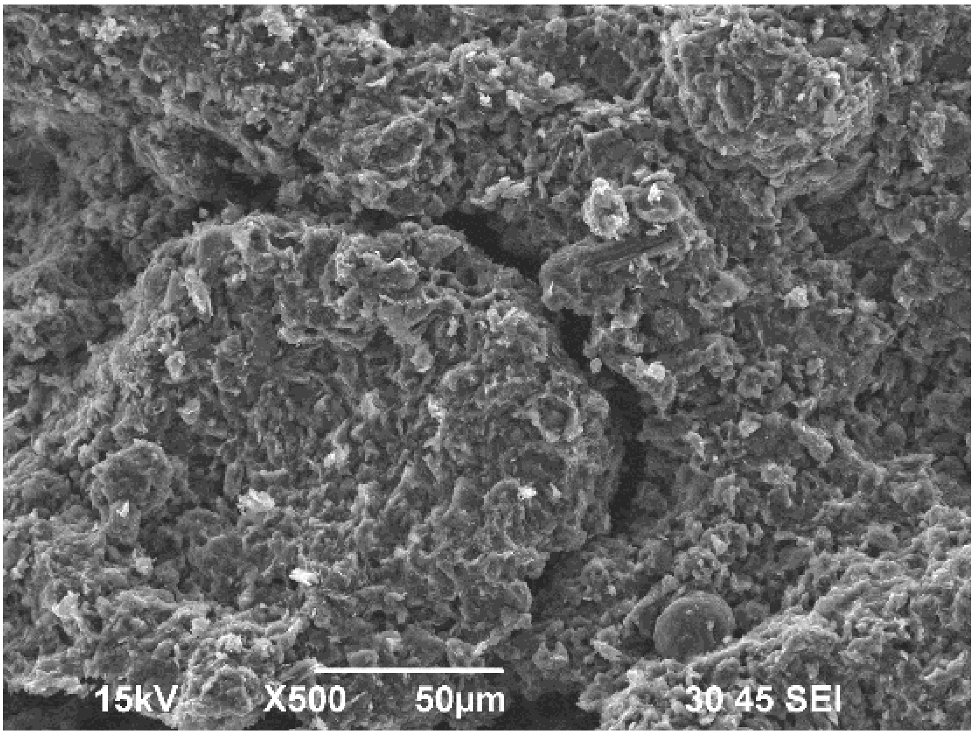

Figure 3-54 Detail SEM image under 30° angle of PCIB sample U111 at detail location 2.

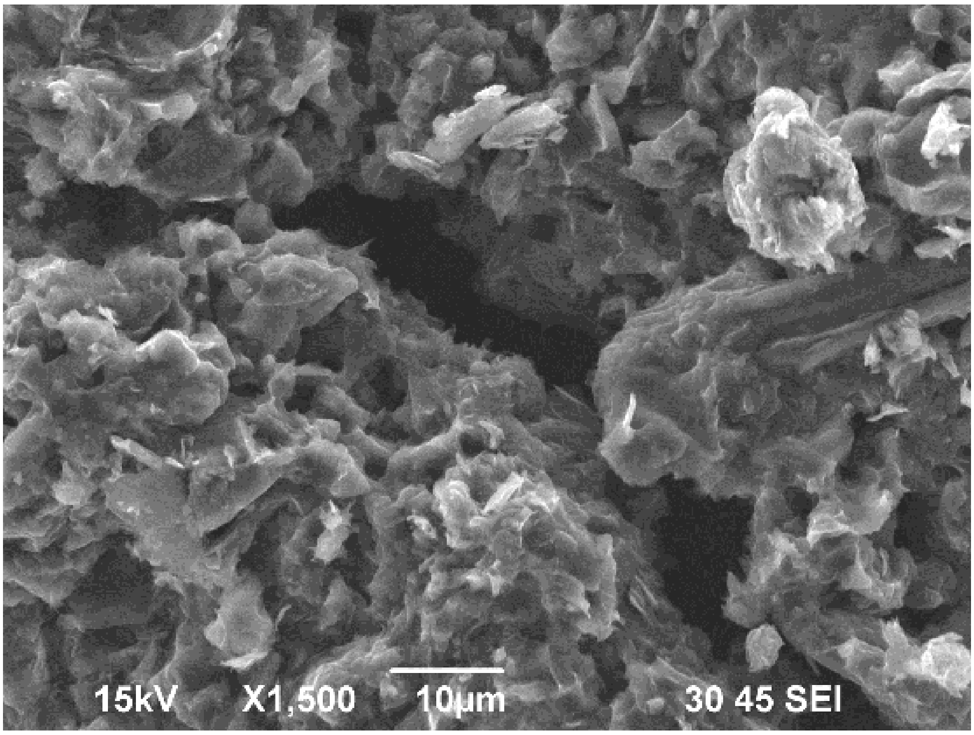

Figure 3-55 Detail SEM image under 30° angle of PCIB sample U111 at detail location 2.

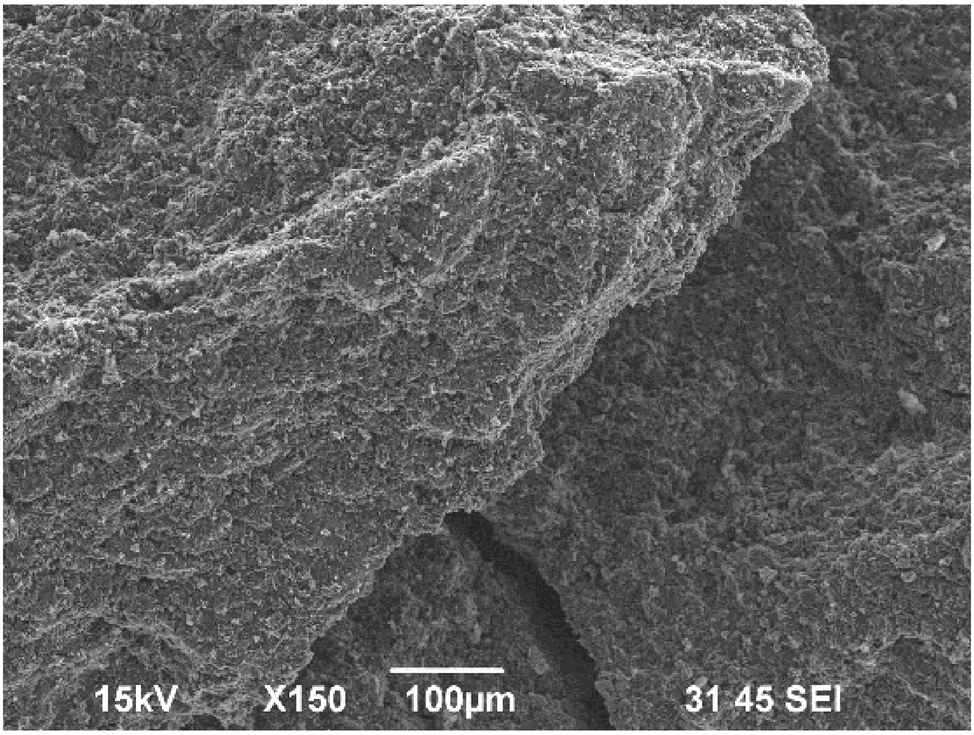

Figure 3-56 Detail SEM image under 30° angle of PCIB sample U111 at detail location 3.

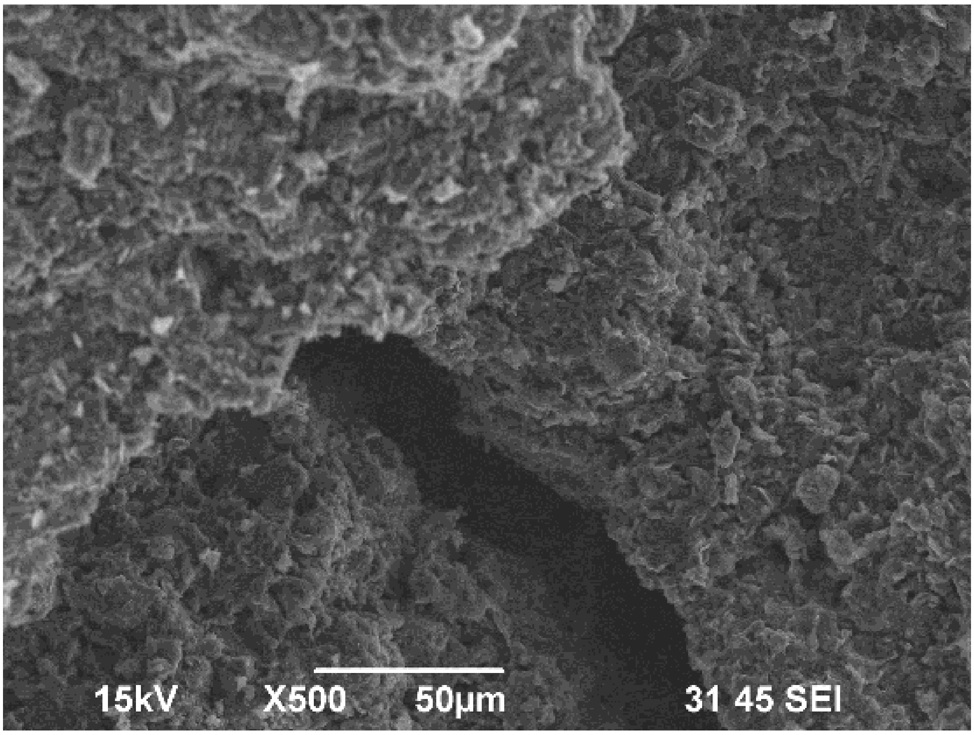

Figure 3-57 Detail SEM image under 30° angle of PCIB sample U111 at detail location 3.

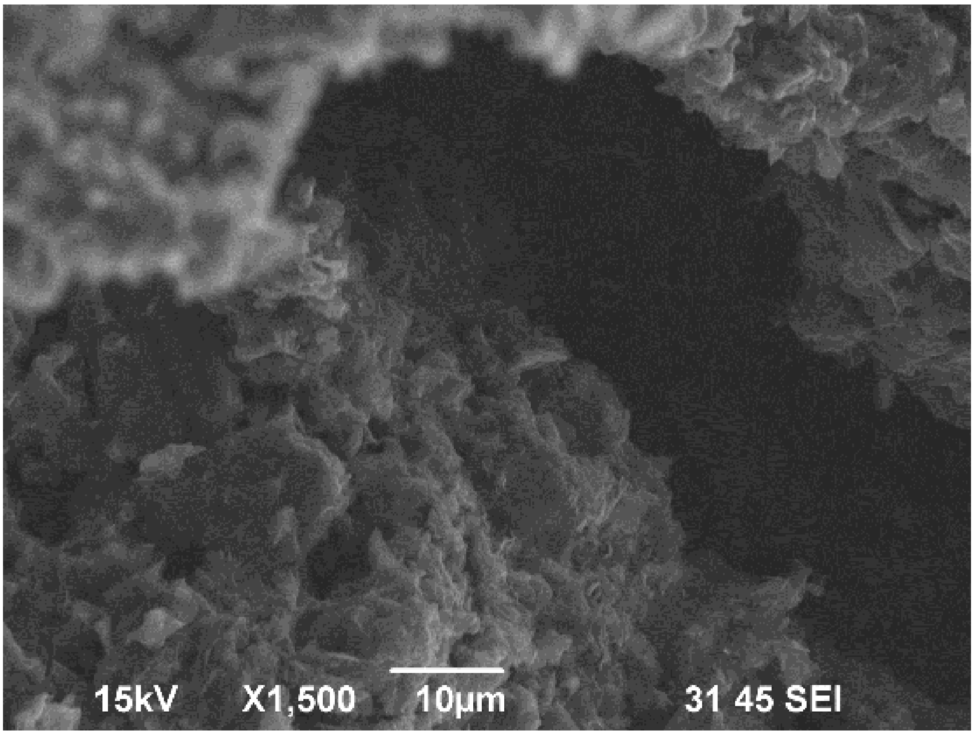

Figure 3-58 Detail SEM image under 30° angle of PCIB sample U111 at detail location 3.

U198, PCIB, 7.7 dpa

Figure 3-59 to Figure 3-68 show the fracture surface of PCIB sample U198, irradiated at 750°C to 7.7 dpa.

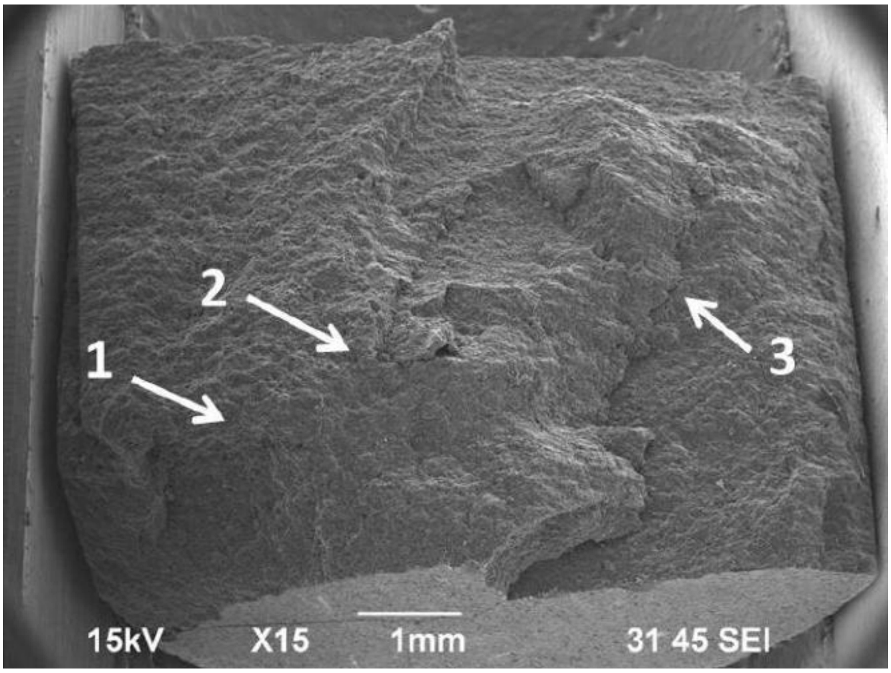

Figure 3-59 Overview SEM images under 30° angle of PCIB sample U198, 7.7 dpa. The numbers indicate the locations of the detail SEM images.

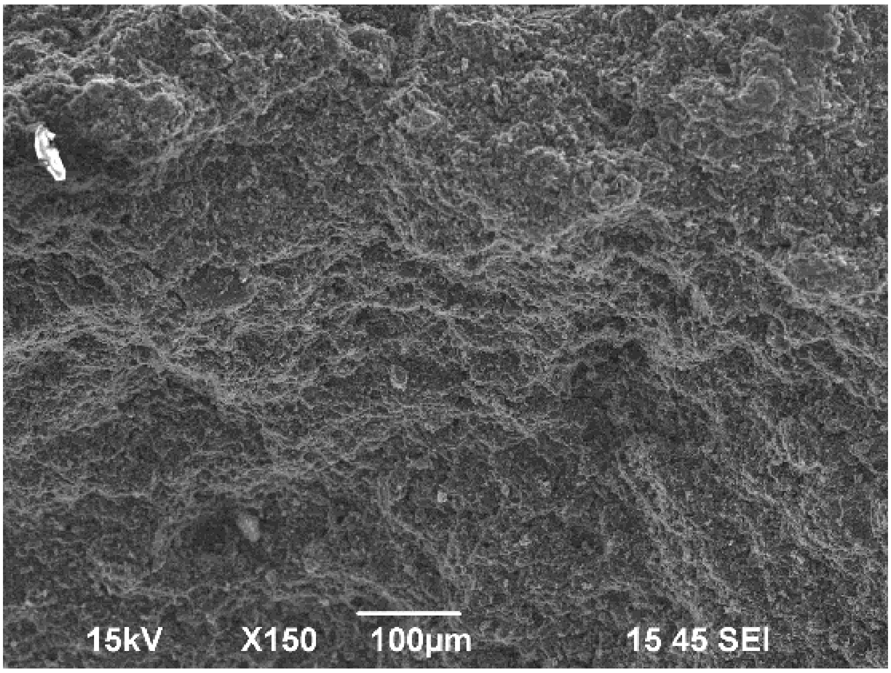

Figure 3-60 Detail SEM image under 30° angle of PCIB sample U198 at detail location 1.

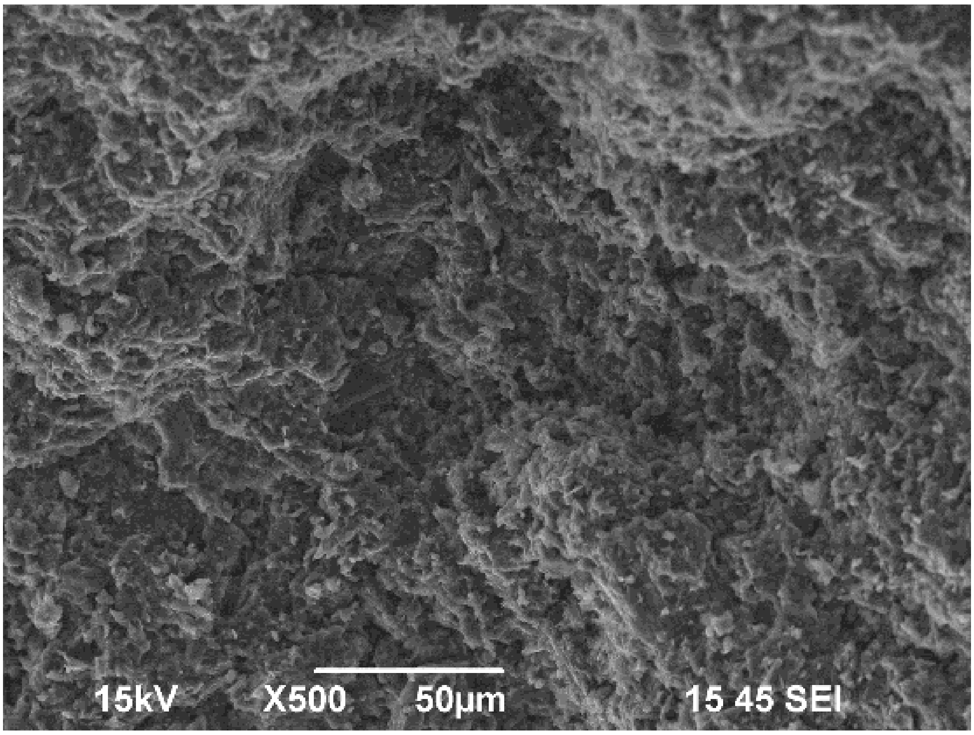

Figure 3-61 Detail SEM image under 30° angle of PCIB sample U198 at detail location 1.

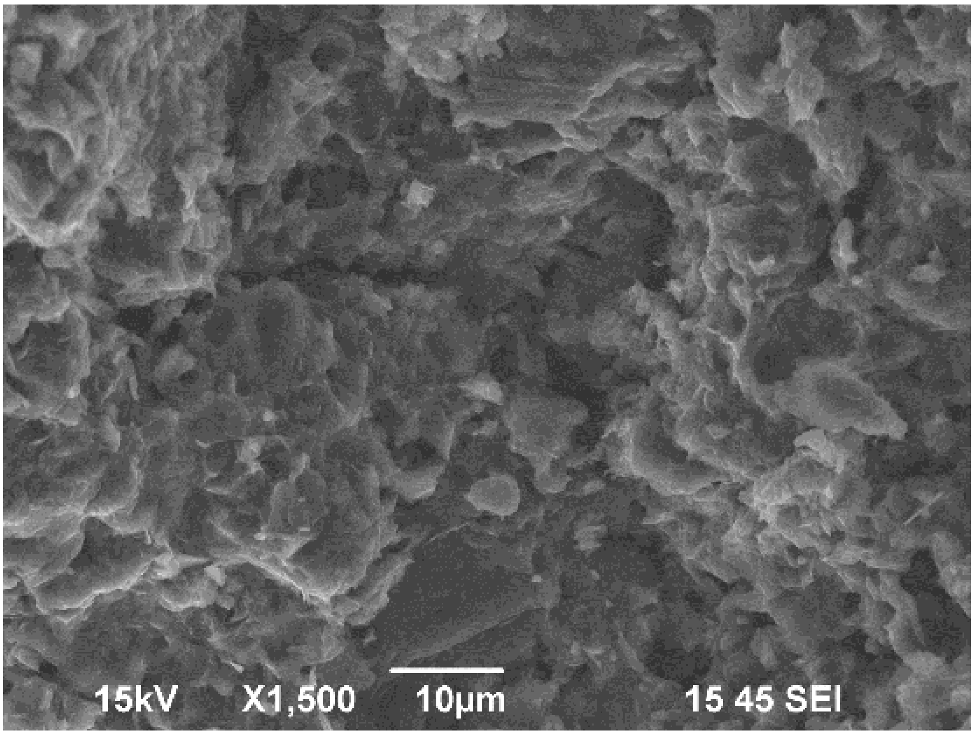

Figure 3-62 Detail SEM image under 30° angle of PCIB sample U198 at detail location 1.

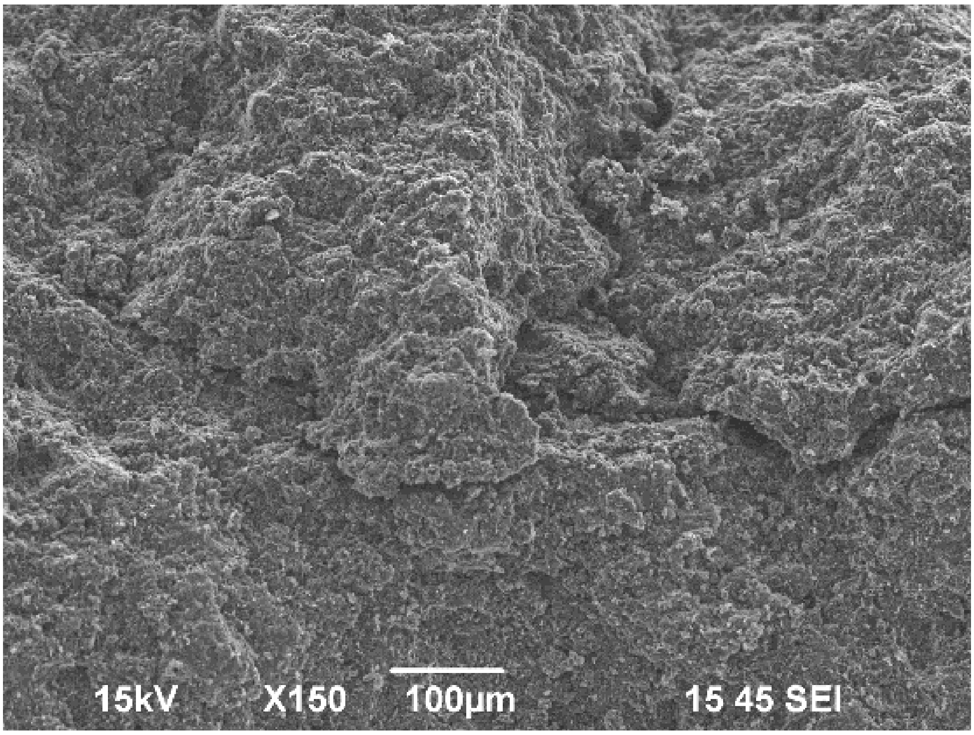

Figure 3-63 Detail SEM image under 30° angle of PCIB sample U198 at detail location2.

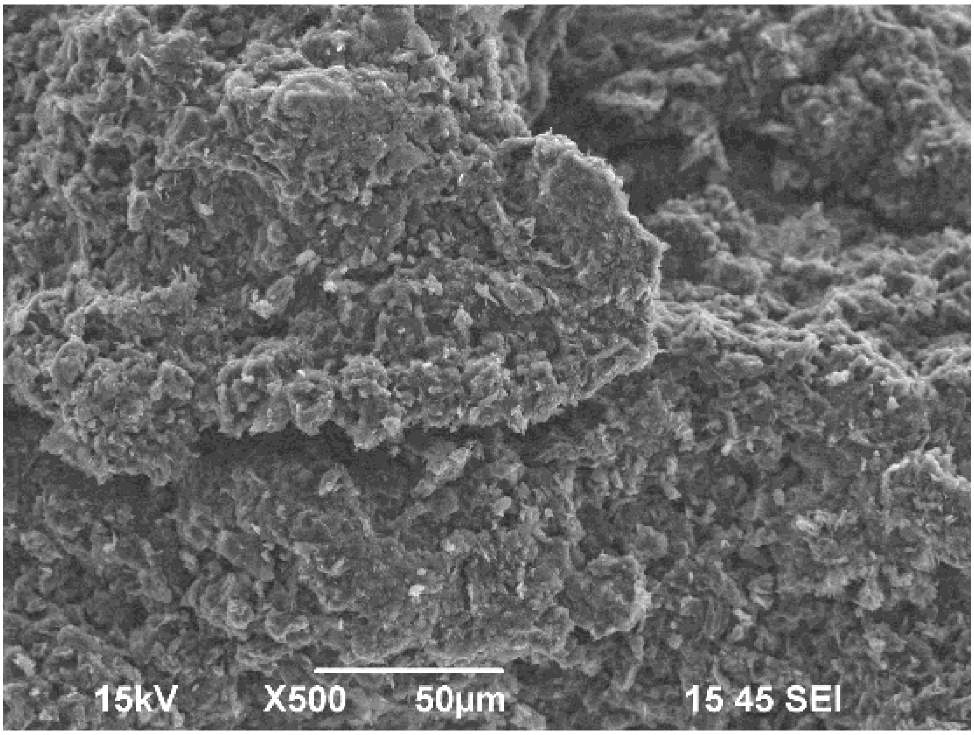

Figure 3-64 Detail SEM image under 30° angle of PCIB sample U198 at detail location 2.

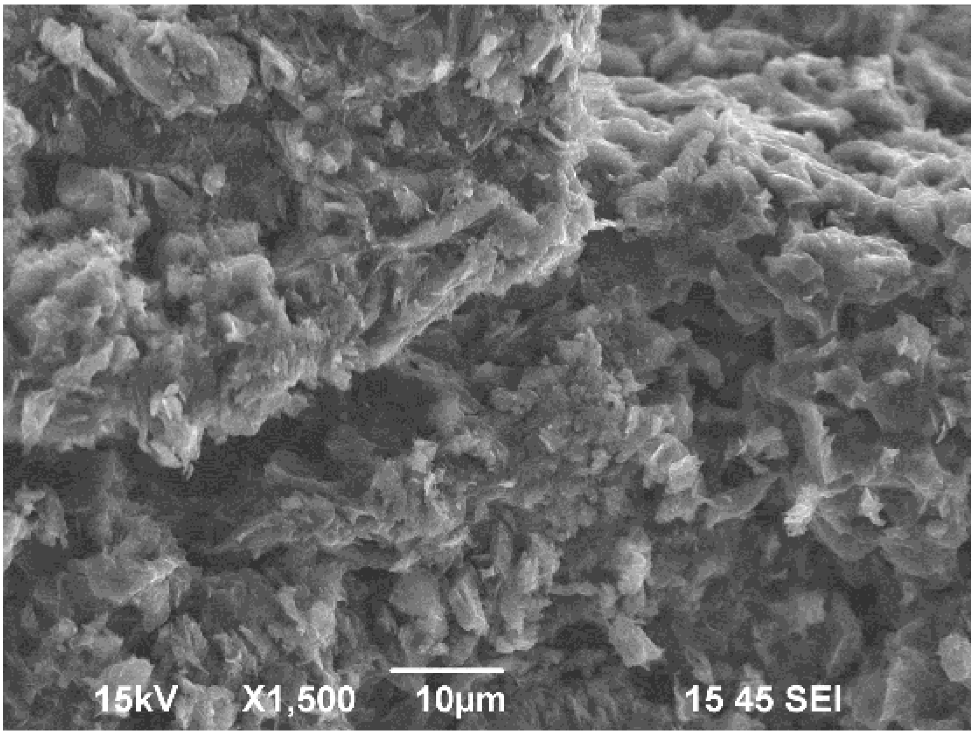

Figure 3-65 Detail SEM image under 30° angle of PCIB sample U198 at detail location 2.

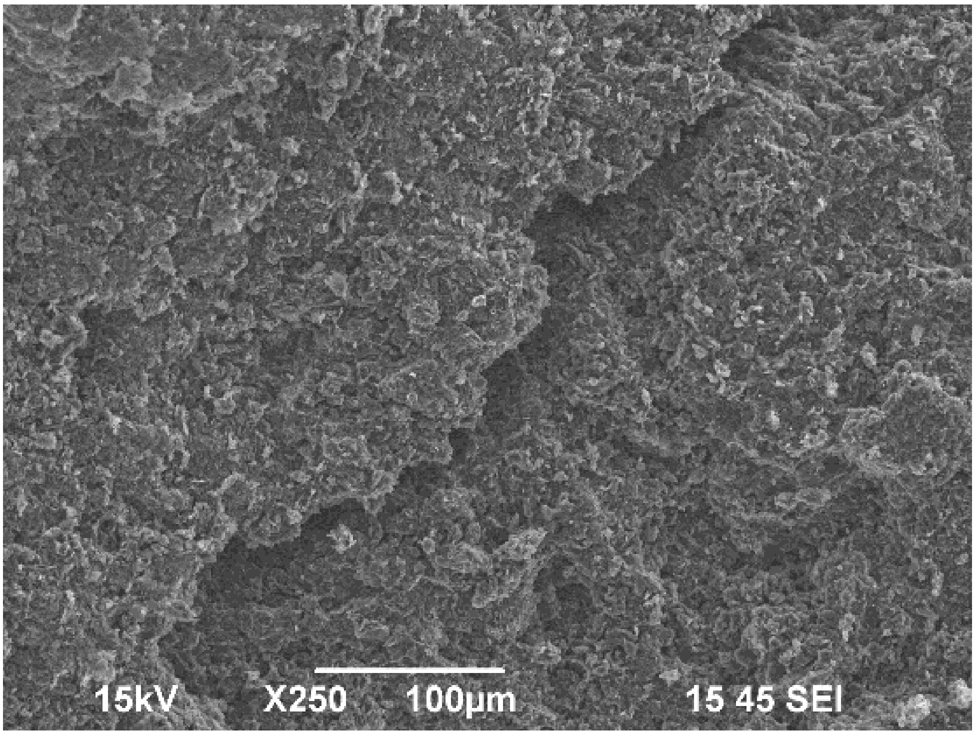

Figure 3-66 Detail SEM image under 30° angle of PCIB sample U198 at detail location 3.

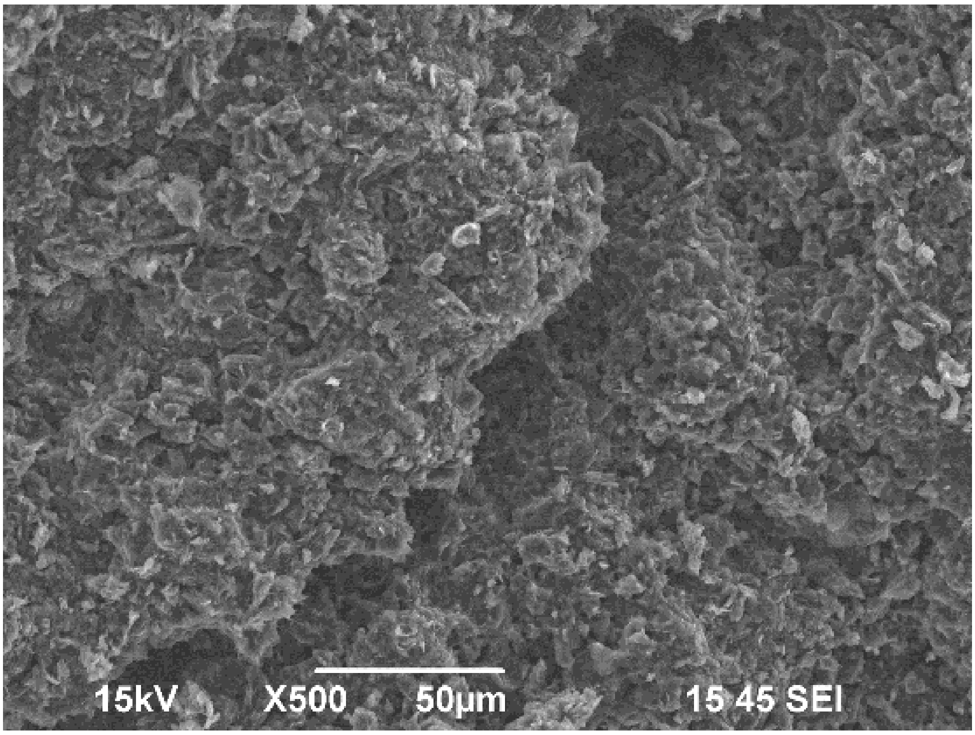

Figure 3-67 Detail SEM image under 30° angle of PCIB sample U198 at detail location 3.

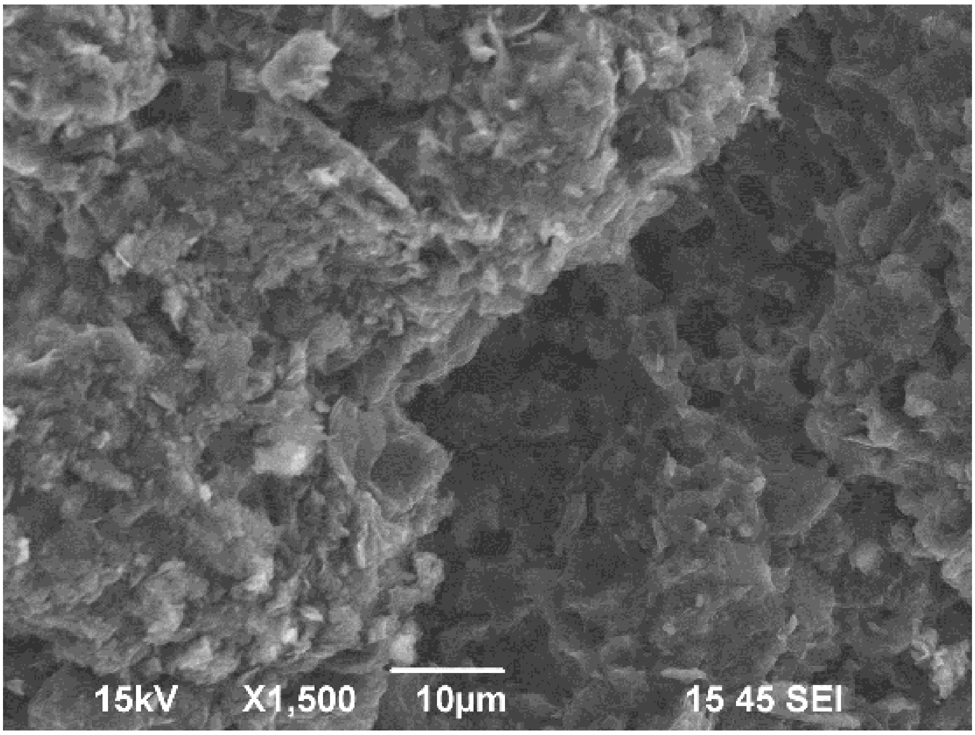

Figure 3-68 Detail SEM image under 30° angle of PCIB sample U198 at detail location 3.

U165, PCIB, 9.8 dpa

Figure 3-69 to Figure 3-78 show the fracture surface of PCIB sample U165, irradiated at 750°C to 9.8 dpa.

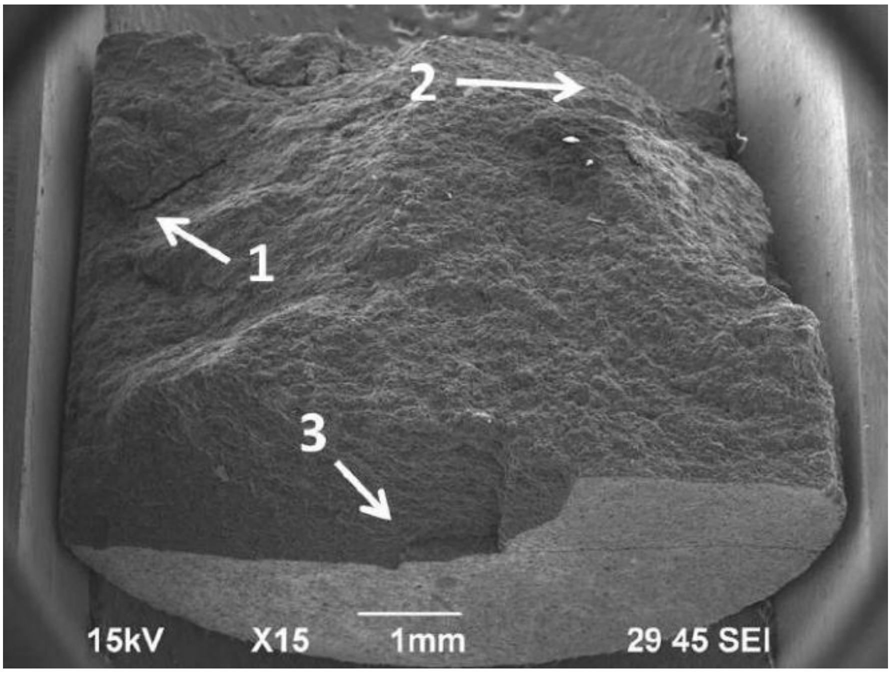

Figure 3-69 Overview SEM images under 30° angle of PCIB sample U165, 9.8 dpa. The numbers indicate the locations of the detail SEM images.

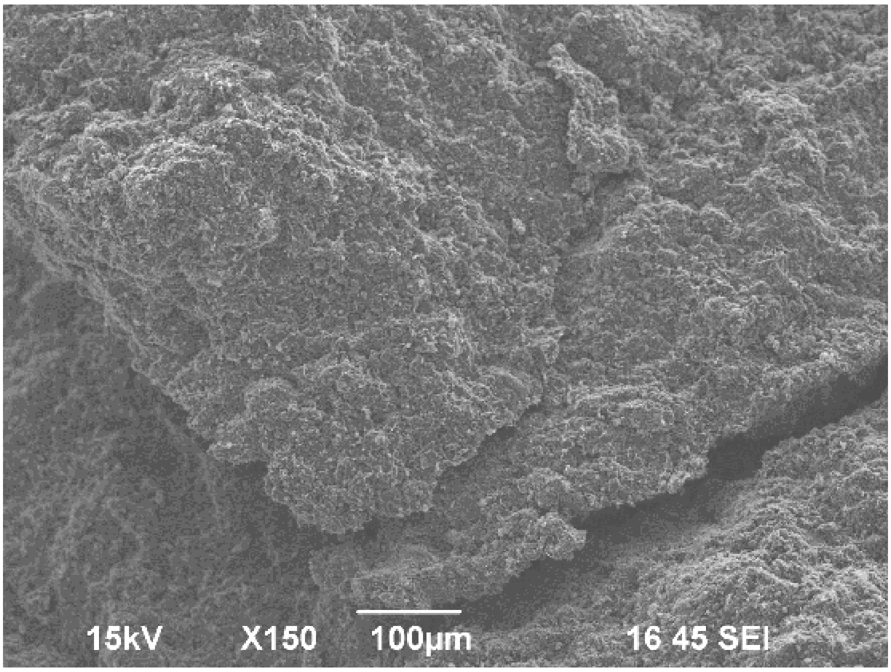

Figure 3-70 Detail SEM image under 30° angle of PCIB sample U165 at detail location 1.

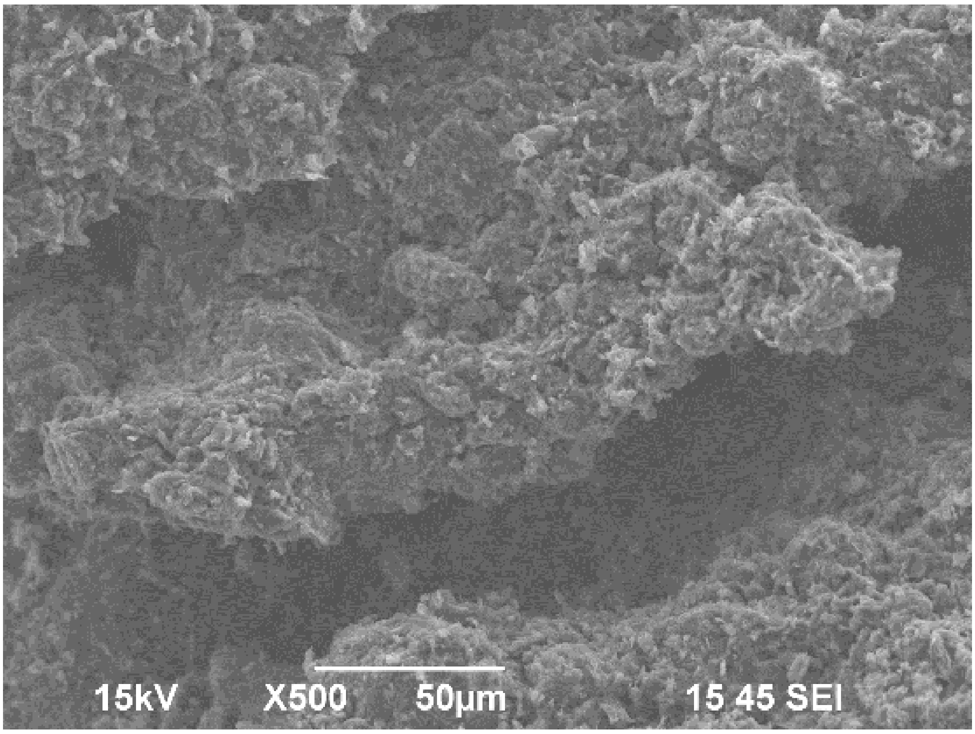

Figure 3-71 Detail SEM image under 30° angle of PCIB sample U165 at detail location 1.

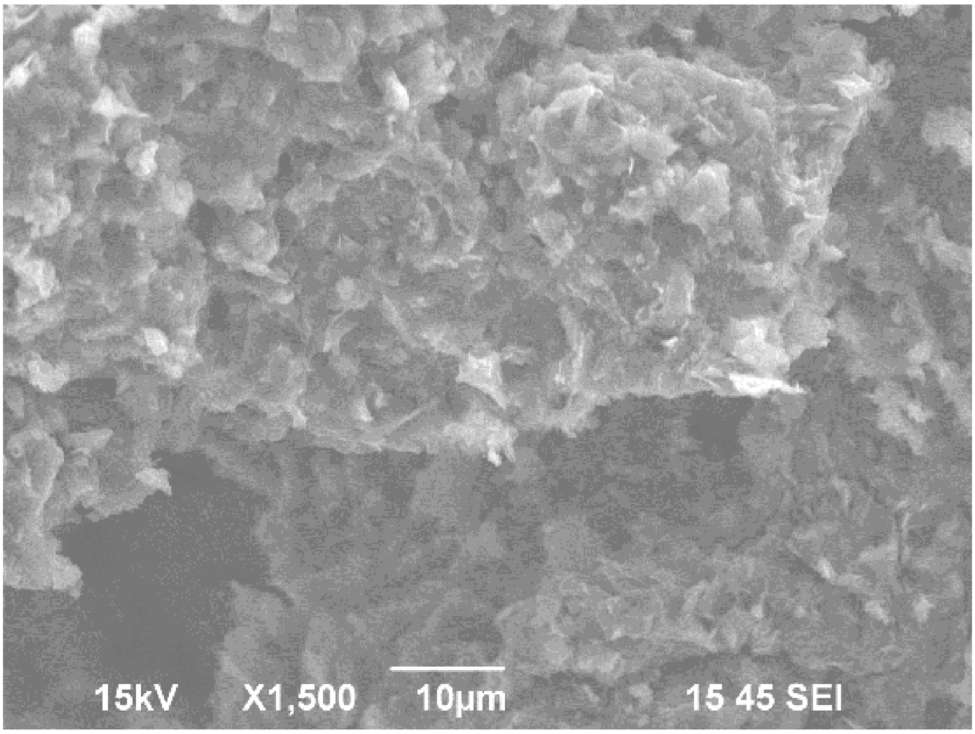

Figure 3-72 Detail SEM image under 30° angle of PCIB sample U165 at detail location 1.

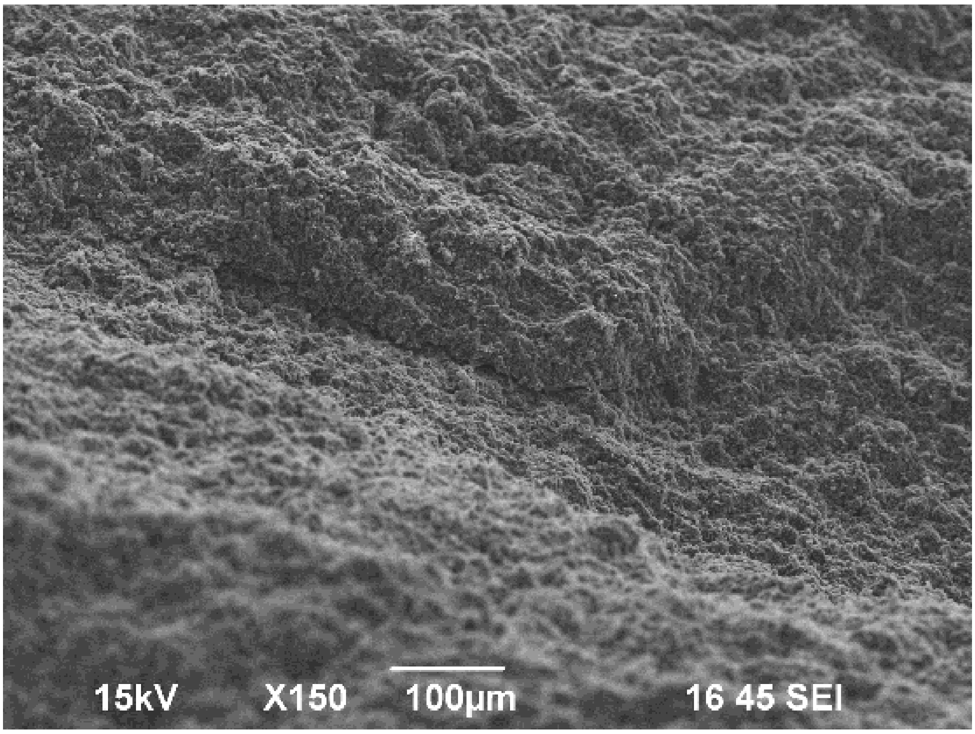

Figure 3-73 Detail SEM image under 30° angle of PCIB sample U165 at detail location 2.

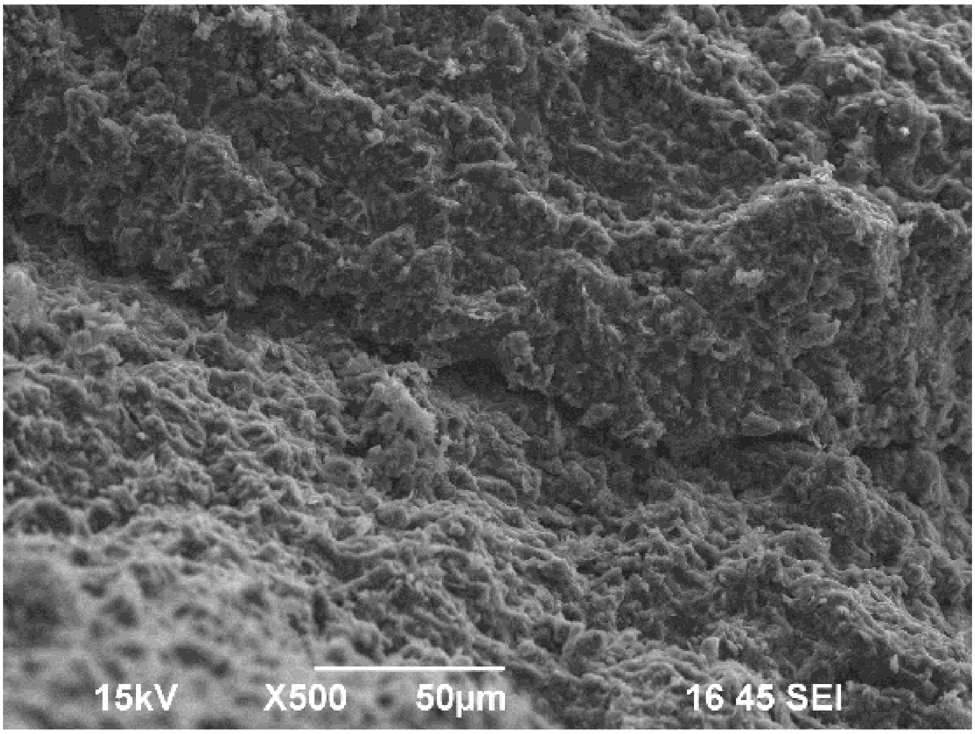

Figure 3-74 Detail SEM image under 30° angle of PCIB sample U165 at detail location 2.

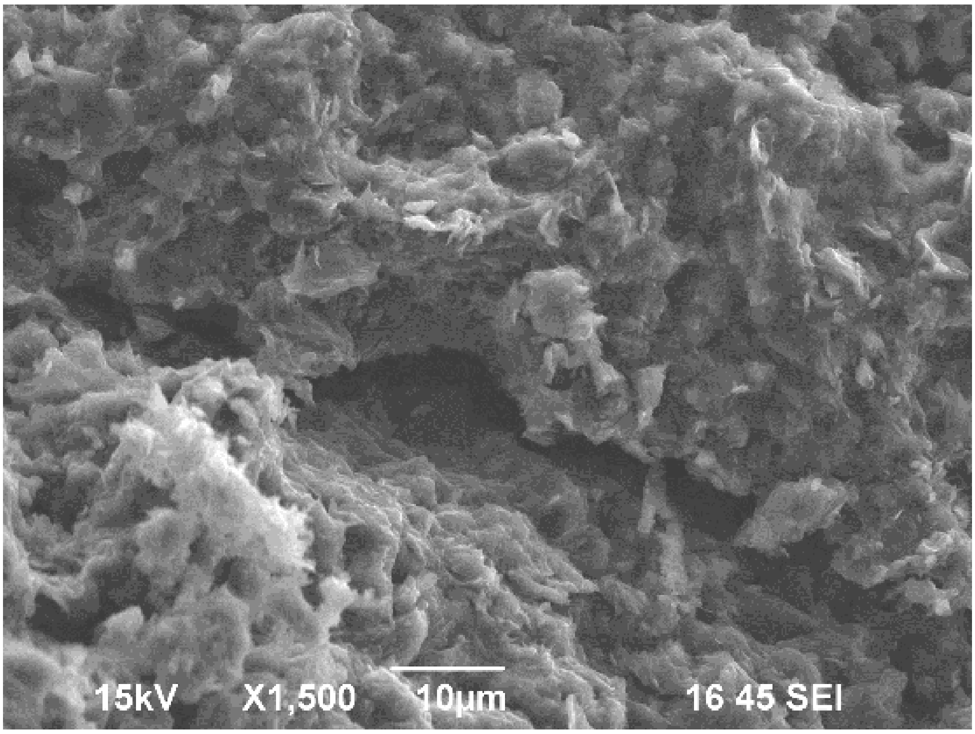

Figure 3-75 Detail SEM image under 30° angle of PCIB sample U165 at detail location 2.

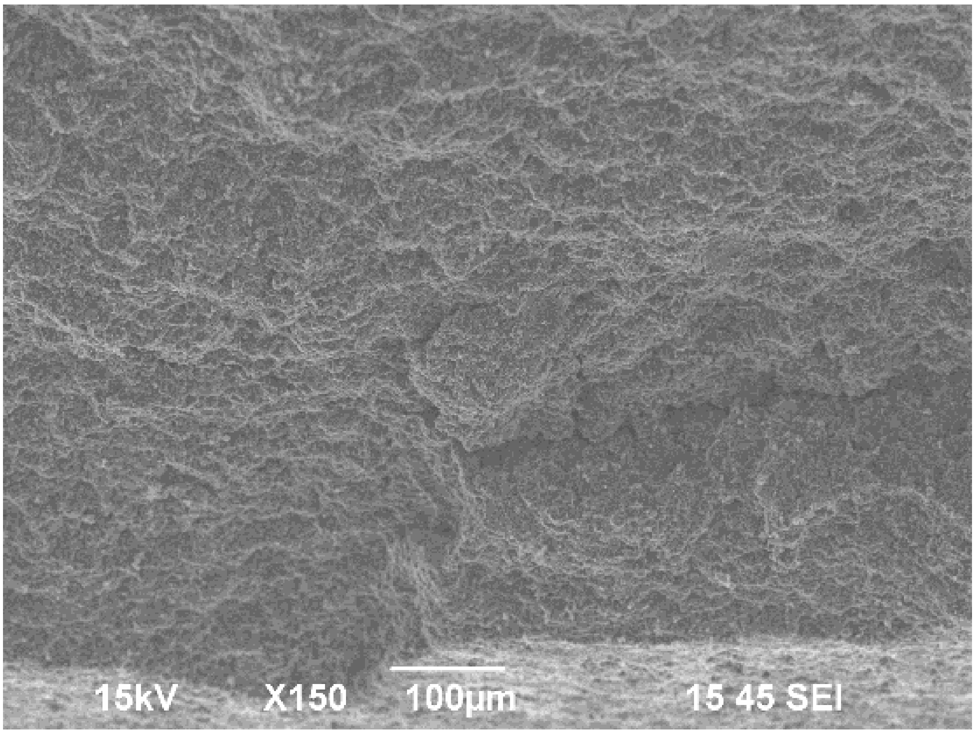

Figure 3-76 Detail SEM image under 30° angle of PCIB sample U165 at detail location 3.

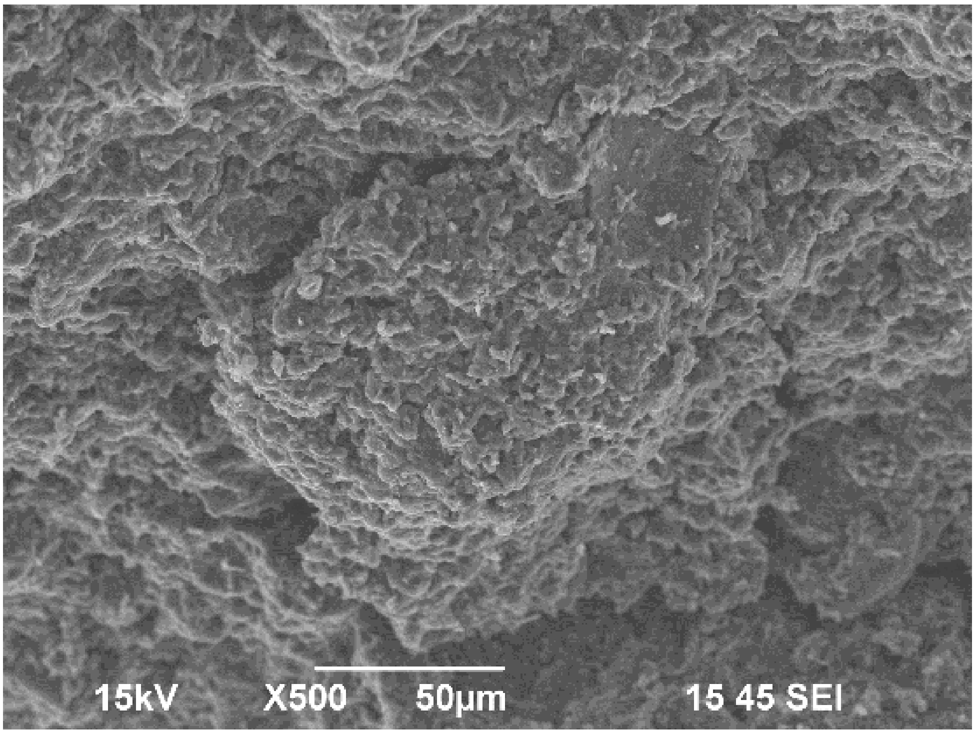

Figure 3-77 Detail SEM image under 30° angle of PCIB sample U165 at detail location 3.

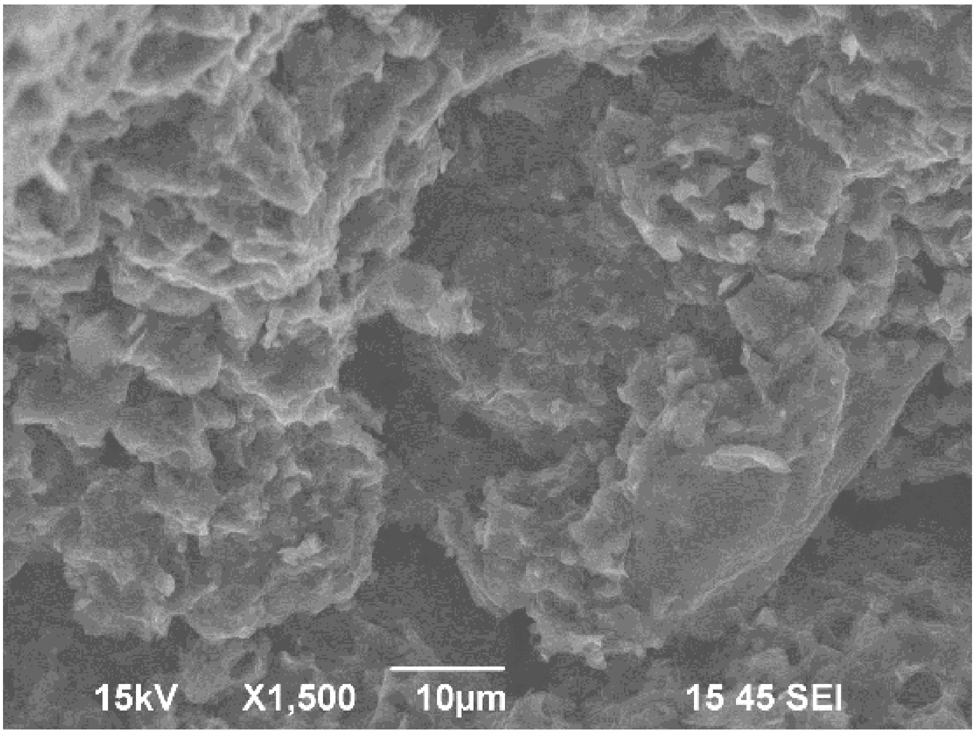

Figure 3-78 Detail SEM image under 30° angle of PCIB sample U165 at detail location 3.

U166, PCIB, 13.4 dpa

Figure 3-79 to Figure 3-85 show the fracture surface of PCIB sample U166, irradiated at 750°C to 13.4 dpa.

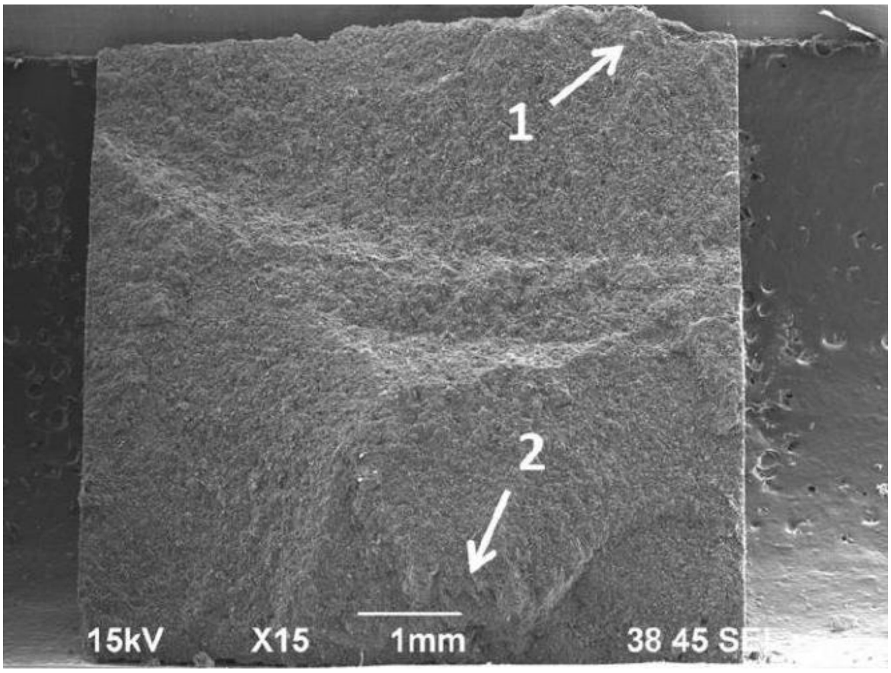

Figure 3-79 Overview SEM images under 30° angle of PCIB sample U166, 13.4 dpa. The numbers indicate the locations of the detail SEM images.

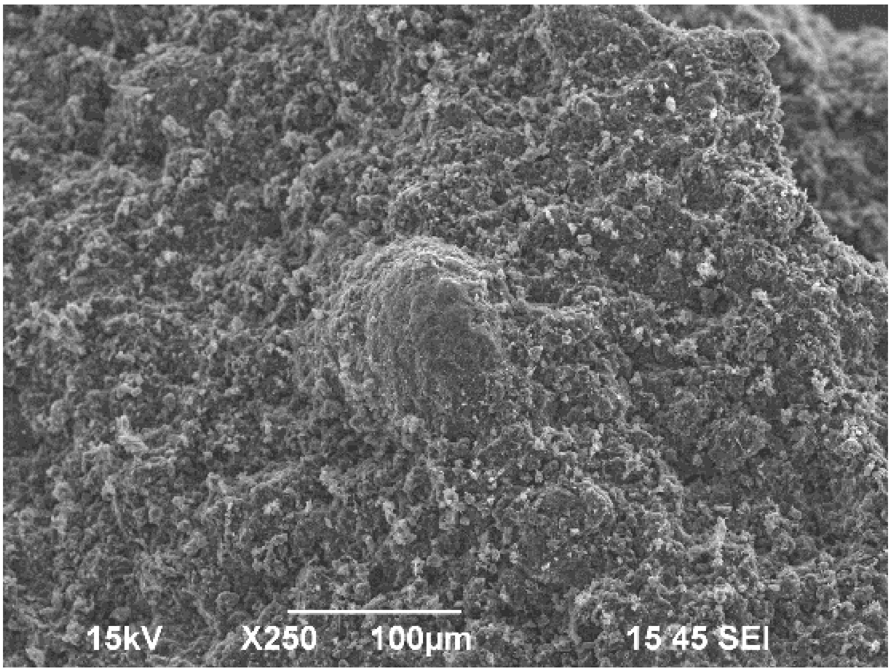

Figure 3-80 Detail SEM image under 30° angle of PCIB sample U166 at detail location 1.

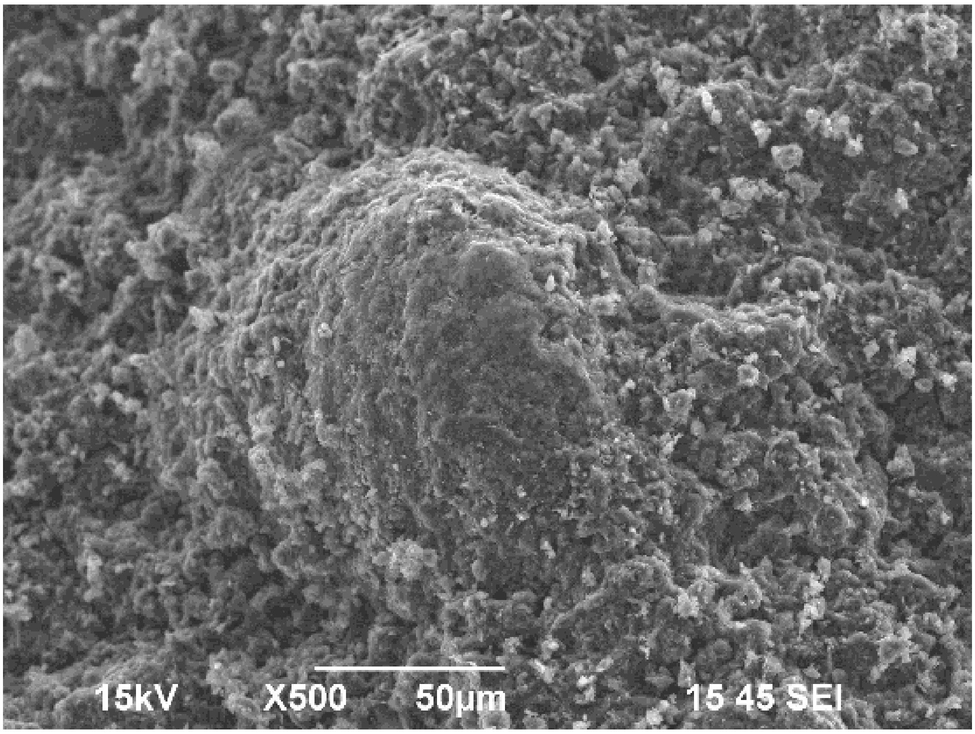

Figure 3-81 Detail SEM image under 30° angle of PCIB sample U166 at detail location 1.

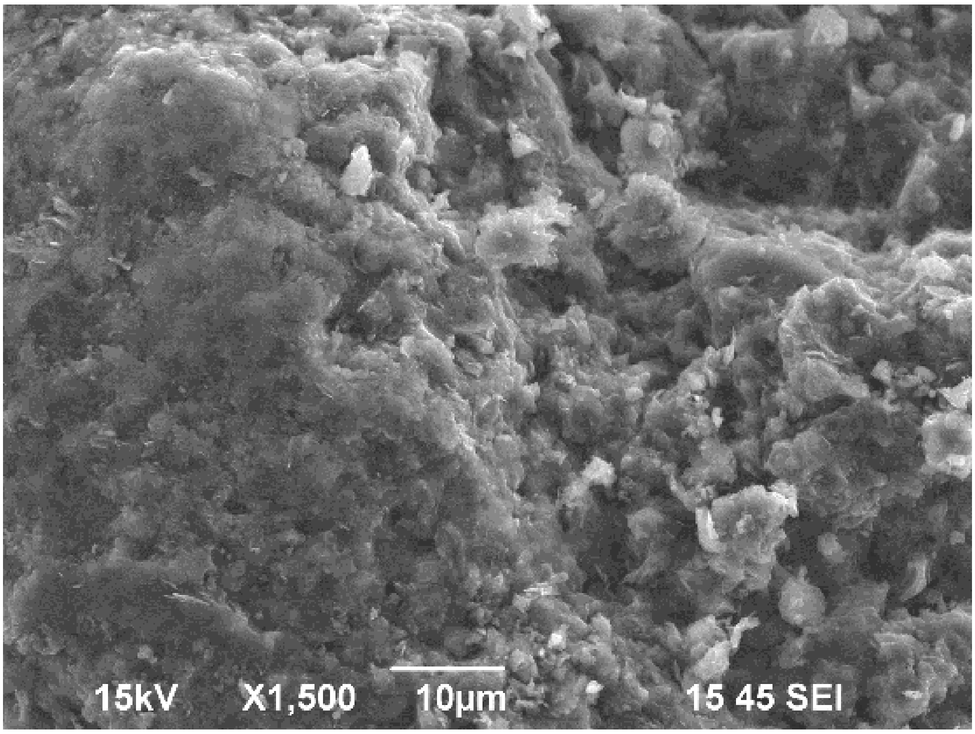

Figure 3-82 Detail SEM image under 30° angle of PCIB sample U166 at detail location 1.

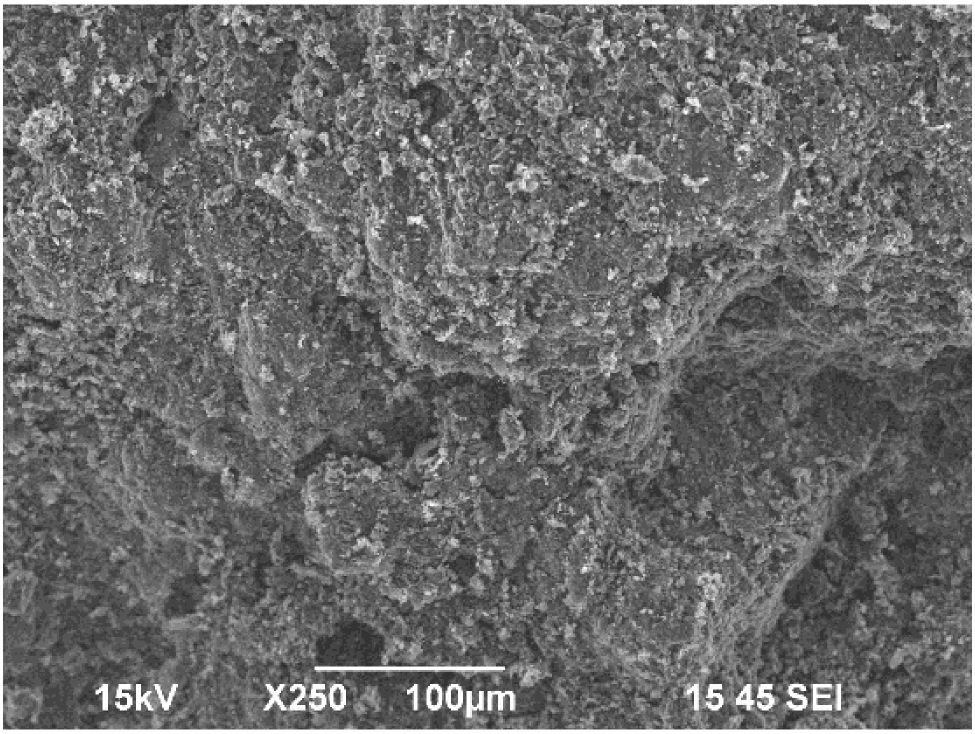

Figure 3-83 Detail SEM image under 30° angle of PCIB sample U166 at detail location 2.

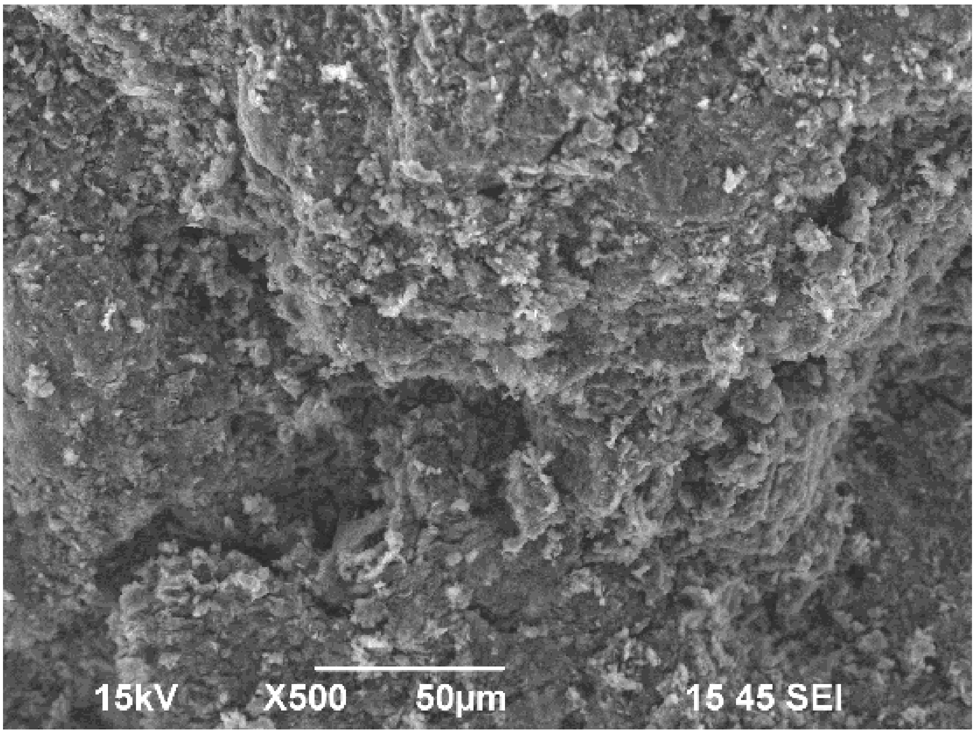

Figure 3-84 Detail SEM image under 30° angle of PCIB sample U166 at detail location 2.

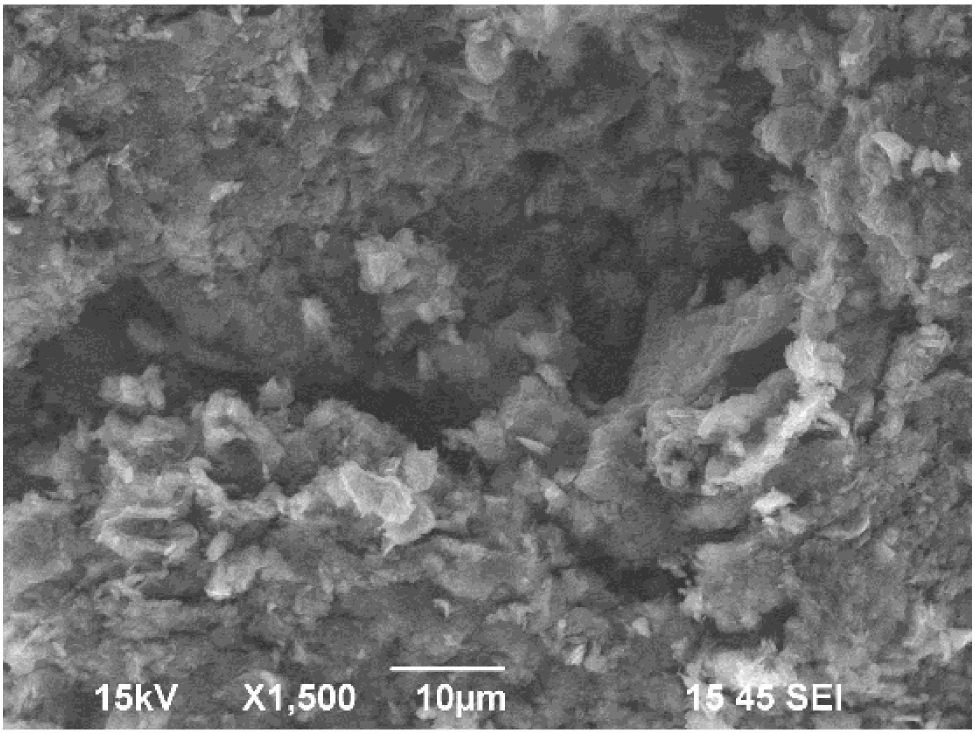

Figure 3-85 Detail SEM image under 30° angle of PCIB sample U166 at detail location 2.

U114, PCIB, 21.1 dpa

Figure 3-86 to Figure 3-95 show the fracture surface of PCIB sample U114, irradiated at 750°C to 21.1 dpa. Two pieces were investigated, one showing a radial fracture surface and one showing an axial fracture surface.

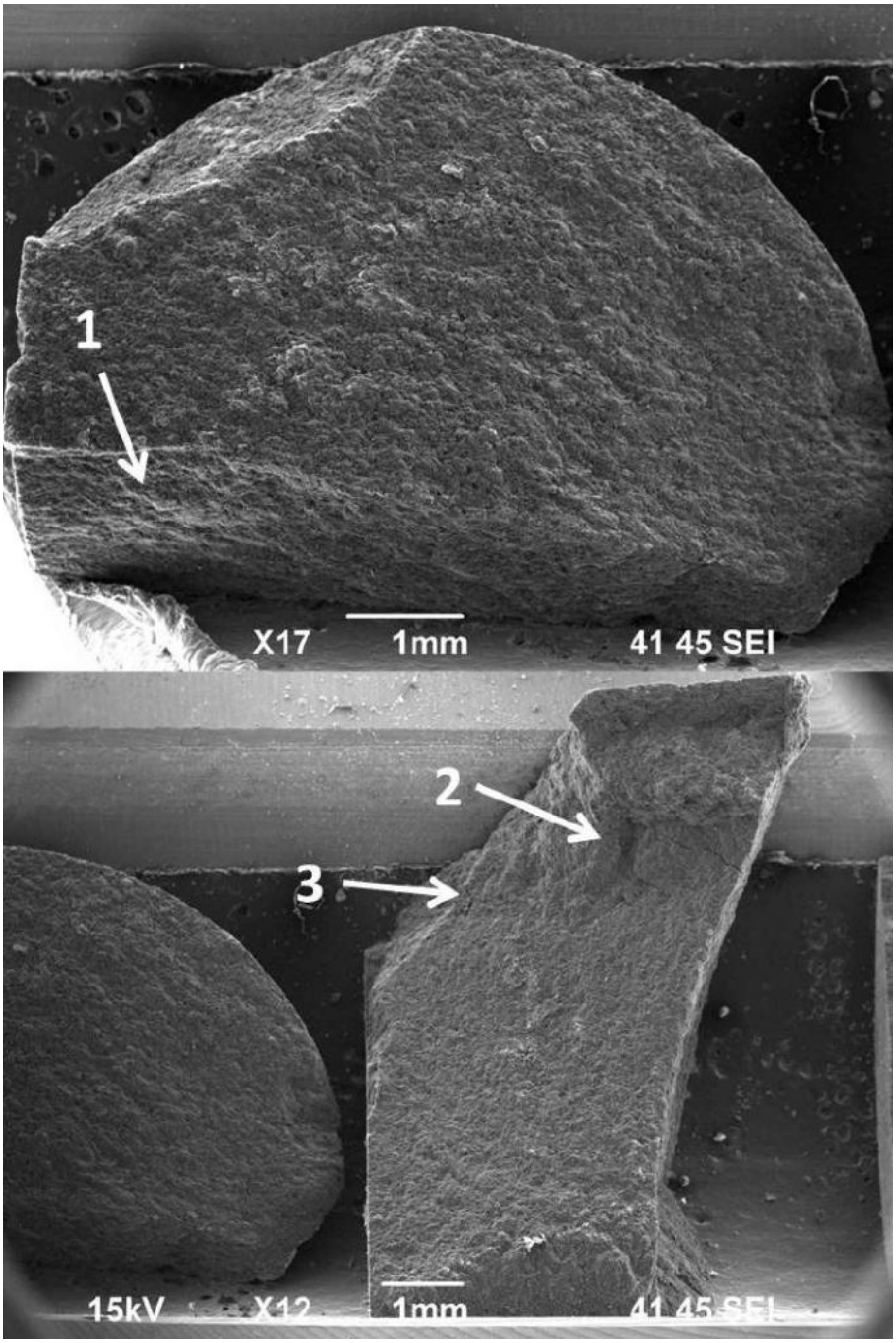

Figure 3-86 Overview SEM images under 30° angle of sample U114, 21.1 dpa. The numbers indicate the locations of the detail SEM images. The top panel shows the radial fracture surface investigated. The bottom panel shows the axial fracture surface.

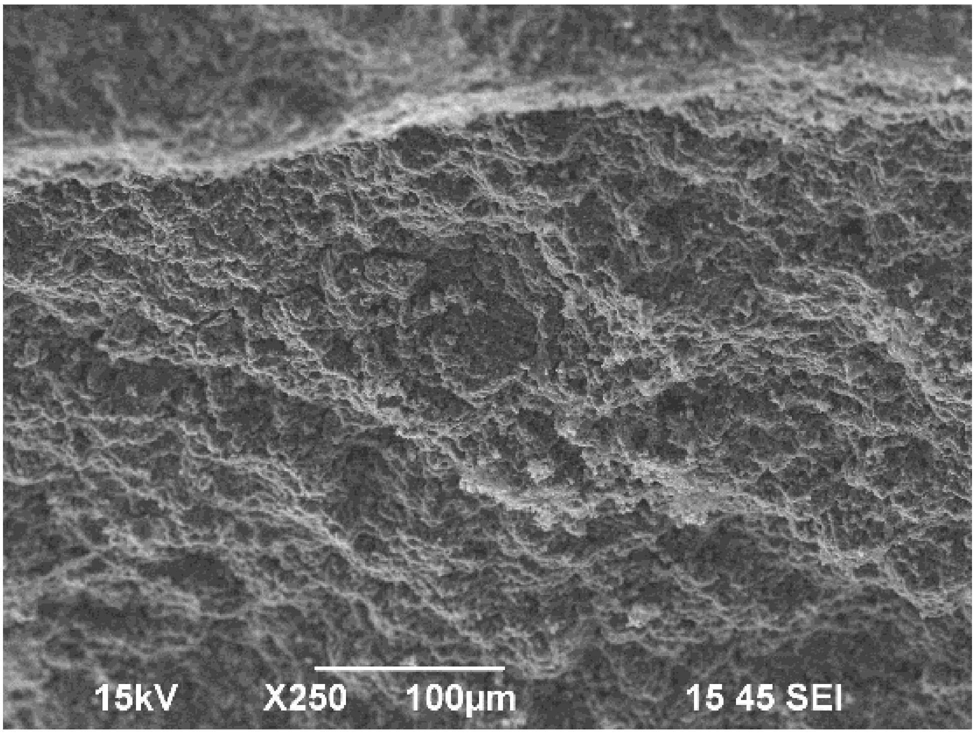

Figure 3-87 Detail SEM image under 30° angle of PCIB sample U114 at detail location 1, on the radial fracture surface.

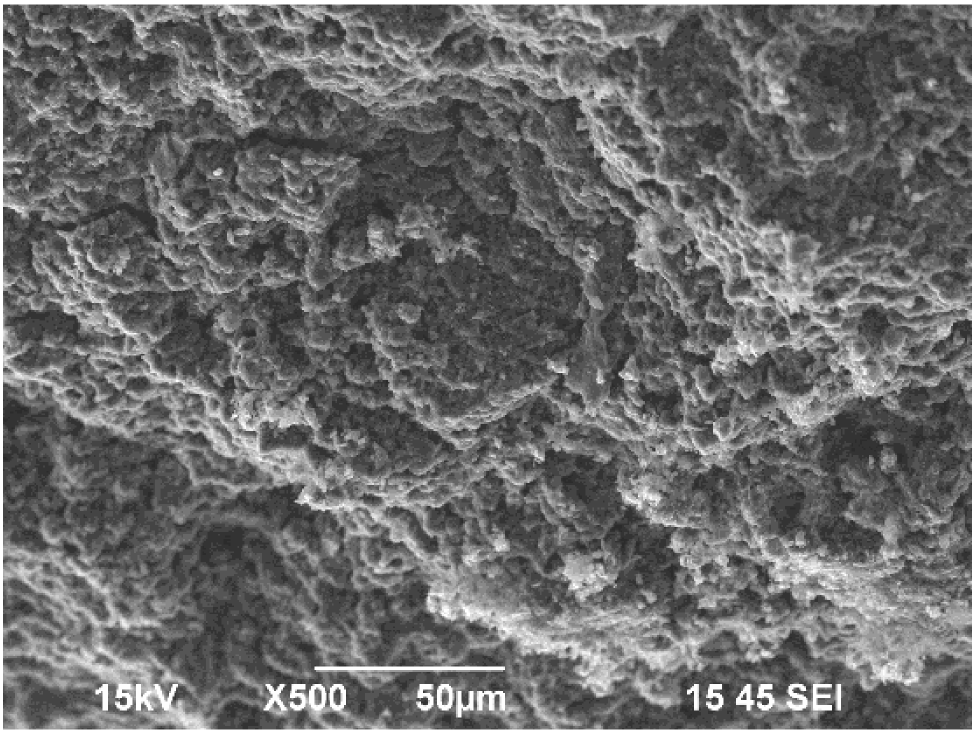

Figure 3-88 Detail SEM image under 30° angle of PCIB sample U114 at detail location 1, on the radial fracture surface.

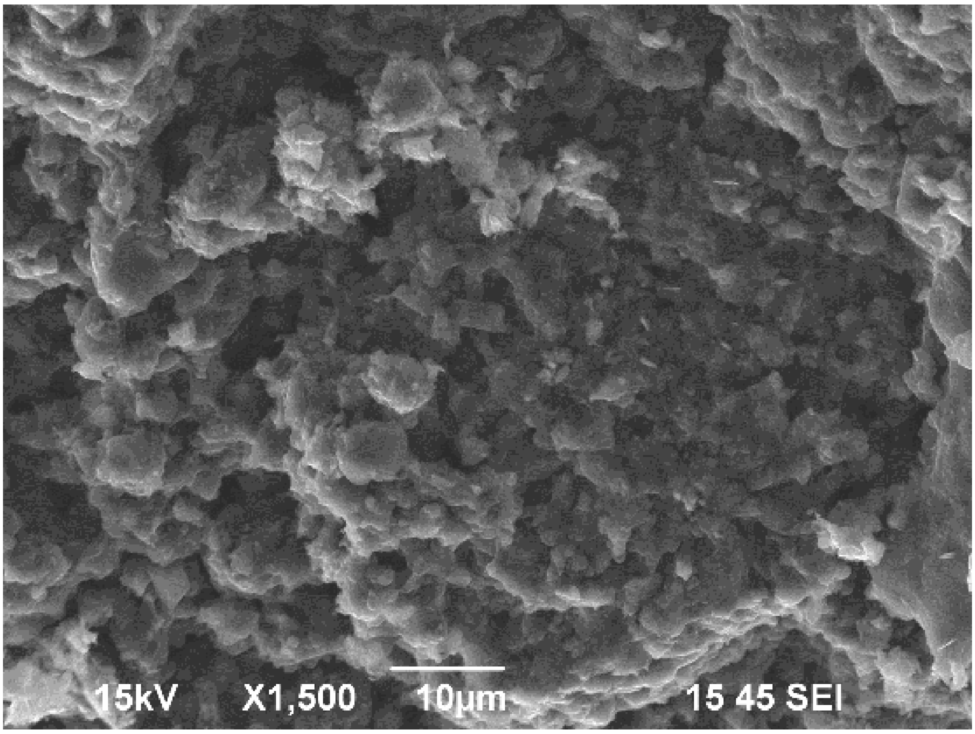

Figure 3-89 Detail SEM image under 30° angle of PCIB sample U114 at detail location 1, on the radial fracture surface.

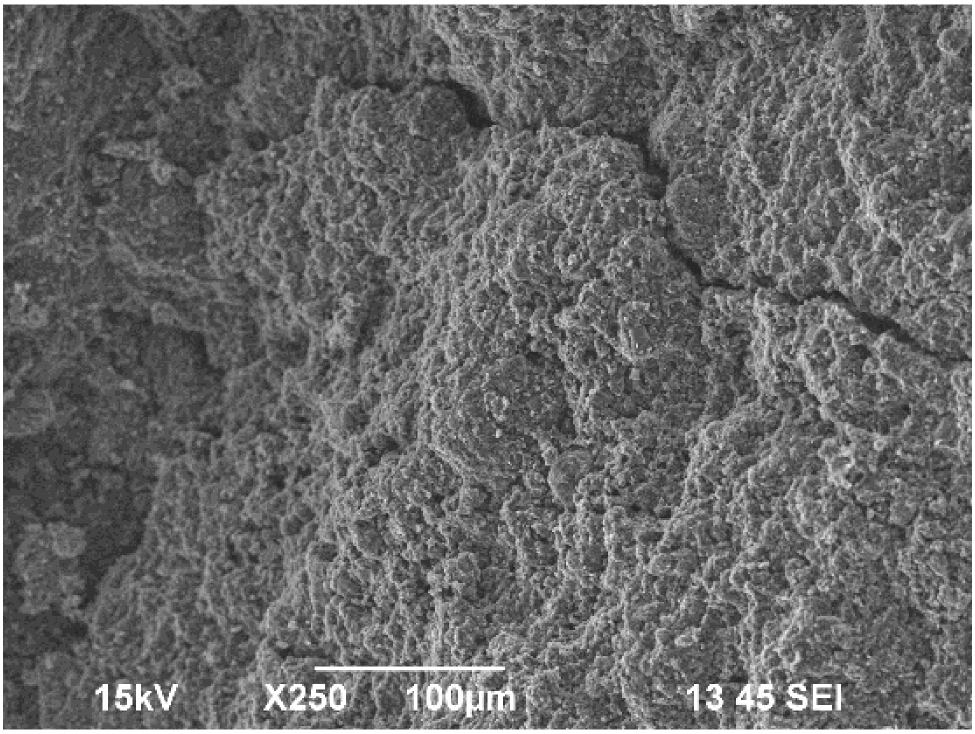

Figure 3-90 Detail SEM image under 30° angle of PCIB sample U114 at detail location 2, on the axial fracture surface.

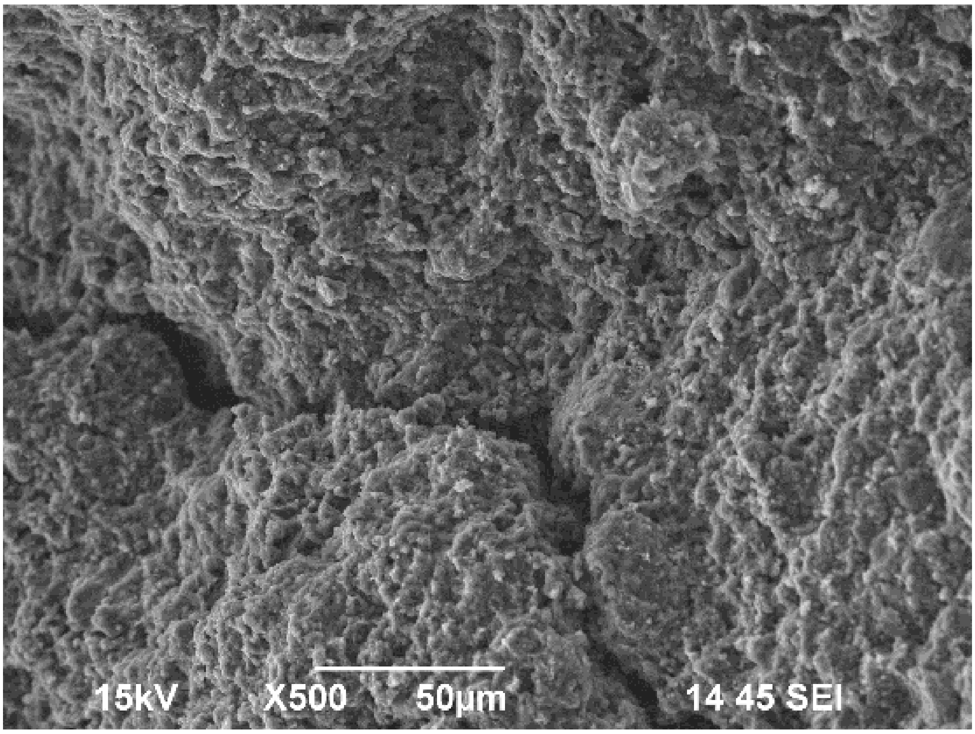

Figure 3-91 Detail SEM image under 30° angle of PCIB sample U114 at detail location 2, on the axial fracture surface.

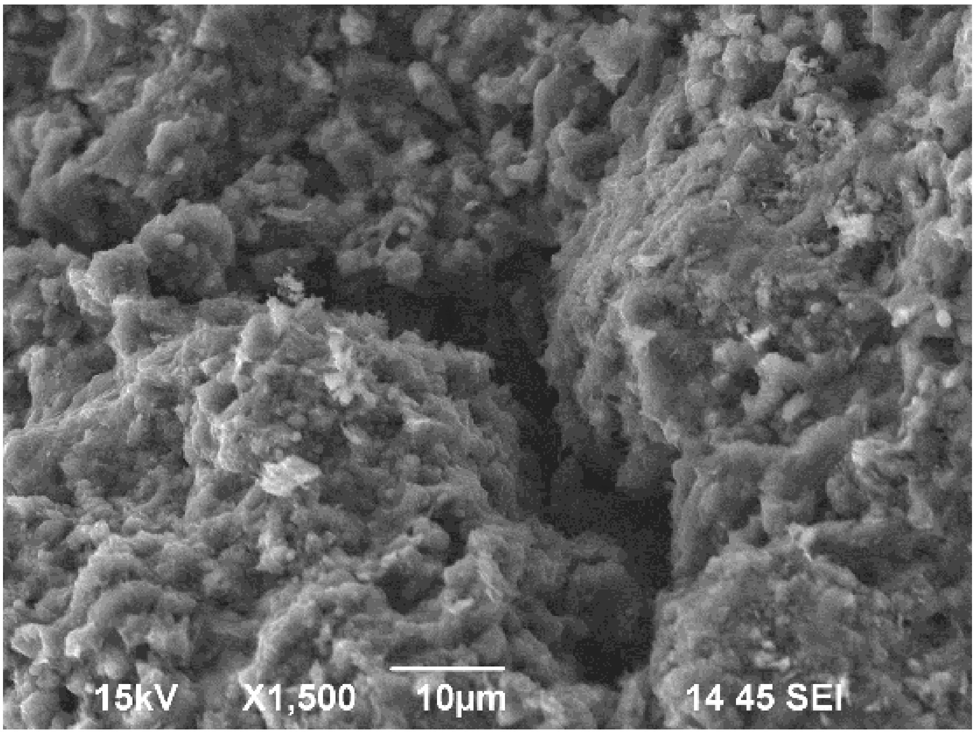

Figure 3-92 Detail SEM image under 30° angle of PCIB sample U114 at detail location 2, on the axial fracture surface.

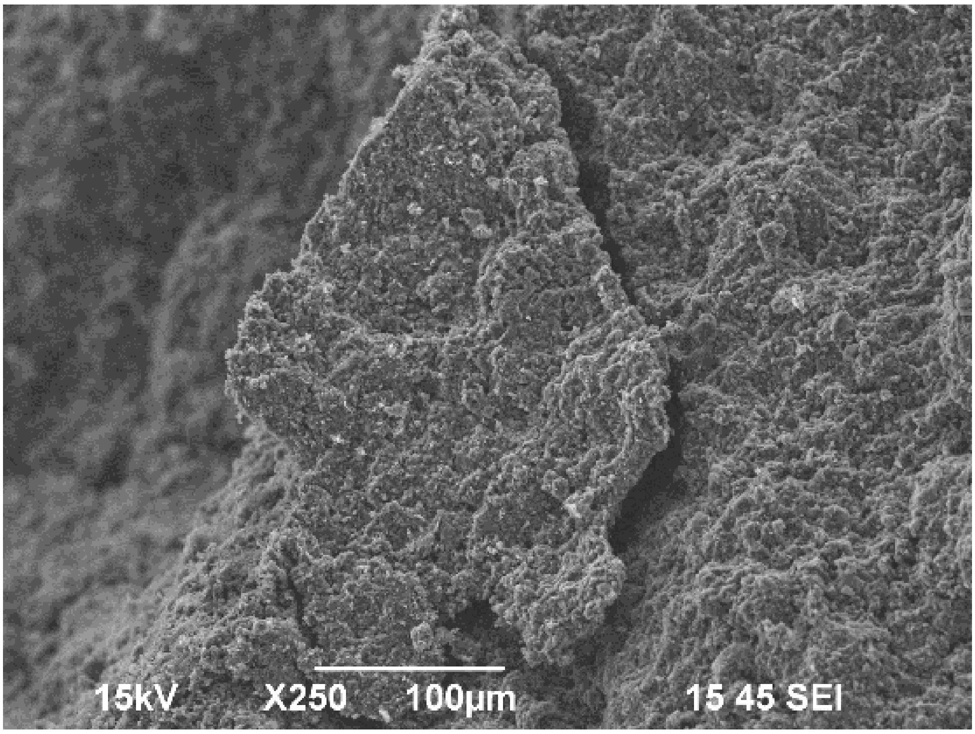

Figure 3-93 Detail SEM image under 30° angle of PCIB sample U114 at detail location 3, on the axial fracture surface.

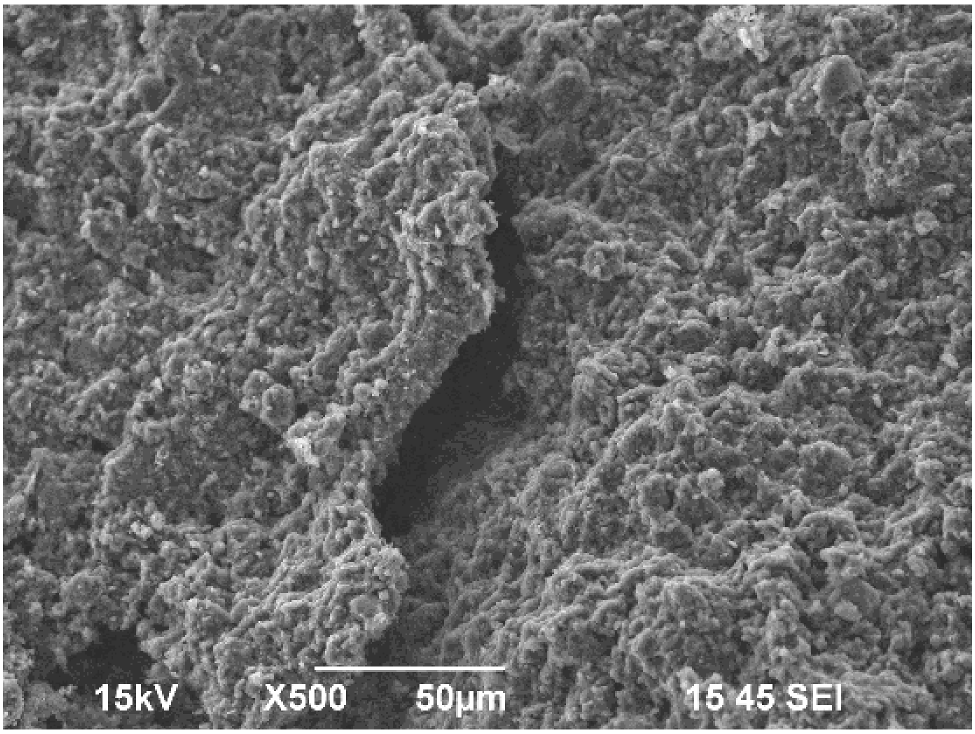

Figure 3-94 Detail SEM image under 30° angle of PCIB sample U114 at detail location 3, on the axial fracture surface.

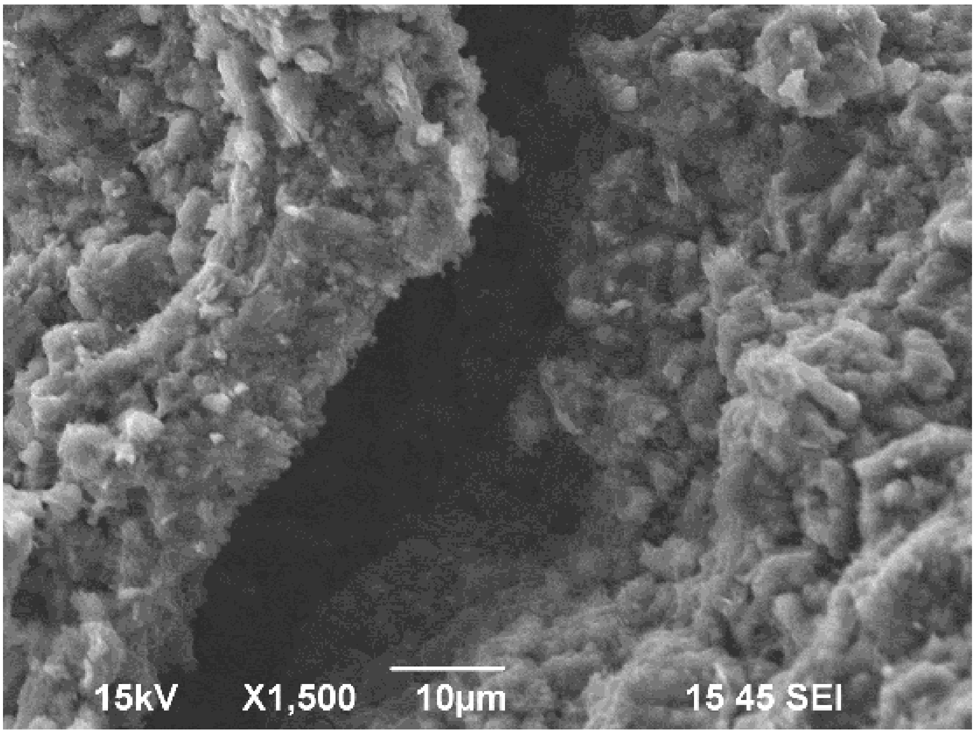

Figure 3-95 Detail SEM image under 30° angle of PCIB sample U114 at detail location 3, on the axial fracture surface.

4 Conclusions

To determine the tensile strength of irradiated HTR graphite grades, diametric compression tests have been successfully conducted on 47 irradiated and 30 unirradiated graphite specimens. In general tensile strength was found to increase with increasing dpa up to around turn-around. After volume change turn-around, the tensile strength decreases again. In some cases the strength almost returns to unirradiated values, in other cases the strength levels out.

On 4 NBG-10 and 6 PCIB specimens that were used for diametric compression fractography using scanning electron microscopy was performed. The images show smoother fracture surfaces for the fine-grained PCIB with respect to the coarse-grained NBG-10, regardless of neutron fluence.

References

[1] F. Schmalz *et al.*, Preliminary irradiation testing of selected graphite grades for HTR, *Final report on HTR-M1 WP3*, 20787/05.71179/P, 19 December 2005.

[2] J.A. Vreeling *et al.*, Designing loading and assembling an irradiation experiment with radioactive samples, *DLM 3.1: Progress on continuation of 750°C graphite irradiation test*, 21457/06.77295/P, 26 October 2006.

[3] J.A. Vreeling*, DML3.8 Continuation of 950°C graphite irradiation, Status March* 2009, NRG-21457/09.94517, 18 March 2009.

[4] J.A. Vreeling, B. Sakintuna, *DML3.13: Full PIE INNOGRAPH-1A and description INNOGRAPH-1B*, NRG-21457/10.101850, 14 April 2010.

[5] J.A. Vreeling, B. Sakintuna, Post Irradiation Examinations of experiment at 950°C, *DML 3.16 Full PIE of INNOGRAPH-2A*, NRG-21457/10.101644, 14 April 2010.

[6] M.C.R. Heijna, D41.12: High dose experiments at 750°C and 950°C, *Full PIE of INNOGRAPH-1B and INNOGRAPH-2B*, NRG-22906/12.111097, 3 April 2012.

[7] M.C.R. Heijna, D41.13: Microstructure analysis on irradiated graphite, *Optical Microscopy and SEM*, NRG-22906/12.117312, 27 November 2012.

[8] O. Wouters, J.A. Vreeling, INNOGRAPH-1B and INNOGRAPH-2A specimen manufacture and pre-characterisation, *DML3.3: Graphite material procurement & characterisation*, NRG-21457/06.77300/P, 23 October 2006.

[9] F.L.L.B. Carniero, A Barcellos, ‘Concrete tensile strength’, Union of Testing and Research Laboratories for Materials and Structures, Paris No. 13, 1953.

[10] T. Akazawa, ‘Tension test method for concrete’, Union of Testing and Research Laboratories for Materials and Structures, Paris No. 16, 1953.

[11] Q.Z. Wang, X.M. Jia, S.Q. Kou, Z.X. Zhang, P.A. Lindqvist, ‘The flattened Brazilian disc specimen used for testing elastic modulus, tensile strength and fracture toughness of brittle rocks: analytical and numerical results’, International Journal of Rock Mechanics and Mining Sciences 41 (2004), p245-253.

[12] S.P. Timoshenko, J.N. Goodier, ‘Theory of elasticity’, McGraw-Hill, New York, 1970.

[13] H. Awaji, ‘Diametral compressive stress considering the Hertzian contact’, Journal of the Society of Materials Science (Japan) 27 (1987), p336-341.

[14] Q.Z. Wang, L.Xin, 'Determination of fracture toughness K_{IC} by using the flattened Brazilian disk specimen for rocks', Engineering Fracture Mechanics 64 (1999), p193-201.

[15] K.N. Kaklis, Z. Agioutantis, E. Sarris, A. Pateli, 'A theoretical and numerical study of discs with flat edges under diametral compression (flat Brazilian test)', 5th GRACM International Congress on Computational Mechanics (2005), Lissamol, Cyprus.

[16] C. Berre, B.J. Marsden, S.L. Fok, A.J. Vreeling, A. de Jong, J. van der Laan, 'Bulk tensile strength measurements of thermally oxidised graphite using the Brazilian disc test', unpublished.

List of tables

Table 1 Selected grades for the INNOGRAPH-1A and -1B irradiation experiments 9

Table 2 Test matrix for the diametric compression tests on irradiated HTR graphite. The samples that are selected for fractography following the diametric compression are high-lighted in light-grey. 83

Table 3 Results of diametric compression tests, including three methods of calculating tensile strength. Also included are the measured contact areas (*w* and 2*b*). Specimen dimensions are given by L (length), D (diameter), and H (diameter at flat side). 85

Table 4 GrafTech PCEA graphite specimens after diametric compression testing.................................. 87

Table 5 GrafTech PCIB graphite specimens after diametric compression testing.................................... 89

Table 6 GrafTech PPEA graphite specimens after diametric compression testing 91

Table 7 SGL NBG-10 graphite specimens after diametric compression testing....................................... 92

Table 8 SGL NBG-17 graphite specimens after diametric compression testing....................................... 93

Table 9 SGL NBG-18 graphite specimens after diametric compression testing....................................... 96

Table 10. Toyo Tanso IG-110 graphite specimens after diametric compression testing. 97

List of figures

Figure 1-1 Schematic overview of the four INNOGRAPH irradiation experiments 8

Figure 2-1 Flattening of the specimens. The figure on the left-hand side exaggeratedly shows the flatting of the cylinder. The figure on the right-hand side is a top-view of the specimen............ 10

Figure 2-2 Schematic drawing of the INNOGRAPH-1B experiment, showing the eight drums that contain the graphite samples 12

Figure 2-3 Schematic volume change versus neutron fluence curve, with indicated characteristic regions in these type of curves: 0) Virgin. 1) Shrinking. 2) Turn-around. 3) Swelling. 4) Cross-over. 5) Swollen. 13

Figure 2-4 Plots of the relative volume change versus dpa for SGL graphite grades irradiated at 750°C in which the samples selected for diametric compression are indicated. 14

Figure 2-5 Plots of the relative volume change versus dpa for GrafTech graphite grades irradiated at 750°C in which the samples selected for diametric compression are indicated. 15

Figure 2-6 Plot of the relative volume change versus dpa for Toyo Tanso IG-110 graphite irradiated at 750°C in which the samples selected for diametric compression are indicated. 15

Figure 2-7 Schematic representation of the diametric compression load distribution for, from left to right, a point contact, distributed contact, a sample with flattened sides, and a sample with one flat side and using a curved anvil. 17

Figure 2-8 Schematic representation of the cutting and tensile strength directions in diametric compression tests. The axes on the right show how the unique axis and non-unique plane are defined for two situations: unique direction parallel to the cutting direction, and unique direction orthogonal to the cutting directions. 17

Figure 2-9 Graphite sample mounted in the tensile stage for diametric compression testing. 18

Figure 3-1 Two typical load-displacement curves for the diametric compression tests on irradiated graphite samples. The black solid line shows failure in two steps, the red dashed line failure in a single step. 20

Figure 3-2 Tensile strength as determined from diametric compression for GrafTech graphite grades PCEA, PCIB, and PPEA irradiated at 750°C. Note that the AG and WG directions are sample cutting directions and not tensile strength directions. 21

Figure 3-3 Tensile strength as determined from diametric compression for Toyo Tanso IG-110 graphite irradiated at 750°C. Note that the AG and WG directions are sample cutting directions and not tensile strength directions. 21

Figure 3-4 Tensile strength as determined from diametric compression for SGL graphite grades NBG-10, NBG-17, and NBG-18 irradiated at 750°C. Note that the AG and WG directions are sample cutting directions and not tensile strength directions. 22

Figure 3-5 Overview SEM image under 30° angle of NBG-10 sample 0S31, 0 dpa. The numbers indicate the locations of the detail SEM images. 23

Figure 3-6 Detail SEM image under 30° angle of NBG-10 sample 0S31 at detail location 1. 23

Figure 3-7 Detail SEM image under 30° angle of NBG-10 sample 0S31 at detail location 1. 24

Figure 3-8 Detail SEM image under 30° angle of NBG-10 sample 0S31 at detail location 1. 24

Figure 3-9 Detail SEM image under 30° angle of NBG-10 sample 0S31 at detail location 2. 25

Figure 3-10 Detail SEM image under 30° angle of NBG-10 sample 0S31 at detail location 2. 25

Figure 3-11 Detail SEM image under 30° angle of NBG-10 sample 0S31 at detail location 3. 26

Figure 3-12 Detail SEM image under 30° angle of NBG-10 sample 0S31 at detail location 3. 26

Figure 3-13 Overview SEM images under 30° angle of both halves of NBG-10 sample S050, 6.5 dpa. The numbers indicate the locations of the detail SEM images. 27

Figure 3-14 Detail SEM image under 0° angle of NBG-10 sample S050 at detail location 1. 28

Figure 3-15 Detail SEM image under 0° angle of NBG-10 sample S050 at detail location 1. 28

Figure 3-16 Detail SEM image under 30° angle of NBG-10 sample S050 at detail location 2. 29

Figure 3-17 Detail SEM image under 30° angle of NBG-10 sample S050 at detail location 2. 29

Figure 3-18 Detail SEM image under 30° angle of NBG-10 sample S050 at detail location 3. This feature is the inverse of the feature shown in Figure 3-17. 30

Figure 3-19 Detail SEM image under 30° angle of NBG-10 sample S050 at detail location 3. This feature is the inverse of the feature shown in Figure 3-18. 30

Figure 3-20 Detail SEM image under 30° angle of NBG-10 sample S050 at detail location 4. 31

Figure 3-21 Detail SEM image under 30° angle of NBG-10 sample S050 at detail location 4. 31

Figure 3-22 Overview SEM images under 30° angle of both halves of NBG-10 sample S051, 12.8 dpa. The numbers indicate the locations of the detail SEM images. 32

Figure 3-23 Detail SEM image under 30° angle of NBG-10 sample S051 at detail location 1. 33

Figure 3-24 Detail SEM image under 30° angle of NBG-10 sample S051 at detail location 2. 33

Figure 3-25 Detail SEM image under 30° angle of NBG-10 sample S051 at detail location 2. 34

Figure 3-26 Detail SEM image under 30° angle of NBG-10 sample S051 at detail location 2. 34

Figure 3-27 Detail SEM image under 30° angle of NBG-10 sample S051 at detail location 2. 35

Figure 3-28 Detail SEM image under 30° angle of NBG-10 sample S051 at detail location 3. 35

Figure 3-29 Detail SEM image under 30° angle of NBG-10 sample S051 at detail location 3. 36

Figure 3-30 Detail SEM image under 30° angle of NBG-10 sample S051 at detail location 3. 36

Figure 3-31 Overview SEM images under 30° angle of NBG-10 sample S042, 22.3 dpa. The numbers indicate the locations of the detail SEM images. 37

Figure 3-32 Detail SEM image under 30° angle of NBG-10 sample S042 at detail location 1. 37

Figure 3-33 Detail SEM image under 30° angle of NBG-10 sample S042 at detail location 1. 38

Figure 3-34 Detail SEM image under 30° angle of NBG-10 sample S042 at detail location 1. 38

Figure 3-35 Detail SEM image under 30° angle of NBG-10 sample S042 at detail location 2. 39

Figure 3-36 Detail SEM image under 30° angle of NBG-10 sample S042 at detail location 2. 39

Figure 3-37 Detail SEM image under 30° angle of NBG-10 sample S042 at detail location 2. 40

Figure 3-38 Overview SEM images under 30° angle of PCIB sample 1U00, 0 dpa. The numbers indicate the locations of the detail SEM images. 41

Figure 3-39 Detail SEM image under 30° angle of PCIB sample 1U00 at detail location 1. 41

Figure 3-40 Detail SEM image under 30° angle of PCIB sample 1U00 at detail location 1. 42

Figure 3-41 Detail SEM image under 30° angle of PCIB sample 1U00 at detail location 1. 42

Figure 3-42 Detail SEM image under 30° angle of PCIB sample 1U00 at detail location 2. 43

Figure 3-43 Detail SEM image under 30° angle of PCIB sample 1U00 at detail location 2. 43

Figure 3-44 Detail SEM image under 30° angle of PCIB sample 1U00 at detail location 3. 44

Figure 3-45 Detail SEM image under 30° angle of PCIB sample 1U00 at detail location 3. 44

Figure 3-46 Detail SEM image under 30° angle of PCIB sample 1U00 at detail location 4. 45

Figure 3-47 Detail SEM image under 30° angle of PCIB sample 1U00 at detail location 4. 45

Figure 3-48 Detail SEM image under 30° angle of PCIB sample 1U00 at detail location 4. 46

Figure 3-49 Overview SEM images under 30° angle of PCIB sample U111, 6.3 dpa. The numbers indicate the locations of the detail SEM images. 47

Figure 3-50 Detail SEM image under 30° angle of PCIB sample U111 at detail location 1. 47

Figure 3-51 Detail SEM image under 30° angle of PCIB sample U111 at detail location 1. 48

Figure 3-52 Detail SEM image under 30° angle of PCIB sample U111 at detail location 1. 48

Figure 3-53 Detail SEM image under 30° angle of PCIB sample U111 at detail location 2. 49

Figure 3-54 Detail SEM image under 30° angle of PCIB sample U111 at detail location 2. 49

Figure 3-55 Detail SEM image under 30° angle of PCIB sample U111 at detail location 2. 50

Figure 3-56 Detail SEM image under 30° angle of PCIB sample U111 at detail location 3. 50

Figure 3-57 Detail SEM image under 30° angle of PCIB sample U111 at detail location 3. 51

Figure 3-58 Detail SEM image under 30° angle of PCIB sample U111 at detail location 3. 51

Figure 3-59 Overview SEM images under 30° angle of PCIB sample U198, 7.7 dpa. The numbers indicate the locations of the detail SEM images. 52

Figure 3-60 Detail SEM image under 30° angle of PCIB sample U198 at detail location 1. 52

Figure 3-61 Detail SEM image under 30° angle of PCIB sample U198 at detail location 1. 53

Figure 3-62 Detail SEM image under 30° angle of PCIB sample U198 at detail location 1. 53

Figure 3-63 Detail SEM image under 30° angle of PCIB sample U198 at detail location2. 54

Figure 3-64 Detail SEM image under 30° angle of PCIB sample U198 at detail location 2. 54

Figure 3-65 Detail SEM image under 30° angle of PCIB sample U198 at detail location 2. 55

Figure 3-66 Detail SEM image under 30° angle of PCIB sample U198 at detail location 3. 55

Figure 3-67 Detail SEM image under 30° angle of PCIB sample U198 at detail location 3. 56

Figure 3-68 Detail SEM image under 30° angle of PCIB sample U198 at detail location 3. 56

Figure 3-69 Overview SEM images under 30° angle of PCIB sample U165, 9.8 dpa. The numbers indicate the locations of the detail SEM images. 57

Figure 3-70 Detail SEM image under 30° angle of PCIB sample U165 at detail location 1. 57

Figure 3-71 Detail SEM image under 30° angle of PCIB sample U165 at detail location 1. 58

Figure 3-72 Detail SEM image under 30° angle of PCIB sample U165 at detail location 1. 58

Figure 3-73 Detail SEM image under 30° angle of PCIB sample U165 at detail location 2. 59

Figure 3-74 Detail SEM image under 30° angle of PCIB sample U165 at detail location 2. 59

Figure 3-75 Detail SEM image under 30° angle of PCIB sample U165 at detail location 2. 60

Figure 3-76 Detail SEM image under 30° angle of PCIB sample U165 at detail location 3. 60

Figure 3-77 Detail SEM image under 30° angle of PCIB sample U165 at detail location 3. 61

Figure 3-78 Detail SEM image under 30° angle of PCIB sample U165 at detail location 3. 61

Figure 3-79 Overview SEM images under 30° angle of PCIB sample U166, 13.4 dpa. The numbers indicate the locations of the detail SEM images. 62

Figure 3-80 Detail SEM image under 30° angle of PCIB sample U166 at detail location 1. 62

Figure 3-81 Detail SEM image under 30° angle of PCIB sample U166 at detail location 1. 63

Figure 3-82 Detail SEM image under 30° angle of PCIB sample U166 at detail location 1. 63

Figure 3-83 Detail SEM image under 30° angle of PCIB sample U166 at detail location 2. 64

Figure 3-84 Detail SEM image under 30° angle of PCIB sample U166 at detail location 2. 64

Figure 3-85 Detail SEM image under 30° angle of PCIB sample U166 at detail location 2. 65

Figure 3-86 Overview SEM images under 30° angle of sample U114, 21.1 dpa. The numbers indicate the locations of the detail SEM images. The top panel shows the radial fracture surface investigated. The bottom panel shows the axial fracture surface. 66

Figure 3-87 Detail SEM image under 30° angle of PCIB sample U114 at detail location 1, on the radial fracture surface. 67

Figure 3-88 Detail SEM image under 30° angle of PCIB sample U114 at detail location 1, on the radial fracture surface. 67

Figure 3-89 Detail SEM image under 30° angle of PCIB sample U114 at detail location 1, on the radial fracture surface. 68

Figure 3-90 Detail SEM image under 30° angle of PCIB sample U114 at detail location 2, on the axial fracture surface. 68

Figure 3-91 Detail SEM image under 30° angle of PCIB sample U114 at detail location 2, on the axial fracture surface. 69

Figure 3-92 Detail SEM image under 30° angle of PCIB sample U114 at detail location 2, on the axial fracture surface. 69

Figure 3-93 Detail SEM image under 30° angle of PCIB sample U114 at detail location 3, on the axial fracture surface. 70

Figure 3-94 Detail SEM image under 30° angle of PCIB sample U114 at detail location 3, on the axial fracture surface. 70

Figure 3-95 Detail SEM image under 30° angle of PCIB sample U114 at detail location 3, on the axial fracture surface. 71

Appendix A Test Matrix

Table 2 Test matrix for the diametric compression tests on irradiated HTR graphite. The samples that are selected for fractography following the diametric compression are high-lighted in light-grey.

Specimen code	Grade	Location	Orientation	dpa
0T04	IG-110	heart	AG	0
0T05	IG-110	heart	AG	0
0T06	IG-110	heart	AG	0
0T07	IG-110	heart	AG	0
0T08	IG-110	heart	AG	0
0T27	IG-110	edge	AG	0
0T28	IG-110	edge	AG	0
0T29	IG-110	edge	AG	0
0T30	IG-110	edge	AG	0
0T31	IG-110	edge	AG	0
T010	IG-110	heart	AG	6.9
T039	IG-110	edge	AG	9.1
T014	IG-110	heart	AG	13.6
T011	IG-110	heart	AG	23.4
T026	IG-110	heart	WG	6.5
T049	IG-110	edge	WG	7.9
T052	IG-110	edge	WG	11.5
T022	IG-110	heart	WG	17.4
T048	IG-110	edge	WG	21.5
0S31	NBG-10	heart	AG	0
S050	NBG-10	heart	AG	6.5
S051	NBG-10	heart	AG	12.8
S042	NBG-10	heart	AG	22.3
0S06	NBG-10	heart	WG	0
S032	NBG-10	heart	WG	6.8
S064	NBG-10	edge	WG	10.4
S068	NBG-10	edge	WG	13.5
S031	NBG-10	heart	WG	16.9
S033	NBG-10	heart	WG	22.2
1S30	NBG-17	heart	AG	0
1S31	NBG-17	heart	AG	0
1S32	NBG-17	heart	AG	0
1S33	NBG-17	heart	AG	0
1S34	NBG-17	heart	AG	0
S619	NBG-17	heart	AG	8.3
S571	NBG-17	edge	AG	10.8
S617	NBG-17	heart	AG	12.6

Specimen code	Grade	Location	Orientation	dpa
S568	NBG-17	edge	AG	13.2
1S07	NBG-17	heart	WG	0
1S08	NBG-17	heart	WG	0
1S09	NBG-17	heart	WG	0
1S10	NBG-17	heart	WG	0
1S11	NBG-17	heart	WG	0
2S31	NBG-18	heart	AG	0
S479	NBG-18	edge	AG	9.2
S524	NBG-18	heart	AG	11.4
S478	NBG-18	edge	AG	12.6
S523	NBG-18	heart	AG	13.2
2S06	NBG-18	heart	WG	0
0U25	PCEA	heart	AG	0
U025	PCEA	heart	AG	7.5
U043	PCEA	heart	AG	11.6
U042	PCEA	heart	AG	13.2
U024	PCEA	heart	AG	17.9
U023	PCEA	heart	AG	22.2
0U00	PCEA	heart	WG	0
U008	PCEA	heart	WG	6.3
U053	PCEA	heart	WG	11.8
U104	PCEA	edge	WG	13
U004	PCEA	heart	WG	17.8
U005	PCEA	heart	WG	22.4
1U00	PCIB	heart	AG	0
U111	PCIB	heart	AG	6.3
U198	PCIB	edge	AG	7.7
U165	PCIB	heart	AG	9.8
U166	PCIB	heart	AG	13.4
U114	PCIB	heart	AG	21.1
1U30	PCIB	heart	WG	0
U127	PCIB	heart	WG	5.8
U126	PCIB	heart	WG	6.6
U193	PCIB	edge	WG	8.6
U192	PCIB	edge	WG	9.3
2U29	PPEA	heart	AG	0
U258	PPEA	heart	AG	12.8
U236	PPEA	heart	AG	19.9
2U05	PPEA	heart	WG	0
U280	PPEA	heart	WG	6

Appendix B Results of the tensile strength measurements

Table 3 Results of diametric compression tests, including three methods of calculating tensile strength. Also included are the measured contact areas (*w* and 2*b*). Specimen dimensions are given by L (length), D (diameter), and H (diameter at flat side).

Specimen code	Grade	Orientation	Location	dpa	σ_H [MPa]	σ_P [MPa]	σ_α [MPa]	F_{fail} [N]	L [mm]	H [mm]	D [mm]	2b [mm]	α [°]	w [mm]	Failure location
0S06	NBG-10	WG	heart	0	15.3	18.4	5.9	1328	5.956	7.696	7.979	3.2	22.0	3.00	Near middle
0S31	NBG-10	AG	heart	0	15.4	18.9	6.0	1358	5.958	7.687	7.962	3.3	22.0	3.00	Right of middle
0T04	IG-110	AG	heart	0	17.0	23.3	7.4	1673	5.938	7.712	7.974	4.0	21.9	3.00	Middle
0T05	IG-110	AG	heart	0	17.3	23.7	7.5	1702	5.937	7.712	7.976	4.0	21.9	3.00	Through middle
0T06	IG-110	AG	heart	0	17.2	23.0	7.3	1653	5.942	7.709	7.979	3.9	22.0	3.00	middle to sides of flat side
0T07	IG-110	AG	heart	0	17.7	23.5	7.4	1688	5.938	7.709	7.976	3.8	22.0	3.00	Near middle
0T08	IG-110	AG	heart	0	18.1	23.6	7.5	1698	5.932	7.709	7.978	3.7	22.0	3.00	Through middle
0T27	IG-110	AG	edge	0	15.8	22.3	7.1	1601	5.926	7.705	7.979	4.2	22.0	3.00	Through middle
0T28	IG-110	AG	edge	0	17.1	22.7	7.2	1630	5.931	7.708	7.98	3.8	22.0	3.00	Through middle
0T29	IG-110	AG	edge	0	15.8	22.3	7.1	1605	5.953	7.697	7.939	4.2	21.9	3.00	Middle to right flat side
0T30	IG-110	AG	edge	0	16.6	21.6	6.8	1546	5.924	7.709	7.974	3.7	22.0	3.00	Middle to right flat side
0T31	IG-110	AG	edge	0	16.7	22.2	6.9	1645	5.925	7.709	7.973	4.0	21.9	3.00	Middle
0U00	PCEA	WG	heart	0	16.1	21.3	6.8	1530	5.938	7.691	7.981	3.8	22.1	3.00	Near middle
0U25	PCEA	AG	heart	0	12.2	15.9	5.1	1148	5.956	7.697	7.985	3.7	22.0	3.00	Right of middle
1S07	NBG-17	WG	heart	0	20.5	26.7	8.5	1923	5.965	7.677	8.022	3.7	22.3	3.00	Left of middle
1S08	NBG-17	WG	heart	0	16.8	21.1	6.7	1515	5.952	7.689	8.022	3.5	22.2	3.00	Left of middle
1S09	NBG-17	WG	heart	0	19.3	24.1	7.6	1730	5.949	7.697	8.023	3.4	22.1	3.00	Through middle
1S10	NBG-17	WG	heart	0	15.0	23.3	7.4	1682	5.965	7.707	8.024	4.6	22.1	3.00	Middle
1S11	NBG-17	WG	heart	0	20.8	26.4	8.4	1906	5.952	7.712	8.023	3.6	22.1	3.00	Near middle
1S30	NBG-17	AG	heart	0	15.8	20.6	6.5	1487	5.957	7.718	7.976	3.7	21.9	3.00	Near middle
1S31	NBG-17	AG	heart	0	20.7	25.2	8.0	1826	5.964	7.721	7.981	3.3	21.9	3.00	Through middle
1S32	NBG-17	AG	heart	0	20.4	24.3	7.7	1762	5.968	7.722	7.982	3.1	21.9	3.00	Through middle
1S33	NBG-17	AG	heart	0	19.8	24.8	7.8	1794	5.979	7.718	7.973	3.5	21.9	3.00	Middle
1S34	NBG-17	AG	heart	0	19.8	24.0	7.6	1728	5.951	7.712	7.973	3.2	21.9	3.00	Middle
1U00	PCIB	AG	heart	0	25.8	34.6	11.0	2503	5.969	7.714	7.981	3.9	21.9	3.00	Left of middle
1U30	PCIB	WG	heart	0	25.5	33.2	10.5	2396	5.952	7.707	7.989	3.7	22.0	3.00	Middle to flat side
2S06	NBG-18	WG	heart	0	14.9	20.0	6.4	1441	5.932	7.716	7.983	3.9	21.9	3.00	Multiple directions
2S31	NBG-18	AG	heart	0	19.0	23.6	7.5	1701	5.947	7.707	7.984	3.4	22.0	3.00	Left of middle
2U05	PPEA	WG	heart	0	18.6	24.1	7.6	1732	5.955	7.696	7.992	3.7	22.1	3.00	Through middle
2U29	PPEA	AG	heart	0	16.4	19.7	6.2	1419	5.959	7.704	7.98	3.1	22.0	3.00	Left of middle
S031	NBG-10	WG	heart	16.9	27.1	32.3	10.1	2442	2442	7.714	8.026	3.2	22.3	3.04	Left of middle
S032	NBG-10	WG	heart	6.8	24.4	28.8	8.9	2138	2138	7.662	7.932	3.1	21.7	2.94	Through middle
S033	NBG-10	WG	heart	22.2	22.1	26.9	8.3	2131	2131	7.895	8.237	3.5	21.9	3.03	Through middle
S042	NBG-10	AG	heart	22.3	16.7	20.6	6.3	1664	1664	7.835	8.193	3.6	21.2	2.90	Left of middle
S050	NBG-10	AG	heart	6.5	19.3	25.5	7.8	1907	1907	7.621	7.898	3.9	21.5	2.89	Through middle
S051	NBG-10	AG	heart	12.8	26.0	34.2	10.5	2525	2525	7.562	7.848	3.9	21.4	2.86	Left of middle
S064	NBG-10	WG	edge	10.4	31.7	39.3	12.6	2847	2847	7.547	7.865	3.5	23.5	3.14	Left of middle
S068	NBG-10	WG	edge	13.5	32.2	38.2	12.5	2807	2807	7.58	7.925	3.1	24.5	3.29	Through middle

Table 3 continued

Specimen code	Grade	Orientation	Location	dpa	σ_H [MPa]	σ_P [MPa]	σ_α [MPa]	F_{fail} [N]	L [mm]	H [mm]	D [mm]	2b [mm]	α [°]	w [mm]	Failure location
S478	NBG-18	AG	edge	12.6	27.3	32.4	10.5	2402	2402	7.574	7.903	3.1	23.8	3.20	Middle to flat side
S479	NBG-18	AG	edge	9.2	26.7	35.6	11.4	2603	2603	7.536	7.855	3.9	23.5	3.13	Through middle
S523	NBG-18	AG	heart	13.2	31.1	34.8	11.2	2582	2582	7.572	7.897	2.6	23.8	3.19	Right of middle
S524	NBG-18	AG	heart	11.4	26.1	33.8	10.9	2496	2496	7.557	7.874	3.8	23.6	3.16	Through middle
S568	NBG-17	AG	edge	13.2	27.6	38.0	11.8	2875	2875	7.673	7.97	4.2	22.1	2.99	First fracture left of middle
S571	NBG-17	AG	edge	10.8	29.9	35.5	11.0	2656	2656	7.633	7.916	3.1	21.9	2.96	Through middle
S617	NBG-17	AG	heart	12.6	30.7	37.2	11.7	2822	2822	7.669	7.979	3.4	22.5	3.05	Right of middle
S619	NBG-17	AG	heart	8.3	34.4	43.8	13.8	3252	3252	7.621	7.919	3.7	22.5	3.03	Through middle
T010	IG-110	AG	heart	6.9	26.5	32.7	9.8	2344	2344	7.664	7.878	3.4	20.7	2.81	To both sides
T011	IG-110	AG	heart	23.4	19.6	24.7	7.4	2071	2071	7.917	8.182	3.7	20.6	2.87	Left of middle
T014	IG-110	AG	heart	13.6	33.9	43.9	13.4	3179	3179	7.544	7.861	3.7	21.4	2.83	3 fractures
T022	IG-110	WG	heart	17.4	31.7	36.5	11.8	2694	2694	7.69	8.027	2.9	23.7	3.23	Left of middle
T026	IG-110	WG	heart	6.5	27.2	36.0	11.7	2597	2597	7.575	7.912	3.9	24.2	3.25	Through middle
T039	IG-110	AG	edge	9.1	33.1	42.1	12.6	3089	3089	7.597	7.823	3.6	20.7	2.79	Through middle
T048	IG-110	WG	edge	21.5	30.8	37.9	11.6	2842	2842	7.878	8.167	3.5	21.5	2.99	3 fractures
T049	IG-110	WG	edge	7.9	32.8	41.5	12.9	2979	2979	7.617	7.889	3.6	22.1	2.98	Somewhat left to middle
T052	IG-110	WG	edge	11.5	35.8	44.6	12.8	3236	3236	7.685	7.896	3.5	19.4	2.63	Through middle
U004	PCEA	WG	heart	17.8	21.7	25.0	7.9	1832	1832	7.613	7.957	2.9	22.9	3.07	Middle to left flat side
U005	PCEA	WG	heart	22.4	19.6	23.9	7.7	1830	1830	7.82	8.185	3.5	23.7	3.28	Through middle
U008	PCEA	WG	heart	6.3	24.1	30.8	9.8	2223	2223	7.588	7.919	3.7	23.1	3.09	Through middle
U023	PCEA	AG	heart	22.2	15.0	17.7	5.6	1404	1404	7.72	8.162	3.2	22.6	3.02	Left of middle
U024	PCEA	AG	heart	17.9	20.6	24.8	7.7	1854	1854	7.598	7.971	3.3	22.2	2.94	Left of middle
U025	PCEA	AG	heart	7.5	20.0	25.5	8.0	1872	1872	7.589	7.899	3.7	22.4	3.00	Through middle
U042	PCEA	AG	heart	13.2	28.3	35.4	11.5	2569	2569	7.466	7.815	3.5	24.1	3.18	Through middle
U043	PCEA	AG	heart	11.6	28.2	35.1	11.3	2547	2547	7.472	7.81	3.5	23.7	3.14	Through middle
U053	PCEA	WG	heart	11.8	28.6	36.7	11.6	2660	2660	7.542	7.835	3.7	22.6	3.01	Left of middle
U104	PCEA	WG	edge	13	37.8	48.4	15.6	3480	3480	7.543	7.86	3.7	23.5	3.15	Through middle
U111	PCIB	AG	heart	6.3	32.9	41.9	13.3	3096	3096	7.645	7.974	3.7	22.9	3.10	Through middle
U114	PCIB	AG	heart	21.1	41.8	48.5	15.4	3788	3788	7.777	8.137	3.0	22.9	3.13	3 fractures
U126	PCIB	WG	heart	6.6	39.8	47.1	14.7	3460	3460	7.662	7.95	3.1	22.1	2.99	On complete left
U127	PCIB	WG	heart	5.8	36.2	45.4	14.2	3326	3326	7.669	7.974	3.6	22.3	3.02	To left side
U165	PCIB	AG	heart	9.8	45.8	54.2	16.1	4063	4063	7.676	7.94	3.1	20.4	2.76	Multiple fracture
U166	PCIB	AG	heart	13.4	47.0	57.6	17.0	4348	4348	7.707	7.967	3.4	20.2	2.73	Multiple fracture
U192	PCIB	WG	edge	9.3	45.7	55.1	17.1	4049	4049	7.69	7.957	3.3	22.0	3.00	3 fractures
U193	PCIB	WG	edge	8.6	41.2	53.0	15.9	3958	3958	7.72	7.962	3.8	20.6	2.81	3 fractures
U198	PCIB	AG	edge	7.7	45.6	57.1	17.9	4212	4212	7.633	7.932	3.6	22.5	3.03	Towards sides of flat side
U236	PPEA	AG	heart	19.9	22.9	28.8	9.1	2206	2206	7.665	8.068	3.6	22.9	3.06	Right of middle
U258	PPEA	AG	heart	12.8	26.1	33.6	10.7	2480	2480	7.535	7.874	3.7	23.2	3.08	Right of middle
U280	PPEA	WG	heart	6	30.7	35.8	11.5	2576	2576	7.551	7.862	3.0	23.3	3.12	Through middle

Appendix C Images of specimens after testing

C.1 GrafTech specimens

Table 4 GrafTech PCEA graphite specimens after diametric compression testing

Specimen code	Grade	Location	Orientation	dpa	Specimen after testing
0U25	PCEA	heart	AG	0	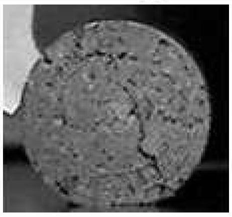
U025	PCEA	heart	AG	7.5	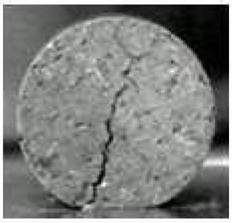
U043	PCEA	heart	AG	11.6	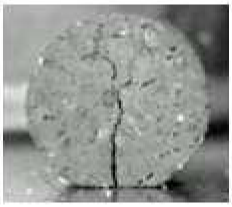
U042	PCEA	heart	AG	13.2	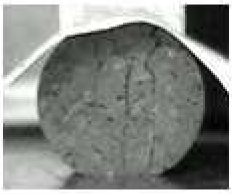
U024	PCEA	heart	AG	17.9	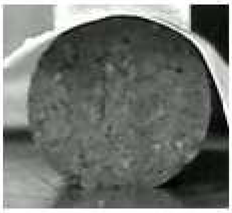

Table 4 continued

Specimen code	Grade	Location	Orientation	dpa	Specimen after testing
U023	PCEA	heart	AG	22.2	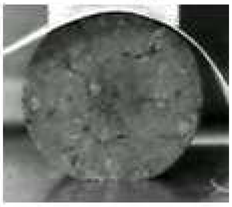
0U00	PCEA	heart	WG	0	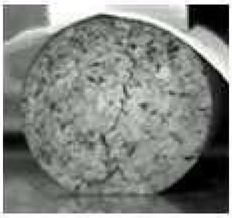
U008	PCEA	heart	WG	6.3	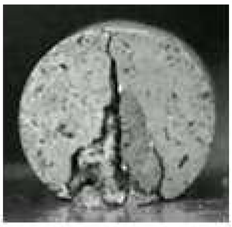
U053	PCEA	heart	WG	11.8	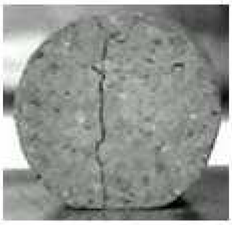
U104	PCEA	edge	WG	13	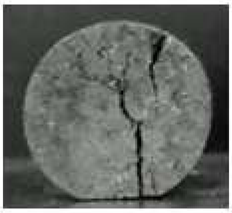
U004	PCEA	heart	WG	17.8	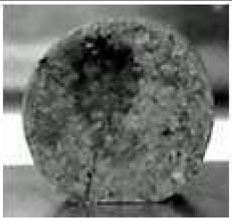
U005	PCEA	heart	WG	22.4	

Table 5 GrafTech PCIB graphite specimens after diametric compression testing

Specimen code	Grade	Location	Orientation	dpa	Specimen after testing
1U00	PCIB	heart	AG	0	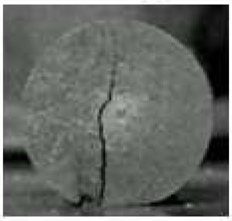
U111	PCIB	heart	AG	6.3	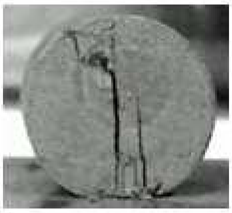
U198	PCIB	edge	AG	7.7	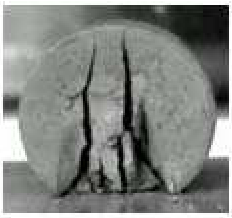
U165	PCIB	heart	AG	9.8	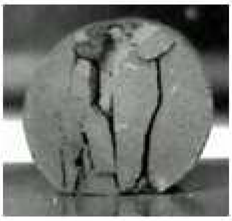
U166	PCIB	heart	AG	13.4	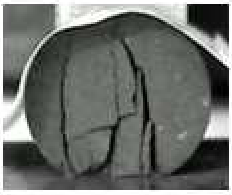
U114	PCIB	heart	AG	21.1	

Table 5 continued

Specimen code	Grade	Location	Orientation	dpa	Specimen after testing
1U30	PCIB	heart	WG	0	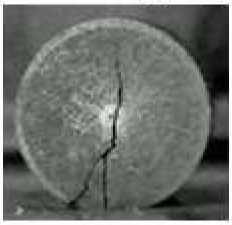
U127	PCIB	heart	WG	5,8	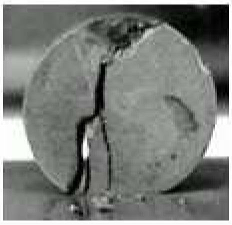
U126	PCIB	heart	WG	6,6	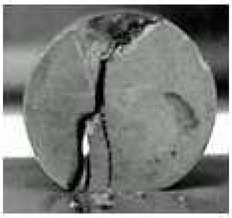
U193	PCIB	edge	WG	8,6	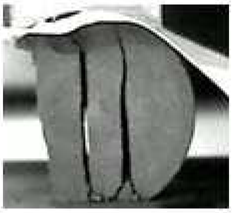
U192	PCIB	edge	WG	9,3	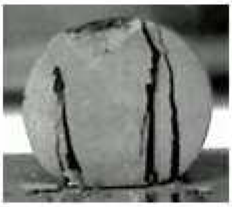

Table 6 GrafTech PPEA graphite specimens after diametric compression testing

Specimen code	Grade	Location	Orientation	dpa	Specimen after testing
2U29	PPEA	heart	AG	0	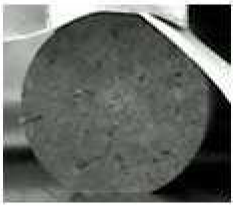
U258	PPEA	heart	AG	12,8	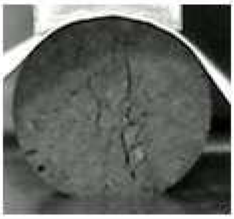
U236	PPEA	heart	AG	19,9	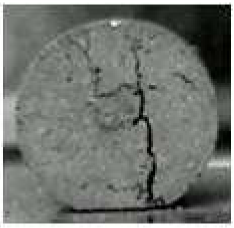
2U05	PPEA	heart	WG	0	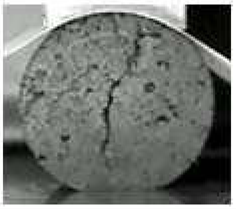
U280	PPEA	heart	WG	6	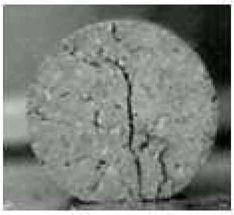

C.2 SGL specimens

Table 7 SGL NBG-10 graphite specimens after diametric compression testing.

Specimen code	Grade	Location	Orientation	dpa	Specimen after testing
0S31	NBG-10	heart	AG	0	
S050	NBG-10	heart	AG	6.5	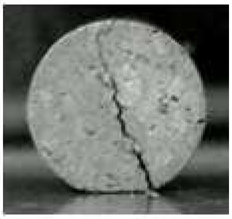
S051	NBG-10	heart	AG	12.8	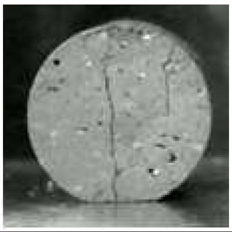
S042	NBG-10	heart	AG	22.3	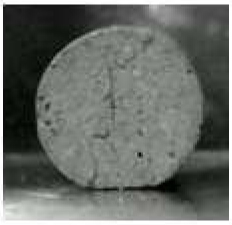
0S06	NBG-10	heart	WG	0	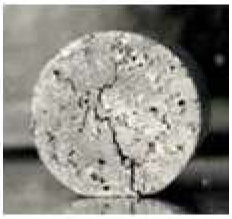
S032	NBG-10	heart	WG	6.8	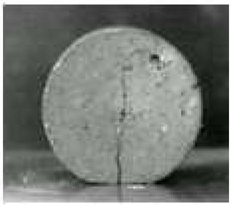

Table 7 continued

Specimen code	Grade	Location	Orientation	dpa	Specimen after testing
S064	NBG-10	edge	WG	10.4	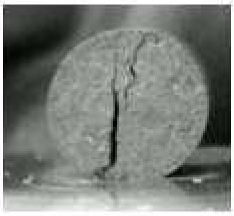
S068	NBG-10	edge	WG	13.5	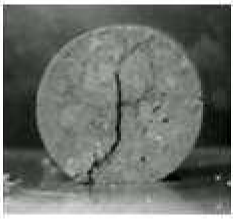
S031	NBG-10	heart	WG	16.9	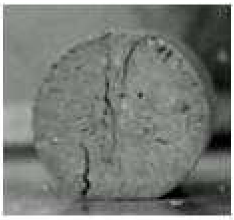
S033	NBG-10	heart	WG	22.2	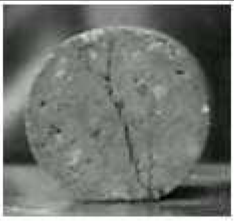

Table 8 SGL NBG-17 graphite specimens after diametric compression testing.

Specimen code	Grade	Location	Orientation	dpa	Specimen after testing
1S30	NBG-17	heart	AG	0	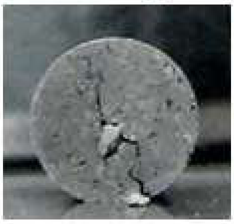
1S31	NBG-17	heart	AG	0	

Table 8 continued

Specimen code	Grade	Location	Orientation	dpa	Specimen after testing
1S32	NBG-17	heart	AG	0	
1S33	NBG-17	heart	AG	0	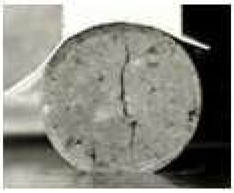
1S34	NBG-17	heart	AG	0	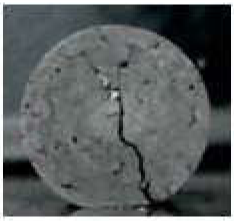
S619	NBG-17	heart	AG	8.3	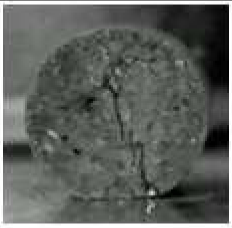
S571	NBG-17	edge	AG	10.8	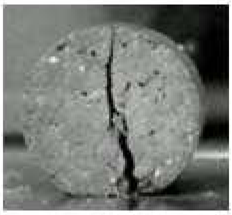
S617	NBG-17	heart	AG	12.6	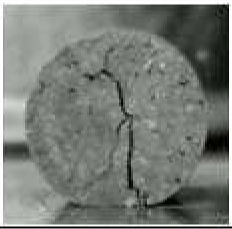
S568	NBG-17	edge	AG	13.2	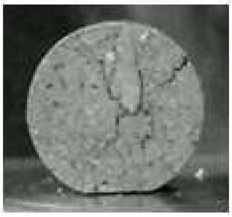

Table 8 continued

Specimen code	Grade	Location	Orientation	dpa	Specimen after testing
1S07	NBG-17	heart	WG	0	
1S08	NBG-17	heart	WG	0	
1S09	NBG-17	heart	WG	0	
1S10	NBG-17	heart	WG	0	
1S11	NBG-17	heart	WG	0	

Table 9 SGL NBG-18 graphite specimens after diametric compression testing

Specimen code	Grade	Location	Orientation	dpa	Specimen after testing
2S31	NBG-18	heart	AG	0	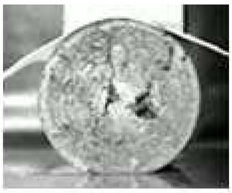
S479	NBG-18	edge	AG	9.2	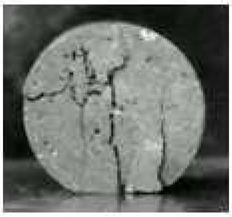
S524	NBG-18	heart	AG	11.4	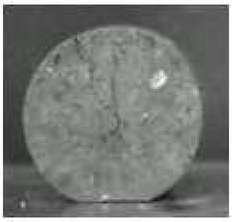
S478	NBG-18	edge	AG	12.6	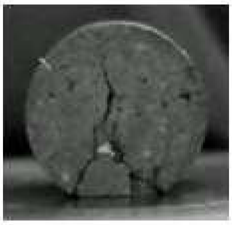
S523	NBG-18	heart	AG	13.2	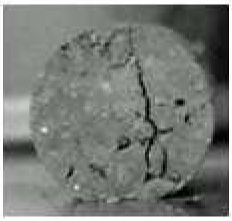
2S06	NBG-18	heart	WG	0